Discovery of novel mechanisms in skeletal muscle and liver underlying the regulation of blood glucose homeostasis

Evan Porter Taddeo

Cromwell, CT

MS, Biological and Physical Sciences, University of Virginia, 2013

BA, Biology, Hamilton College, 2011

A Dissertation presented to the Graduate Faculty of the University of Virginia in Candidacy for the Degree of Doctor of Philosophy

Department of Pharmacology

University of Virginia

July 2015

Kyle L. Hoehn, Ph.D.

Ira G. Schulman, Ph.D.

Thurl E. Harris, Ph.D.

Susanna R. Keller, M.D.

Brant E. Isakson, Ph.D.

Bimal N. Desai, Ph.D.

ABSTRACT

Maintaining blood glucose levels is a fundamental process for sustaining life. During fasting, the liver constantly replenishes the circulating glucose supply through hepatic glucose production (HGP). After consuming a meal, insulin shuts down HGP and stimulates peripheral uptake and utilization of glucose by skeletal muscle. These processes go awry in insulin resistant individuals, resulting in lower insulin-stimulated glucose uptake, exacerbated HGP and eventually type 2 diabetes. Despite considerable attention, the mechanism of insulin resistance in muscle and liver remains unclear.

HGP and skeletal muscle glucose uptake /utilization rely on mitochondrial function. Abnormal mitochondrial function can contribute to insulin resistance. Yet, the mechanisms linking altered mitochondrial function to defects in whole-body glucose metabolism are not well understood. The primary objective of my thesis project was to investigate the role of mitochondria in skeletal muscle glucose uptake and HGP in the context of insulin resistance. Herein, I report the discovery of the mitochondrial permeability transition pore (mPTP) as a link between mitochondrial dysfunction and insulin resistance in skeletal muscle. Tissue-specific mPTP inhibition also elucidated a critical role for mitochondrial function in liver glucose utilization. Finally, I demonstrate a new role for the bioactive lipid-hydrolyzing enzyme lipid phosphate phosphatase 1 (LPP1) in HGP and liver mitochondria homeostasis during fasting. In sum, we conclude that the mitochondrion serves as a vital energy stress sensor, promoting mPTP-dependent insulin resistance in muscle and adjusting HGP in response to the liver lipid environment. This work uncovers new pathways connecting mitochondria to glucose homeostasis that may be probed in the future for potential therapeutic targets to treat diabetes.

ACKNOWLEDGMENTS

There are numerous individuals that have made my success a possibility. First and foremost, I would like to thank my family and friends. I would never have made it this far without their support. My parents, Dr. Robert Taddeo and Judith Taddeo, RN, my sister, Emily Taddeo Patrei and brother-in-law Jon Patrei have offered unwavering love and encouragement. My grandparents, Petrina and Herbert Porter and Ruth and Bill Taddeo always inspired me to work hard and follow my dreams. I would like to thank Dr. David Hangauer who not only spurred my interest in pharmacology by facilitating my enrollment in a summer internship at Kinex Pharmaceuticals in Buffalo, NY, but has given me invaluable advice for carefully selecting a postdoctoral mentor. I would also like to acknowledge my good friends, especially Eric Walton, Michael Anthony, Michael Osborne, George Kentros, Andrew Branting, Jake Lacy, Gary Bedrosian and Haley Peterson. Your friendship has meant the world to me, and your support has been instrumental in my growth as a person. I must pay homage to my good friend, Isaac Nardi, who has always been there for me through the highs and lows. Finally, I would like to thank my Hamilton College Biology thesis advisors, Drs. David Gapp and Ashleigh Smythe who cultivated my love of science and gave me an opportunity to pursue any and all of my research interests.

Throughout my graduate career, the University of Virginia Pharmacology Department has been a crucial element in my development as an independent scientist. First and foremost, I would like to thank my mentor, Dr. Kyle Hoehn. I simply would not be the scientist I am today without his knowledge, guidance, and support. Under Kyle, I developed into an independent researcher with a diligent work ethic and little fear of

failure, and for this I am thankful. He has done an excellent job preparing me for a future career in science. I look forward to working with him as a scientific peer. I would also like to acknowledge my Thesis Committee members, Ira Schulman, Thurl Harris, Susanna Keller, Brant Isakson and Bimal Desai for their helpful scientific input and advice for selecting a postdoctoral mentor. Lab meetings with Thurl and continuous collaboration with Brant have greatly enriched my experiences at UVa and fostered my growth as a scientist.

I must also pay tribute to a long-time collaborator and friend, Dr. Zhen Yan, who was not only a key part of my PhD project, but always pushed me to think critically about my own data and be cognizant of the broader significance of my work. Dr. Rhianna Laker, a postdoc in the Yan lab, has been a wonderful collaborator, spearheading the investigation of tissue-specific metabolic regulation by the mPTP. Rhianna has also been a great friend from whom I have learned much about various things, including but not limited to, Australian culture and being a postdoc. I am very grateful for the constant assistance of Dr. Jose Tomsig in measuring and interpreting mass spectrometry-based lipidomics data throughout the course of my PhD. Of course, I cannot forget all of the hard work by Jolene Kidd and Tammy Snow. Both Jolene and Tammy certainly kept me in line and on schedule during my PhD. I would not have made it this far without them.

I am extremely grateful for the opportunity to work with the members of my lab. Marin Healy, Brandon Kenwood, David Breen, Frances Byrne, Jenny Chow, Jason Liao, Stefan Hargett and Sujoy Lahiri have all made my experience enjoyable and unforgettable. For this reason, I looked forward to coming into lab every day. Marin and Brandon especially have always pushed me to be a better scientist and a better person.

For this I will be forever grateful. I hope that we may maintain professional relationships, but more importantly friendships, in the future no matter what lay ahead.

Finally, I would like to thank Dr. Orian Shirihai at Boston University for taking me on as a postdoctoral fellow. I am very excited to join the lab of Dr. Shirihai and take the next step in my scientific career under his guidance.

TABLE OF CONTENTS

SUMMARY OF FIGURES

SUMMARY OF TABLES

APPENDIX OF ABBREVIATIONS

2-DOG. *2-Deoxyglucose*
AGK. *Acylglycerol Kinase*
AGPAT. *Acylglycerophosphate Acyltransferase*
ANT. *Adenine Nucleotide Translocase*
BKA. *Bongkrekic Acid*
BSA. *Bovine Serum Albumin*
C1P. *Ceramide-1-Phosphate*
CCTα. *CTP:phosphocholine Cytidylyltransferase α*
CerK. *Ceramide Kinase*
CerS. *Ceramide Synthase*
CK. *Choline Kinase*
CsA. *Cyclosporin A*
CypD. *Cyclophilin D*
DAGs. *Diacylglycerols*
EK. *Ethanolamine Kinase*
ET. *CTP:phosphoethanolamine Cytidylyltransferase*
ETC. *Electron Transport Chain*
FFAs. *Free Fatty Acids*
G6pase. *Glucose-6-Phosphatase*
GAPDH. *Glyceraldehyde 3-Phosphate Dehydrogenase*
GLUT4. *Glucose Transporter 4*
GPAT. *Glycerol-3-Phosphate Acyltransferase*
GTTs. *Glucose Tolerance Tests*
HFD. *High Fat Diet*
HGP. *Hepatic Glucose Production*
HK2. *Hexokinase 2*
ITTs. *Insulin Tolerance Tests*
KO. *Knockout*
LFD. *Low Fat Chow Diet*
LKO. *Liver-Specific Knockout*
LPA. *Lysophosphatidic Acid*
LPC. *Lysophosphatidylcholine*
LPP1. *Lipid Phosphate Phosphatase 1*
MAG. *Monoacylglycerol*
MAS. *Mitochondrial Assay Solution*
MCAD. Medium Chain Acyl-CoA Dehydrogenase
MCK. Muscle Creatine Kinase
MDA. *Malondialdehyde*
MHC. *Myosin Heavy Chain*
MKO. *Muscle-Specific Knockout*
mPTP. *Mitochondrial Permeability Transition Pore*
$O_2^{\cdot}$. *Superoxide*
OCR. *Oxygen Consumption Rate*
OXPHOS. *Oxidative Phosphorylation*

PA. *Phosphatidic Acid*
PAs. *Phosphatidic Acids*
PCs. *Phosphatidylcholines*
PDH. *Pyruvate Dehydrogenase*
PEMT. *Phosphatidylethanolamine N-methyltransferase*
pen/strep. *Penicillin/Streptomycin*
PEPCK. *Phosphoenolpyruvate Carboxykinase*
PEs. *Phosphatidylethanolamines*
PLD. *Phospholipase D*
PM. *Plasma Membrane*
POL. *Palmitate Oleate Linoleate*
PSD. *Phosphatidylserine Decarboxylase*
PSs. *Phosphatidylserines*
PSS. *Phosphatidylserine Synthase*
PTTs. *Pyruvate Tolerance Tests*
qRT-PCR. Quantitative Reverse Transcription Polymerase Chain Reaction
RCR. *Respiratory Control Ratio*
Rg'. *Rate of Glucose Transport*
S1P. *Sphingosine-1-Phosphate*
SEM. *Standard Error of the Mean*
SOD2. *Superoxide Dismutase*
SphK. *Sphingosine Kinase*
STAT3. *Signal Transducer and Activator of Transcription 3*
TBARS. *Thiobarbituric Acid Reactive Substances*
TCA. *Tricarboxylic Acid*
TEM. *Transmission Electron Microscopy*
VDAC. *Voltage Dependent Anion Channel*
WAT. *White Adipose Tissue*
WT. *Wild Type*
βHAD. *β-hydroxyacyl-CoA Dehydrogenase*

CHAPTER 1: REGULATION OF WHOLE-BODY GLUCOSE HOMEOSTASIS BY SKELETAL MUSCLE AND LIVER

1.1 Glucose metabolism in skeletal muscle and liver

1.1.1 Insulin-stimulated skeletal muscle glucose utilization

After ingestion of a meal, insulin released by the pancreas promotes the uptake of circulating glucose into peripheral tissues, ultimately lowering blood glucose levels. Skeletal muscle accounts for roughly 85% of whole-body insulin-stimulated glucose disposal[1], with adipose, heart and other tissues collectively accounting for the other 15%, pointing to skeletal muscle as a critical site for insulin action. In skeletal muscle, insulin also determines the fate of intracellular glucose, directing it towards glycogen storage or oxidation for energy, with the majority of glucose (~70%) being salvaged as glycogen[2]. In muscle, insulin signals through a well-characterized insulin receptor/IRS/PI3K/Akt pathway[3,4] that ultimately mobilizes glucose transporter 4 (GLUT4) to the plasma membrane (PM), allowing for the uptake and metabolism of glucose. This signaling pathway and downstream steps in glucose metabolism are fundamentally altered in the diabetic state.

Skeletal muscle insulin resistance is a hallmark of type 2 diabetes. As a consequence of insulin resistance, insulin is less capable of stimulating glucose uptake and glycogen storage in muscle, ultimately contributing to hyperglycemia that is characteristic of diabetes. Impaired insulin-stimulated glucose uptake in muscle has been observed in both diabetic patients[1,5] and in rodent models of diabetes[6,7]. In fact, skeletal muscle glucose disposal in type 2 diabetics is roughly 50% of that in healthy controls[5]. This decrease in glucose uptake is due in part to inefficient translocation of GLUT4 to the PM of muscle cells[1,8]. Aberrant GLUT4 translocation disrupts glucose homeostasis in rodents as well. Feeding mice a high fat diet (HFD) attenuates insulin-stimulated glucose

uptake in skeletal muscle by blunting insulin-responsive GLUT4 PM localization[7]. Genetic impairment of GLUT4 trafficking in mice results in insulin resistance and significantly reduces skeletal muscle and whole-body glucose uptake[9], indicating that aberrant GLUT4 translocation may be a common defect underlying the diminished muscle glucose uptake in the insulin resistant state. Similar defects are seen with intracellular muscle glucose metabolism, as insulin resistant subjects show reduced insulin-stimulated glycogen formation[10,11]. The lower insulin-mediated glucose metabolism observed in insulin resistant muscle can be associated with defects in insulin signaling[1], such as reduced Akt activation[12]. It is thought that excess fatty acids are a culprit in mediating this inhibition of Akt in muscle[4]. However, skeletal muscle insulin resistance is not always associated with changes at this major node of insulin signaling[13,14], suggesting the involvement of alternative pathways. Taken together, alterations in insulin-mediated skeletal muscle glucose metabolism are a major contributing factor in the pathogenesis of type 2 diabetes, but a comprehensive understanding of the underlying mechanisms is still lacking.

Insulin stimulates glucose uptake by binding to its receptor tyrosine kinase in the PM of muscle cells. Binding of insulin leads to autophosphorylation and activation of the insulin receptor, which tyrosine phosphorylates IRS adaptor proteins. IRS phosphosites serve as a scaffold for the lipid kinase PI3K, which produces PIP_3 from membrane lipids. The serine/threonine kinase Akt binds PIP_3 at the membrane which induces a conformational change that facilitates PDK1-mediated phosphorylation of Akt at Thr308[3]. Akt is also phosphorylated at Ser473 by mTORC2, and both of these phosphorylations are requisite for full activation of Akt[15]. Activated Akt phosphorylates

the Rab GTPase-activating protein AS160, and 14-3-3 binding to phosphorylated AS160 inhibits its Rab GTPase-activating protein function[15,16]. AS160 inhibition results in a buildup of GTP-loaded Rab proteins on vesicles containing GLUT4[15], promoting the movement of these vesicles along cytoskeletal elements from intracellular storage depots to the PM (Figure 1). AS160-mediated GLUT4 movement may be complemented by insulin activation of the PI3K-independent Cbl/C3G/TC10 pathway [17]. Cbl is phosphorylated by the insulin receptor and translocated to caveolin-enriched lipid rafts on the cell surface[18]. Cbl then recruits the CrkII/C3G complex to lipid rafts, where C3G activates the small GTP-binding protein TC10[19] which helps target GLUT4 vesicles to specific membrane zones for fusion. However, the relative importance of the Cbl pathway has been questioned. Knockdown *in vitro* of Cbl pathway components does not affect insulin-stimulated GLUT4 trafficking and glucose uptake[20]. The results of this study were supported by the discovery that genetic ablation *in vivo* of Cbl enhances insulin sensitivity and increases skeletal muscle glucose uptake[21]. Once at the cell periphery, GLUT4 vesicles are tethered to exocyst complexes, PM-localized multi-protein complexes assembled in response to Akt[15] and TC10 activation[16] that serve as target sites for vesicle fusion (Figure 1). Fusion of GLUT4 vesicles with the cell surface is controlled by the formation of SNARE protein complexes comprised of syntaxin 4 and SNAP-23 at the PM and VAMP2 on GLUT4 vesicles[22]. In response to insulin, the insulin receptor phosphorylates SNARE regulatory proteins, such as Munc18c[23], which facilitates the interaction of these membrane proteins and exocytosis of GLUT4. Once inserted into the membrane, GLUT4 allows glucose entry into the myocyte and subsequent metabolism.

Immediately upon entry into myocytes, glucose is phosphorylated by hexokinase 2 (HK2) to form glucose-6-phosphate, most of which is stored as glycogen as an energy source[2]. Insulin stimulates glycogenesis by a different branch of the insulin signaling pathway downstream of PI3K/Akt that ends up inhibiting the glycogen-catabolizing enzyme glycogen phosphorylase and activating glycogen synthase, the rate limiting enzyme of glycogen production. Insulin-mediated Akt activation promotes glycogen synthase activity through three major mechanisms (Figure 1) all of which ultimately counteract inhibitory phosphorylation of the synthase: 1) Akt inactivates the glycogen synthase-targeting kinase GSK3β by phosphorylation at Ser9[24], 2) Akt promotes dephosphorylation of glycogen synthase by the protein phosphatase PP1[25], and 3) Akt blocks cAMP-mediated activation of the glycogen synthase-inhibiting kinase PKA[26]. Released from inhibition, glycogen synthase incorporates UDP-glucose formed from glucose-6-phosphate into nascent glycogen particles. Activation of glycogen synthase only accounts for part of insulin-stimulated glycogenesis, as the hormone also suppresses the glycogen catabolizing enzyme glycogen phosphorylase by PP1-mediated dephosphorylation[27] (Figure 1). Thus, the net effect of insulin on skeletal muscle glycogen metabolism is an increase in the incorporation of glucose into glycogen.

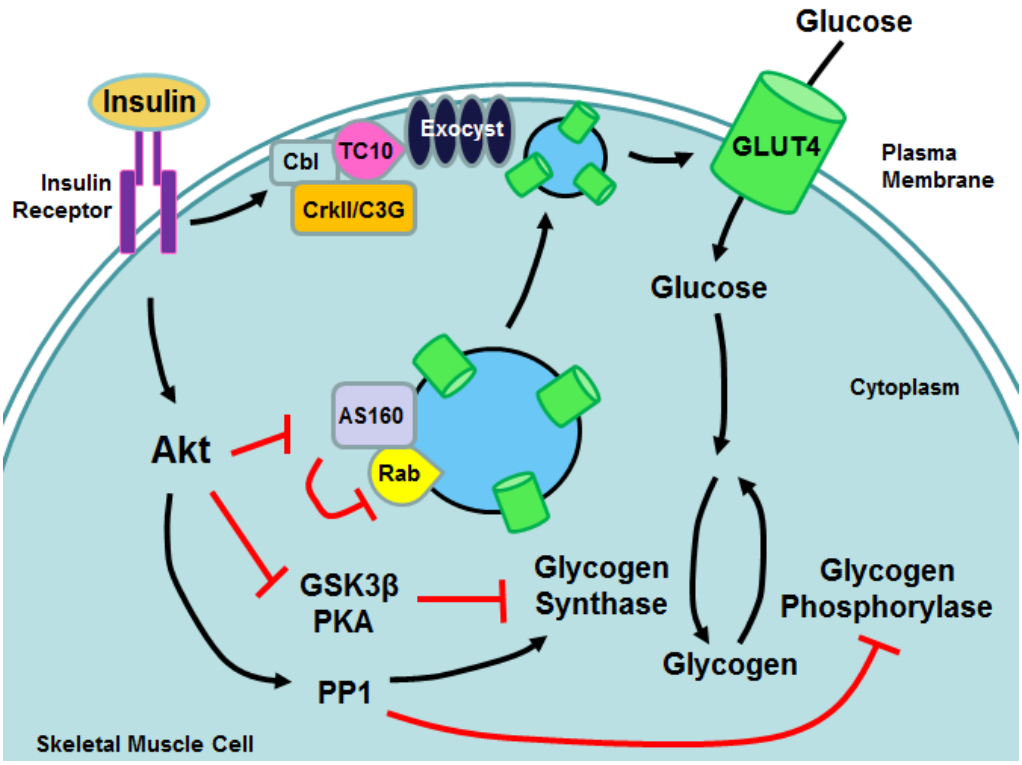

Figure 1. Insulin-stimulated glucose uptake and glycogen storage in skeletal muscle. Insulin binds to the insulin receptor in muscle cells, resulting in Akt-mediated GLUT4 translocation to the PM and formation of targeting sites via TC10 interaction with exocyst complexes. GLUT4-containing vesicles associate with target sites and fuse with the cell surface, facilitating membrane insertion of GLUT4 and subsequent glucose uptake. Insulin-mediated Akt activation also stimulates the storage of incoming glucose as glycogen through activation of glycogen synthase and deactivation of glycogen phosphorylase.

1.1.2 Regulation of hepatic glucose production by glucagon and insulin

Upon fasting, hepatic glucose production (HGP) increases to maintain blood glucose levels within the normal range (70-100 mg/dL)[28]. HGP is defined as the total liver output of glucose derived from both glycogenolysis and gluconeogenesis. In the absence of dietary nutrients, HGP facilitates the constant supply of glucose to all tissues, especially the brain and red blood cells, which depend exclusively on glucose for energy. The release of glucose through glycogenolysis accounts for about 30-60% of HGP in humans during the first12-16hrs of fasting, the other 40-70% derived from gluconeogenesis[29,30]. However, during prolonged fasting (≥24hrs), the proportion of HGP from gluconeogenesis increases to roughly 90% as the hepatic glycogen content becomes depleted[31]. After consumption of a meal, HGP is suppressed to avoid further increases in blood glucose. This balance of HGP induction and inhibition is carefully controlled, mainly through the actions of glucagon and insulin[32], respectively (Figure 2). An imbalance in this hormonal regulation can lead to excessive HGP and contribute to the constitutively high blood glucose that is a hallmark of type 2 diabetes[33]. Thus, tight control over HGP is critical for the preservation of whole-body glucose homeostasis.

Aberrant regulation of HGP contributes to hyperglycemia in type 2 diabetes. Diabetes is associated with elevated glucagon levels[34,35] and decreased insulin inhibition of HGP[33,36]. In line with these hormonal changes, diabetic patients show exaggerated basal HGP during fasting[37] and in the presence of insulin[38]. The increased HGP in diabetic patients may be attributed to elevated gluconeogenesis[33,39] and/or glycogenolysis[38]. Thus, altered hormonal regulation of both HGP components results in higher circulating glucose levels in diabetics. Importantly, metformin, the most-widely

prescribed diabetes treatment lowers blood glucose levels in diabetics primarily by attenuating HGP[40,41,42]. Therefore, HGP remains a critical therapeutic target for treatment of diabetes, emphasizing the need to comprehend the underlying mechanisms regulating this complex process.

Fasting induces HGP mainly through the actions of glucagon, which is counteracted by insulin in the fed state (Figure 2). Glucagon is released by the pancreas and acts on the liver to acutely stimulate hepatic glycogenolysis and activate the gluconeogenic transcriptional program after extended fasting[43]. Postprandial insulin secretion by the pancreas immediately reduces glycogen breakdown and downregulates gluconeogenic gene transcription over a longer time period[36]. Liver glucose synthesis is also fueled by release of the gluconeogenic precursors glycerol from adipose tissue[44,45] and amino acids and lactate from skeletal muscle[46,47] which is also under hormonal control depending on nutritional status.

Glucagon rapidly induces HGP in the liver by increasing glycogen breakdown and modulating substrate flux through the gluconeogenic pathway. Glucagon increases glycogenolysis by stimulating the rate limiting enzyme for glycogen breakdown, glycogen phosphorylase[43,48]. Binding of glucagon to its cognate GPCR in hepatocytes increases cAMP production via adenylyl cyclase and activates PKA, which phosphorylates and activates glycogen phosphorylase. Glucagon also directly impinges upon the gluconeogenic pathway and modifies the activities of glucose metabolism enzymes to favor the *de novo* synthesis of glucose. To drive glucose formation, glucagon stimulates PKA-mediated phosphorylation and activation of fructose-1,6-bisphosphatase[49], which catalyzes the formation of fructose-6-phosphate as the

penultimate step in gluconeogenesis. Through the same PKA-dependent pathway, glucagon also inhibits flux of phosphoenolpyruvate through pyruvate kinase[50]. Overall, glucagon redirects phosphoenolpyruvate away from pyruvate formation and towards gluconeogenesis driven by enhanced fructose-1,6-bisphosphatase activity.

Insulin acutely inhibits HGP by countering the actions of glucagon on glycogen metabolism and gluconeogenic substrate flux. In the liver, insulin stimulates storage of glucose as glycogen while simultaneously impeding glycogenolysis[51]. Insulin signaling through Akt leads to deactivating phosphorylation of GSK3β (Ser9)[24], inactivation of glycogen phosphorylase[52] and the activation of protein phosphatase 1[25,52] which removes inhibitory phosphorylation on glycogen synthase. The net effect is activation of glycogen synthase and increased glycogenesis. These signaling events are complimented by insulin-mediated activation of the cAMP-degrading enzyme phosphodiesterase 3B[53], resulting in lower cAMP levels. Insulin also increases expression of glucokinase, which phosphorylates glucose to provide glucose-6-phosphate for glycolysis[54]. In addition, insulin stimulates production of fructose-2,6-bisphosphate, which activates the glycolytic enzyme phosphofructokinase 1[55] and inhibits fructose-1,6-bisphosphatase[56]. Insulin-mediated dephosphorylation of pyruvate kinase, the last enzyme in the glycolytic pathway, stimulates conversion of phosphoenolpyruvate to pyruvate for mitochondrial oxidation[57]. Therefore, insulin rapidly abates HGP through inhibition of glycogen breakdown and stimulation of substrate flux through glycolysis.

After prolonged fasting, HGP is sustained by glucagon-mediated transcriptional upregulation of key gluconeogenic genes (Figure 3). Downstream of glucagon-induced increases in cAMP, PKA phosphorylates and activates the transcription factor CREB at

Ser133[58]. Activated CREB forms a complex with the transcriptional coactivators CBP, p300 and CRTC2 to promote transcription of the deacetylase Sirt1, the gluconeogenic genes phosphoenolpyruvate carboxykinase (PEPCK) and glucose-6-phosphatase (G6pase) and the progluconeogenic transcription factor PGC1α [58,59]. In response to increased NAD^+ levels during fasting, Sirt1 deacetylates and activates FOXO1 and PGC1α[60]. PGC1α coordinates with FOXO1 and HNF4α to enhance transcription of gluconeogenic genes.

Insulin opposes the transcriptional actions of glucagon on gluconeogenic genes in hepatocytes (Figure 3). The insulin/Akt/FOXO1 pathway is a critical mechanism by which insulin inhibits PEPCK and G6Pase expression. Insulin induces Akt-mediated phosphorylation of FOXO1 at Ser256, which excludes FOXO1 from the nucleus and inhibits gluconeogenic gene transcription[61]. Insulin also dismantles the CREB transcriptional complex through phosphorylation-induced nuclear exclusion of CRTC2[58,62]. Insulin induces expression of the transcriptional repressor SHP1, which interferes with HNF4α-dependent transcription of PEPCK, G6Pase and fructose-1,6-bisphosphatase[63]. Thus, insulin can counteract the transcriptional activation of HGP through direct signaling or indirectly through induction of transcriptional repressors.

Fasting-induced HGP is also fueled by increasing the supply of gluconeogenic substrates to the liver (Figure 2). In adipose tissue, adrenal medulla-derived catecholamines stimulate lipolysis, the catabolism of triglycerides into free fatty acids (FFAs) and glycerol. In adipocytes, catecholamines bind to β-adrenergic receptors and activate the cAMP/PKA pathway, whereby PKA phosphorylates and activates hormone sensitive lipase, the rate limiting enzyme in lipolysis[64]. Adipose tissue lipases cleave

triglycerides stored in lipid droplets, ultimately releasing glycerol and FFAs, which enter circulation and travel to the liver. Glycerol is phosphorylated by glycerol kinase and enters the gluconeogenic pathway[65], while oxidation of FFAs drives HGP through production of acetyl-CoA, ATP, NADH and subsequent activation of fructose-1,6-bisphosphatase[44]. In skeletal muscle, fasting promotes the release of amino acids and lactate into the bloodstream. Amino acid release is thought to be mediated by glucocorticoids. In muscle, glucocorticoids bind to the intracellular glucocorticoid receptor and stimulate the expression of genes involved in protein catabolism[47]. A few of the released amino acids, including alanine and glutamine are classified as glucogenic due to their use as gluconeogenic precursors in the liver. Fasting also activates the Cori cycle, in which lactate produced via anaerobic glycolysis in skeletal muscle is released and sent to the liver[46]. Both glucogenic amino acids and skeletal muscle-derived lactate are converted to pyruvate to provide substrates for gluconeogenesis.

Insulin curtails the supply of gluconeogenic substrates to the liver. Insulin inhibits lipolysis and promotes lipogenesis in adipose, while blocking protein degradation[66] in skeletal muscle (Figure 2). A major mechanism by which insulin inhibits lipolysis in adipose is through activation of phosphodiesterase 3B[53] and reduction of cAMP. Insulin is thought to block skeletal muscle protein catabolism by inhibiting the ubiquitin proteasome system[67]. The net effect of insulin on fat and muscle is a reduction in circulating lipids and amino acids utilized for HGP.

Despite the extensive study of HGP, we are far from fully understanding the regulation of this complex process. For instance, Sirt1 whose HGP-promoting actions are well established, may also decrease gluconeogenic gene expression and HGP by

deacetylating CRTC2, leading to degradation of CRTC2[68]. Furthermore, despite the importance of insulin action in the liver to inhibit HGP, hepatic insulin signaling is dispensable for the suppression of HGP by insulin in mice[32]. These controversies along with the contribution of excessive HGP to type 2 diabetes, only emphasize the need for a better understanding of HGP regulation in health and disease.

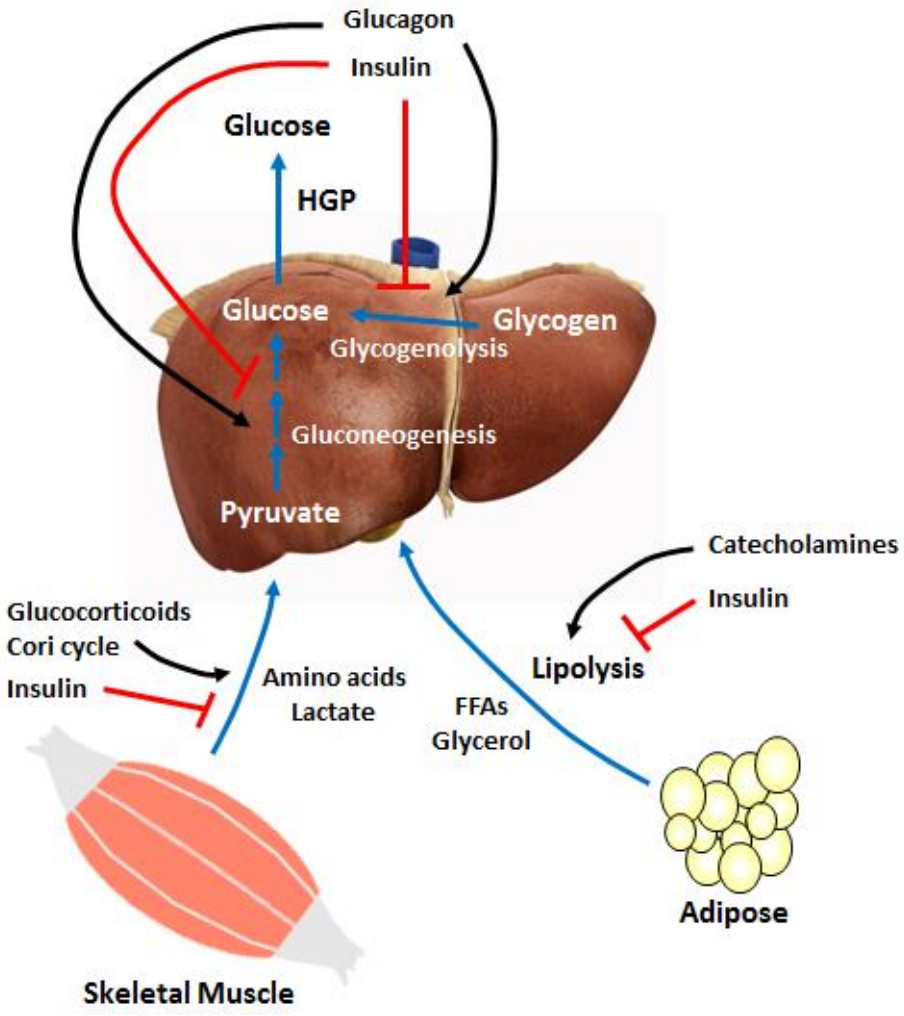

Figure 2. Regulation of HGP by the actions of hormones on peripheral tissues. Glucagon stimulates HGP by promoting glycogenolysis and gluconeogenesis within the liver. Catecholamines and glucocorticoids increase the delivery of gluconeogenic substrates to the liver from adipose and skeletal muscle, respectively. Lactate released by skeletal muscle during the Cori cycle is also used by the liver for gluconeogenesis. Insulin opposes these actions of glucagon, catecholamines and glucocorticoids to decrease HGP.

1.1.3 Signal transducer and activator of transcription 3 as an inhibitor of HGP

Inflammatory signaling provides another route for HGP inhibition. The cytokines IL-13[69] and IL-6[70,71] suppress gluconeogenic gene expression and HGP *in vitro* and *in vivo.* HGP suppression by these cytokines is dependent upon activation of the downstream signaling mediator signal transducer and activator of transcription 3 (STAT3). In response to cytokines and growth factors, STAT3 is phosphorylated on Y705, which promotes nuclear translocation and initiates transcriptional regulation of gluconeogenic genes by STAT3[72]. Liver-specific ablation of STAT3 in mice results in insulin resistance and higher expression of PEPCK and G6pase, while constitutively active STAT3 suppresses these genes and HGP in mice[71], demonstrating the importance of STAT3 for liver glucose homeostasis. Phosphorylation at Y705 is necessary for STAT3-mediated repression of PEPCK and G6pase expression and HGP[73]. Furthermore, STAT3 is tyrosine- phosphorylated in the fed state and dephosphorylated during fasting due in part to Sirt1-mediated deacetylation of STAT3[73], indicating that the inhibitory actions of STAT3 on HGP are physiologically regulated by nutritional status. Taken together, STAT3 is a sensor of energy homeostasis that represses HGP (Figure 3).

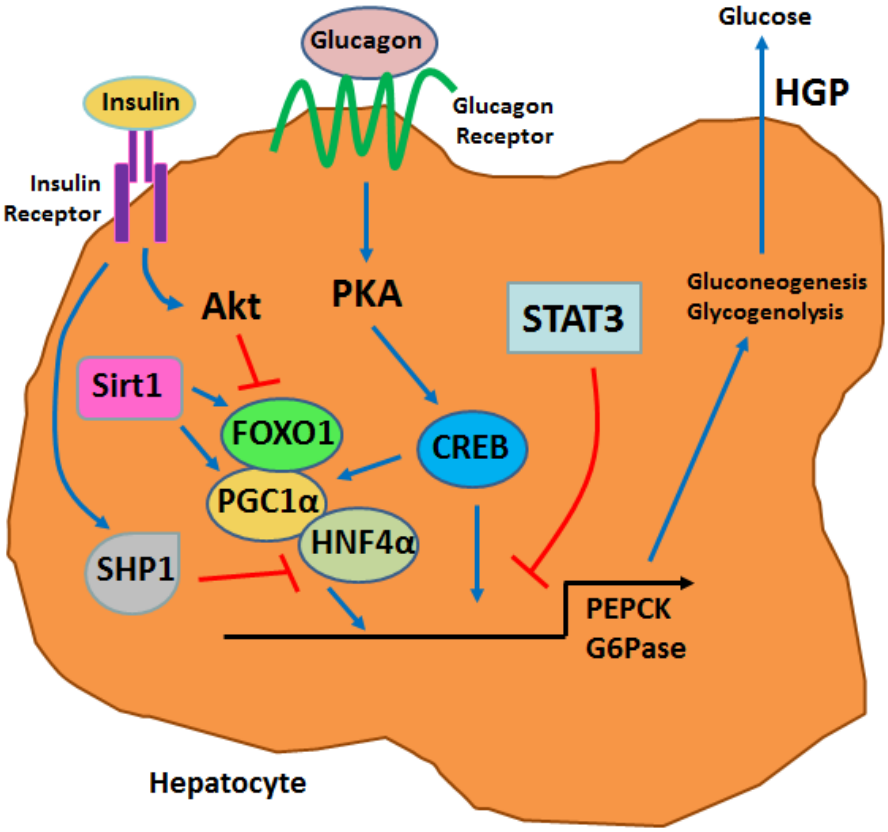

Figure 3. Signaling pathways controlling the gluconeogenic transcriptional program in hepatocytes.

Glucagon signals through PKA to induce PEPCK and G6Pase expression in a CREB-dependent manner. Sirt1 activates FOXO1 and PGC1α which coordinate with HNF4α to help stimulate maximal gluconeogenic gene expression and HGP. Insulin opposes gluconeogenic gene expression through Akt/FOXO1 signaling and through SHP1 transcriptional repression. STAT3 complements the inhibitory actions of insulin on HGP.

1.2 Bioactive lipids and glucose homeostasis

1.2.1 Bioactive lipid metabolism

Bioactive lipids are broadly defined as a class of functional lipids that directly activate specific signaling pathways. These lipid ligands include lysophosphatidic acid (LPA), sphingosine -1-phosphate (S1P), ceramide-1-phosphate (C1P), and phosphatidic acid (PA) among others[74,75]. Many of these bioactive lipids are derived from membrane phospholipids. With highly regulated modes of synthesis, secretion into circulation and degradation, bioactive lipids control local signaling within a cell but have the capacity to act as endocrine modulators of whole body physiology. By binding to lipid-specific families of GPCRs, bioactive lipids regulate a spectrum of cellular functions, such as cell growth[75,76], migration[77], inflammatory responses[78] and energy homeostasis[79]. The fact that serum LPA[79] and S1P[80] are elevated in mice and humans with metabolic disease and may correlate with insulin sensitivity[80] highlights the significant role bioactive lipids play in regulating whole body nutrient metabolism[81].

Bioactive lipids can be derived from or are precursors for membrane phospholipids. The major membrane phospholipids include phosphatidylcholine (PC), phosphatidylethanolamine (PE), and phosphatidylserine (PS), with PC and PE as the most abundant phospholipids in membranes[82]. Steady state levels of PC and PE remain essentially constant based on the ability of the cell to match phospholipid break down with enhanced synthesis. Phospholipids can either be synthesized *de novo* via the Kennedy pathway or interconverted by swapping head groups[82,83] (Figure 4A). PC formation begins with choline as an initial substrate, which is phosphorylated to phosphocholine by cytoplasmic choline kinase (CK). Phosphocholine is then converted to

CDP-choline by CTP:phosphocholine cytidylyltransferase α (CCTα), the rate limiting enzyme in *de novo* PC synthesis that is located throughout the cell. Finally, cholinephosphotransferases (CPT and CEPT) in the plasma membrane, Golgi and mitochondria, combine CDP-choline and DAG to form PC. PE is formed by a similar pathway in which ethanolamine is phosphorylated by cytoplasmic ethanolamine kinase (EK) to form phosphoethanolamine, which is converted to CDP-ethanolamine by the endoplasmic reticulum-localized CTP:phosphoethanolamine cytidylyltransferase (ET). The phosphotransferases EPT and CEPT combine CDP-ethanolamine and DAG to make PE[82,83]. The synthesis of PE and PC is intertwined, as CEPT can form both PC and PE, and the mitochondrial-associated endoplasmic reticulum membrane enzyme phosphatidylethanolamine N-methyltransferase (PEMT) methylates PE to form PC[84]. The less abundant phospholipid PS is synthesized from PC (and to a lesser extent PE) by phosphatidylserine synthase (PSS) enzymes located in mitochondrial-associated endoplasmic reticulum membranes[85]. PS can then be decarboxylated to form PE by endomembrane- and mitochondria-localized phosphatidylserine decarboxylase (PSD) enzymes[86]. Thus, several pathways exist to maintain phospholipid levels, either by production of new lipids or modification of existing lipids.

Bioactive lipid generation depends on phospholipid content (Figure 4B). Phospholipase D (PLD) 1 and 2 convert PC to the bioactive lipid PA. PA can either be dephosphorylated to DAG and subsequently esterified to triacylglycerol or undergo fatty acid removal by PLA to form LPA[82]. During triacylglycerol synthesis in the endoplasmic reticulum, glycerol-3-phosphate acyltransferase (GPAT) utilizes glycerol-3-phosphate to form LPA, which can be reconverted to PA by acylglycerophosphate acyltransferase

(AGPAT)[87]. LPA levels are also determined by a balance between acylglycerol kinase (AGK) –mediated synthesis via phosphorylation of monoacylglycerol (MAG) and dephosphorylation of LPA back to MAG[88]. The majority of circulating LPA is derived from the secreted enzyme autotaxin[89], which removes choline from lysophospatidylcholine (LPC). LPA[90], PA and PS[91] can stimulate the formation of another bioactive lipid, S1P by cytoplasmic sphingosine kinases (SphK). S1P can be dephosphorylated by a number of membrane-bound phosphatases to sphingosine, which can be converted to ceramide by ceramide synthase (CerS) in the endoplasmic reticulum or mitochondrion. Golgi-localized ceramide kinase (CerK) phosphorylates ceramide to form the bioactive lipid C1P, which is also counterbalanced by a group of phosphatases, about which very little is known[78]. This balance between bioactive lipid synthesis and degradation is particularly important in determining signaling pathways activated in insulin-sensitive peripheral tissues.

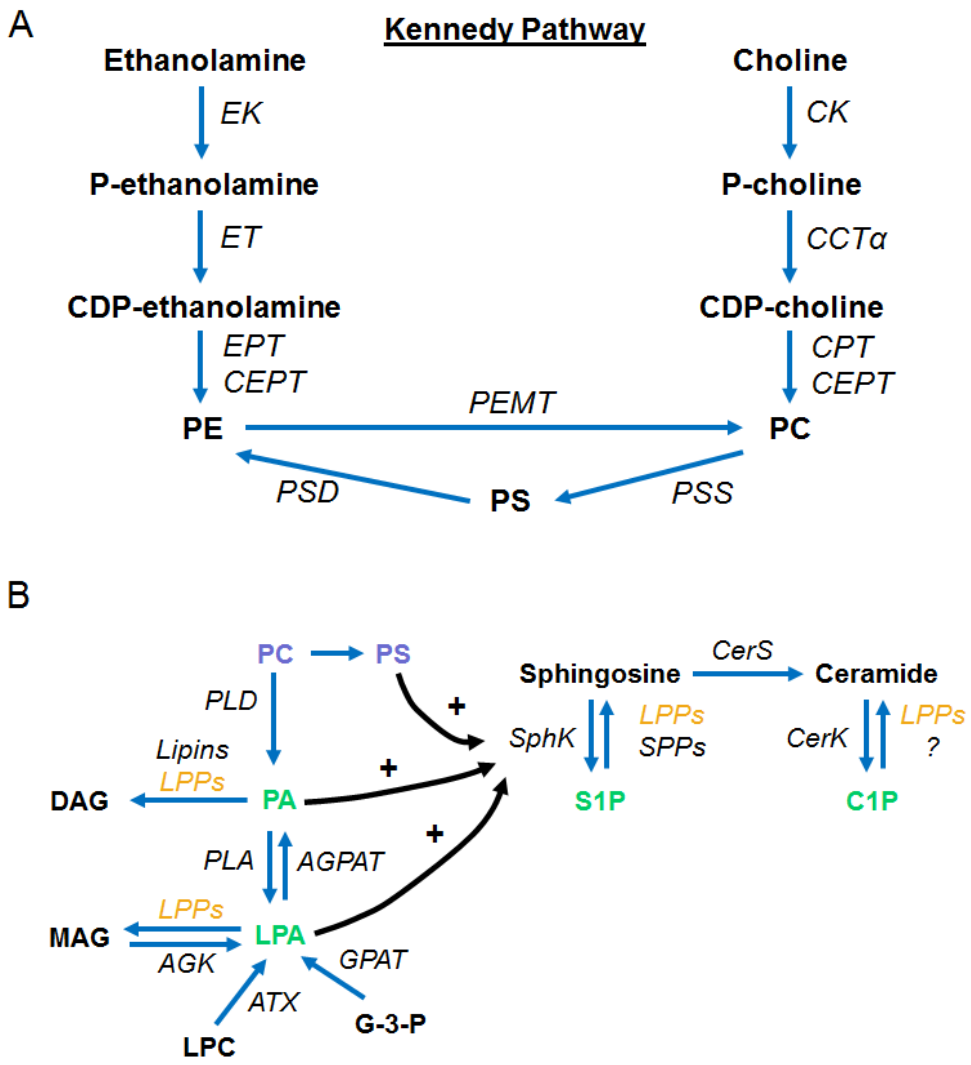

Figure 4. Synthesis and degradation of phospholipids and bioactive lipids.

(A) Synthesis of phospholipids by the Kennedy pathway. PC and PE are formed from choline and ethanolamine, respectively. PS can be made through the conversion of PE to PC. (B) Pathways connecting phospholipids (purple) and bioactive lipids (green). Bioactive lipid metabolism is closely associated with phospholipids and is balanced by phosphatases such as LPPs (gold). Arrows with a "+" symbol indicate stimulation of SphK activity.

1.2.2 Bioactive lipid control of glucose metabolism in muscle and liver

Bioactive lipids control skeletal muscle glucose utilization. Acute administration of LPA in normal and diabetic mice lowers blood glucose levels through activation of LPA receptors, an effect that is attributed to stimulation of Akt-dependent GLUT4 translocation and glucose uptake in skeletal muscle cells[92]. Despite this finding, deletion of the LPA-generating enzyme autotaxin improves glucose tolerance in mice on HFD[93]. Furthermore, chronic pharmacological blockade of LPA receptors in HFD-fed mice improves skeletal muscle glucose uptake and increases glucose oxidation[79], indicating that LPA can have opposing effects on muscle glucose metabolism. S1P also seems to have divergent functions in skeletal muscle. S1P signals through the S1P2 GPCR to stimulate ROS-mediated inactivation of protein tyrosine phosphatase 1B, which leads to increased basal phosphorylation of the insulin receptor and enhanced glucose uptake[94]. On the other hand, fatty acid treatment of skeletal muscle cells increases sphingosine kinase 1-dependent production of S1P, which signals through the S1P3 receptor to stimulate IL-6 production, a cytokine that can interrupt insulin signaling in muscle[95]. PA also influences skeletal muscle glucose uptake downstream of insulin signaling, as insulin-stimulated PA production by PLD mediates fusion of GLUT4-containing vesicles with the PM[96]. Much less is known about C1P in skeletal muscle. C1P induces Akt phosphorylation and inactivates GSK3β in cultured skeletal muscle cells[97], suggesting that C1P may stimulate glycogen formation. Taken together, bioactive lipids show divergent effects on skeletal muscle glucose uptake and metabolism.

The liver is an important hub of bioactive lipid signaling. LPA and S1P are rapidly cleared from circulation via hepatic uptake[98], suggesting that the liver may be an

important site for integration of bioactive lipid turnover and liver energy homeostasis. In support of this idea, LPA can both activate glycogen phosphorylase[99] and stimulate phosphorylation and inactivation of GSK3β[100], suggesting LPA may have dual roles in glycogen metabolism. Chronic treatment of HFD-fed mice with the LPA receptor antagonist Ki16425 increased liver glucokinase expression and glycogen content, but decreased expression of PEPCK and G6pase in the fasted state[79]. These findings highlight an important role for LPA in liver glucose flux between glycogen storage and HGP. Interestingly, PA, an intracellular precursor to LPA, inhibits insulin signaling[101] and promotes HGP in primary mouse hepatocytes through induction of PEPCK and G6pase[101]. Of note, the latter study showed that LPA had no effect on HGP. Virtually nothing is known about C1P in liver glucose utilization. C1P may have a yet undiscovered role, as the livers of obese rats show significantly lower C1P levels compared to lean controls[102]. In hepatocytes, palmitate is converted to S1P, which signals through the S1P2 receptor to hinder insulin signaling[103]. However, adiponectin-mediated enhancement of insulin signaling in the livers of mice is associated with higher S1P levels[104]. Likewise, hepatic overexpression of the sphingomyelin-hydrolyzing enzyme acid sphingomyelinase increases Akt activation and glycogen deposition in the liver through production of S1P, ultimately improving glucose tolerance[105]. These contradictory findings emphasize the persistent gap in knowledge regarding the role of bioactive lipids in liver glucose homeostasis.

1.2.3 Lipid phosphate phosphatase 1 as a regulator of bioactive lipid signaling

Lipid phosphate phosphatase 1 (LPP1) is an integral membrane protein that catalyzes the hydrolysis of bioactive lipid phosphates (Figure 4B). LPP1 is one of three

LPP isoforms (LPP1-3) and encoded by the *Ppap2a* gene[106]. LPP1 is ubiquitously expressed, with considerable amounts of mRNA detected in the muscle and liver[107], but not much is known regarding tissue-specific regulation of LPP1 expression in health and disease. The phosphatase is transcriptionally induced by androgens[108] and estrogens[109] and by PPARγ in vascular endothelial cells[110], but is downregulated in adipocytes during differentiation[111]. Interestingly, streptozotocin-induced diabetes upregulates LPP1 expression in the livers of mice (GEO Profiles, ID: 105483051), but the implications of this transcriptional upregulation remain unknown.

LPP1 is a 300 amino acid long monomeric protein that contains six transmembrane α-helices (I-VI) linked by five hydrophilic loop regions, an extracellular glycosylation site (G) and three active site domains (C1-3) that are conserved across LPP isoforms[106,112] (Figure 5). These active site domains are located in the third and fifth extracellular loops and include the adjacent transmembrane regions[106]. The C1 domain functions in lipid substrate recognition, while the C2 and C3 domains contain key amino acids for catalysis[106]. Conserved histidine residues in C2 and C3 mediate the phosphotransferase reaction that ultimately yields a dephosphorylated lipid and free phosphate[106,112]. Unlike the functionally related group of lipid phosphatases lipins, LPP1 catalysis is insensitive to N-ethylmaleimide and does not require Mg^{2+}[113].

LPP1 dephosphorylates a number of bioactive lipid substrates including LPA, PA, S1P and C1P[113,114]. LPP1 shows a preference for glycerolipids over sphingolipids[107], with LPA being the primary LPP1 substrate. The K_m for the degradation of extracellular LPA has been estimated at 49-67μM in fibroblasts[115], which is higher than physiological serum concentrations of LPA (high nM to low μM)[114]. This indicates that LPP1 has the

capacity to increase its activity in proportion to circulating levels of LPA. LPP1 is a critical determinant of LPA levels both *in vitro* and *in vivo*. The half-life of circulating LPA in mice is roughly 3min, but mice lacking functional LPP1 have elevated levels of circulating LPA and delayed LPA clearance (half-life of 12min)[107]. However, mild overexpression of LPP1 in mice leads to abnormally small body size, lower birth weight, aberrant hair growth and impaired spermatogenesis, without reducing plasma LPA levels[116]. Thus, LPP1 expression regulates many physiological processes through means that are both dependent on, or independent of, LPP1 degradation of LPA. The enzymatic action of LPP1 differentially regulates signaling by LPA and other LPP1 substrates, depending on subcellular location of LPP1.

LPP1 monomers can form oligomers, but oligomerization is not required for activity, and may instead direct LPP1 to different subcellular locations[106]. LPP1 localizes to the PM, endoplasmic reticulum, and Golgi apparatus[112]. Membrane topology of LPP1 indicates that the active sites face either the extracellular side of the PM or the lumen of endomembrane compartments[106,112] (Figure 5). Enrichment of LPP1 in lipid rafts, supports a role for LPP1 in receptor-mediated signaling cascades[117]. The membrane localization of LPP1 places the phosphatase in a prime position to regulate the balance between phosphorylated and dephosphorylated bioactive lipids inside and outside of the cell.

1.2.4 Physiological role of lipid phosphate phosphatase 1

LPP1 regulates a variety of cellular processes through modulation of extracellular and intracellular signaling. LPP1 halts signaling of extracellular bioactive lipids (e.g. LPA) through their cognate GPCRs on the PM (Figure 5). This external activity of LPP1

blocks LPA- and S1P-induced activation of ERK[77], and decreases subsequent PLD-dependent PA generation[118] and migration[77] in fibroblasts. LPP1 also inhibits extracellular LPA-dependent rises in intracellular Ca^{2+}, NF-κB activation and IL-8 secretion from bronchial epithelial cells[119]. Platelets contain high levels of LPP1, which attenuates morphological changes and aggregation induced by exogenous LPA[120]. Thus, LPP1 functions as a critical brake on bioactive lipid signaling through cell surface receptors.

LPA hydrolysis by LPP1 forms monoacylglycerol, which itself may be biologically inert, but can be rephosphorylated to LPA once taken up into cells[114]. Similarly, sphingosine derived from LPP1 hydrolysis of S1P can reenter cells and be phosphorylated by SphKs. A similar LPP1-dependent reuptake mechanism has been observed with C1P. Since the products of LPP1 hydrolysis can be rephosphorylated after cell entry[114], LPP1 may also influence intracellular signaling.

LPP1 also controls signaling downstream of PM receptors (Figure 5). The actions of LPP1 on LPA-mediated ERK activation and subsequent proliferation and migration in mouse embryonic fibroblasts can also occur downstream of LPA receptor activation, as LPP1 still blocked fibroblast migration stimulated by a non-dephosphorylatable LPA receptor agonist[118]. Furthermore, increasing LPP1 activity in fibroblasts inhibited LPA-induced PLD activity and intracellular PA accumulation even in the presence of excess exogenous LPA[118]. Further evidence of LPP1 intracellular function arose from the observation that LPP1 activity regulates ERK activation downstream of thrombin, a growth factor that signals through PM GPCRs[77]. Increasing LPP1 expression also abates platelet derived growth factor-stimulated migration in mouse embryonic fibroblasts by

decreasing the ratio of intracellular PA:DAG and downregulating PKC[77]. The effects of LPP1 overexpression on relative PA and DAG levels were also seen in human embryonic kidney cells[121]. By modulating LPA inside the cell, LPP1 may dictate transcriptional activation of the intracellular LPA targets, such as the pro-inflammatory nuclear LPA1 receptor and PPARγ[106]. Intracellular LPA is also crucial for proper mitochondrial function. LPA is produced by mitochondrial glycerophosphate acyltransferase[122], but when mitochondrial LPA production is attenuated by ablation of this acyltransferase, mitochondria cannot fuse properly and instead fragment[123]. Whether LPP1 localizes to mitochondria to regulate LPA production and/or mitochondrial dynamics is not known (Figure 5). Therefore, LPP1 regulates critical physiological signaling pathways by manipulating levels of extracellular and intracellular bioactive lipids.

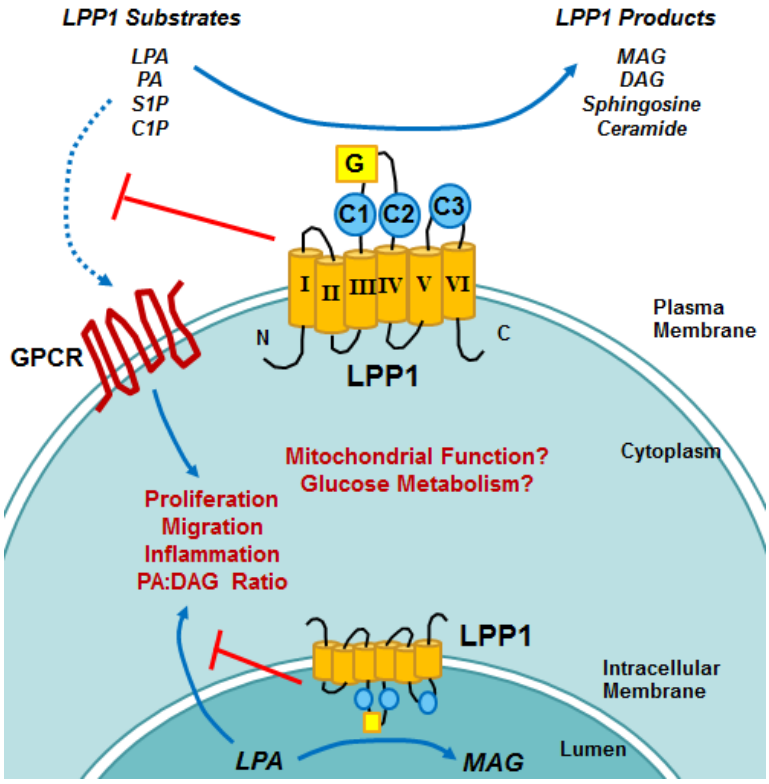

Figure 5. Structure and functions of LPP1.

LPP1 consists of six transmembrane α-helices (I-VI), a glycosylation site (G), and three conserved catalytic sites (C1-C3). LPP1 is positioned in the plasma membrane and internal membranes such that the active sites face either the extracellular space or lumen of intracellular compartments, respectively. Through dephosporylation, LPP1 blocks signaling and downstream biological processes initiated by extracellular and intracellular lipid substrates. Whether LPP1 is important for bioactive lipid control of mitochondrial function or glucose metabolism remains unknown. It is also important to note that products of LPP1 hydrolysis may reenter cells and stimulate intracellular signaling as well. This figure is based on Figure 7 from a previous paper cited here[106].

1.3 Mitochondrial function in glucose homeostasis

1.3.1 Mitochondrial function in skeletal muscle and liver glucose metabolism

Mitochondria provide most of the energy required to drive both glucose uptake and HGP. Mitochondria exhibit great metabolic flexibility, utilizing fatty acids or glucose to produce energy depending on the particular tissue and nutritional status[124] (Figure 6). Oxidation of glucose-derived pyruvate or fatty acids produces acetyl-CoA, which can enter the tricarboxylic acid (TCA) cycle. The TCA cycle produces the reducing equivalents NADH and $FADH_2$ which donate electrons to the electron transport chain (ETC) and fuel ATP synthesis via oxidative phosphorylation (OXPHOS)[124]. In addition, the TCA enzyme succinyl-CoA synthetase produces GTP, another critical high-energy phosphate molecule[125]. Production of these molecules is highly dependent on mitochondrial calcium levels, as many of the TCA cycle dehydrogenase enzymes and ETC complexes are activated by calcium[126,127]. However, accumulation of mitochondrial calcium can enhance production of ROS, such as superoxide ($O_2^{\cdot}$) from the ETC[127], mainly from Complexes I and III[128,129] (Figure 6). Mitochondria mitigate oxidative stress by upregulating antioxidant enzymes, including superoxide dismutase 2 (SOD2)[129]. SOD2 converts $O_2^{\cdot}$ to H_2O_2, which is broken down by catalase to H_2O and O_2. Mitochondrial ROS production in excess of the antioxidant capacity can damage proteins, lipids and DNA[127] and compromise generation of ATP and GTP[130,131]. The transcription factor Nrf2 is a central regulator of mitochondrial redox state, energy substrate utilization and OXPHOS[132,133]. In response to oxidative stress or increased energy demand, Nrf2 activates a transcriptional program that resolves mitochondrial ROS and stimulates fatty acid oxidation, TCA cycle flux and ATP production via OXPHOS[133]. Thus, mitochondria

must successfully integrate multiple signals in order to sustain muscle glucose uptake and HGP.

Skeletal muscle glucose uptake is an energetically costly process. Trafficking of GLUT4 in response to insulin consumes ATP and GTP[134] (Figure 6). Movement of GLUT4-containing vesicles along microtubules from perinuclear regions to the PM is mediated by the ATP-consuming molecular motor kinesin[16]. Once in close proximity to the PM, vesicles move towards exocytosis targeting sites by traversing a network of actin filaments, the organization of which requires ATP[134]. The GTPase TC10 requires GTP in order to facilitate assembly of the GLUT4 vesicle targeting sites on the PM, while RALA uses GTP to guide vesicles to these targeting sites[16]. Finally, N-ethylmaleimide sensitive factor consumes ATP when freeing vesicle constituent proteins from PM fusion proteins after exocytosis of GLUT4[135]. Given the importance of calcium for mitochondrial energy production, it is not surprising that insulin-stimulated glucose uptake in the muscle cells depends on mitochondrial calcium handling[136]. ROS are an inevitable byproduct of respiring mitochondria and seem to regulate glucose uptake in muscle as H_2O_2 produced by SOD2 can stimulate GLUT4-mediated glucose transport[137,138], but the mechanisms linking mitochondrial redox status to GLUT4 dynamics are not well understood. Thus, sustaining mitochondrial function is critical to support insulin-stimulated GLUT4-mediated glucose uptake in muscle.

Glucose production by the liver also requires a considerable amount of energy[51] (Figure 6). Gluconeogenesis is the main energy-consuming component of HGP. The initial step of gluconeogenesis from pyruvate, lactate and glucogenic amino acids is catalyzed by pyruvate carboxylase in the mitochondrion. Pyruvate carboxylase utilizes

ATP to convert pyruvate to oxaloacetate, which is next converted to phosphoenolpyruvate by the GTP-consuming cytosolic enzyme PEPCK. A few steps downstream, phosphoglycerate kinase catalyzes the ATP-dependent formation of the intermediate1,3-bisphosphoglycerate from 3-phosphoglycerate[51]. Relative to gluconeogenesis, the breakdown of glycogen does not expend much energy. Glycogen phosphorylase utilizes ATP in the phosphorylation of glycogen to form glucose-1-phosphate, which subsequently is converted to glucose-6-phosphate. During fasting, liver mitochondria provide energy for HGP mainly by oxidizing fatty acids. This is supported by studies showing that inhibition of fatty acid oxidation causes a dramatic drop in gluconeogenesis[139,140]. Glucagon stimulates mitochondrial calcium uptake[141], and this mitochondrial calcium is important in determining hepatic oxidative stress and gluconeogenic flux[142]. Recent work has elucidated a physiological signaling pathway between ROS and HGP[143]. The oxidative stress sensor Nrf2 is particularly important for liver mitochondria function and glucose metabolism. This is supported by the observation that Nrf2 regulates fatty acid oxidation[144], gluconeogenesis[145] and the hepatic response to ROS[146], but the relative importance of mitochondrial ROS in the regulation of HGP remains unclear.

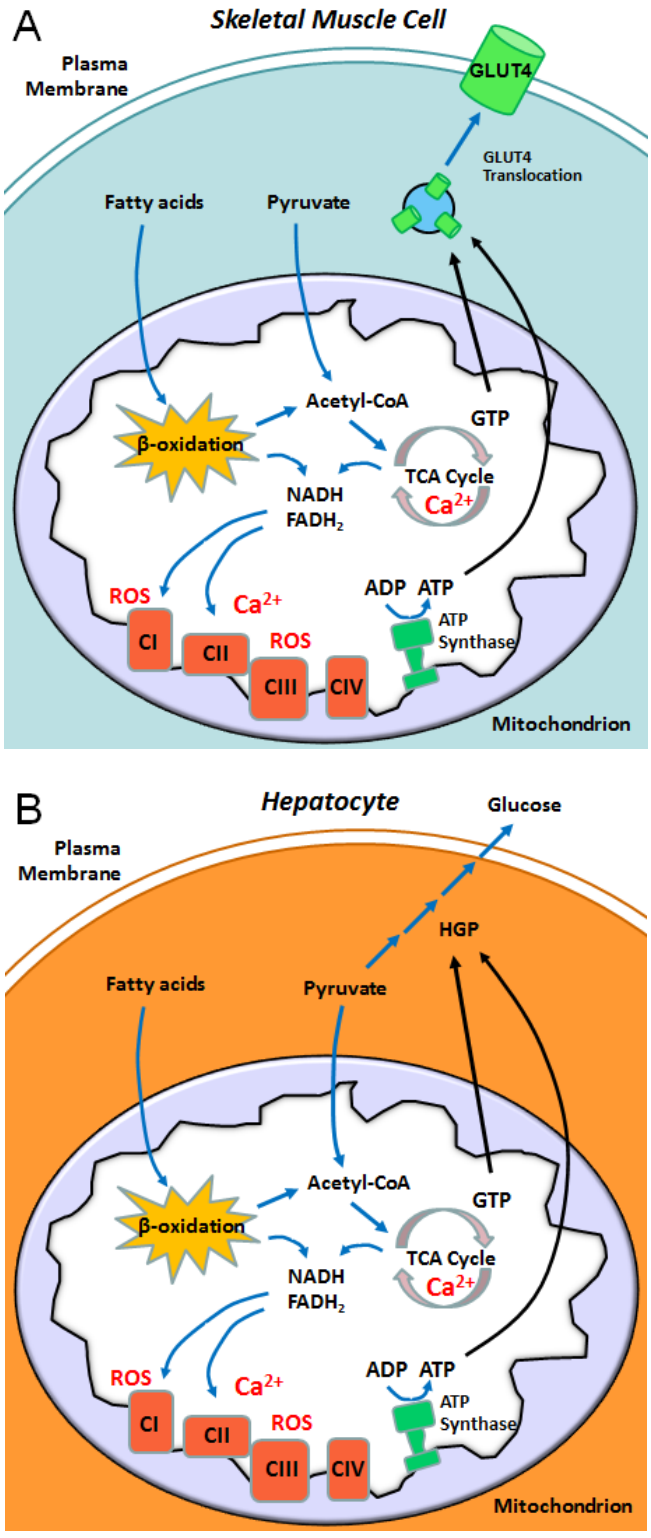

Figure 6. Mitochondrial function in skeletal muscle cell and hepatocyte glucose metabolism.

Mitochondria utilize fatty acids or pyruvate to generate acetyl-CoA, which feeds into the TCA cycle. Both the TCA cycle and β-oxidation yield the reducing equivalents NADH and $FADH_2$ which donate electrons to the ETC and drive ATP synthesis. Along with ATP, GTP formed by the TCA cycle fuels both GLUT4 trafficking in skeletal muscle (A) and HGP in hepatocytes (B). Mitochondrial calcium stimulates the TCA cycle and OXPHOS. ROS are normally produced during OXPHOS by Complexes I and III of the ETC. However, in excess, both mitochondrial calcium and ROS may hinder mitochondrial energy support of GLUT4 dynamics and HGP. This figure is based on a review cited here[124].

1.3.2 Mitochondrial dysfunction in skeletal muscle and liver insulin resistance

Mitochondrial dysfunction is closely associated with insulin resistance. Mitochondrial dysfunction is defined as an alteration in any of the numerous processes carried out by mitochondria, including ATP production via OXPHOS, synthesis and breakdown of metabolites, maintenance of morphology, calcium homeostasis and production and detoxification of ROS[147]. Perturbations in these mitochondrial functions, especially ROS and calcium homeostasis, are linked with insulin resistance in both skeletal muscle and liver[4,138,142,148].Given that mitochondria are critical for glucose uptake and HGP (Figure 6), it is not surprising that aberrant mitochondrial function can contribute to the impairment of insulin-stimulated carbohydrate metabolism in these tissues.

Mitochondrial dysfunction plays a significant role in skeletal muscle insulin resistance. Insulin-resistant subjects have decreased expression of mitochondrial respiratory chain subunits[149], lower oxidative enzyme activities[150], changes in mitochondrial content[151], altered mitochondrial morphology[150] and hindered mitochondrial OXPHOS capacity in conjunction with higher lipid content in muscle[152]. Similar decreases in skeletal muscle mitochondrial function have been observed in humans and rodents after acute lipid infusion[153] or short-term HFD[154], indicating that mitochondrial dysfunction may contribute to subsequent skeletal muscle insulin resistance. Nutrient oversupply stimulates excessive mitochondrial ROS production, which may antagonize mitochondrial function and lead to impairments in insulin action in muscle[155]. Treatment of cultured skeletal muscle cells with the ETC Complex III inhibitor antimycin A abolishes insulin-stimulated GLUT4 translocation to the PM in a

manner that is dependent upon mitochondrial $O_2^{\cdot}$ production[138]. As calcium levels are a critical determinant of mitochondrial ROS, it is not surprising that disruption of mitochondrial calcium uptake impairs insulin signaling and glucose uptake[156]. A hallmark of insulin resistant skeletal muscle is swollen, misshapen mitochondria[157,158], which can be due to imbalances in the mitochondrial fusion/fission cycle. Excessive mitochondrial fission increases mitochondrial oxidative stress, inhibits ATP production by OXPHOS and hampers insulin-stimulated glucose uptake in skeletal muscle cells[159]. Countering of this excessive mitochondrial fission improves insulin sensitivity, another case in which mitochondrial dysfunction may precede insulin resistance. Overall, multiple modes of mitochondrial dysfunction may contribute to the development of skeletal muscle insulin resistance.

Mitochondrial inefficiency is also associated with hepatic insulin resistance. Insulin resistant patients with non-alcoholic steatohepatitis and/or type 2 diabetes show impaired ETC enzyme activities[160] and ATP production[161,162] in the liver, altered fatty acid oxidation[160,163] and abnormalities in mitochondrial morphology[164]. Interestingly, mice with a primary defect in mitochondrial fatty acid oxidation develop hepatic insulin resistance concomitant with impaired insulin-mediated suppression of HGP[165]. Stimulation of fatty acid oxidation in the livers of high fat/high sucrose-fed mice alleviates insulin resistance and improves glucose tolerance[166], indicating that mitochondrial deficits in substrate oxidation were underlying insulin resistance in that particular model. As in muscle, insulin resistance in liver is also linked with increased mitochondrial ROS production[148]. Palmitate can induce insulin resistance in hepatocytes through the generation of mitochondrial ROS[167]. Moreover, insulin resistant mice

overexpressing SOD2 show improved hepatic insulin sensitivity and lower blood glucose levels[168]. Excessive accumulation of mitochondrial calcium may also hamper insulin action in liver. Experimental induction of mitochondria/endoplasmic reticulum contact in hepatocytes overloads mitochondria with calcium, depresses mitochondrial respiration, and leads to insulin resistance, as evidenced by decreased glucose disposal and increased HGP[142]. Taken together, mitochondrial dysfunction is an important factor in insulin resistance in both liver and skeletal muscle.

The exact role of mitochondrial dysfunction in insulin resistance remains a controversial issue. Several studies have provided evidence to counter the hypothesis that mitochondrial dysfunction is an intrinsic defect of insulin resistance and type 2 diabetes[169]. Patients with type 2 diabetes[170] or HFD-fed rodents[171] may not show any differences in skeletal muscle mitochondrial function. In some circumstances, insulin resistant skeletal muscle shows a compensatory increase in mitochondrial function[172]. Interestingly, mice lacking the insulin receptor in muscle have mitochondrial defects[173]. Moreover, type 2 diabetics showed comparable muscle ATP production rate to healthy controls when glucose and insulin were kept at the same low levels, but the diabetes patients failed to increase ATP production after increasing insulin[174]. This same phenomenon of reduced insulin-stimulated ATP production was observed in rats fed HFD[175], raising the possibility that mitochondrial dysfunction is downstream of impaired insulin action in muscle.

A similar debate rages on with respect to hepatic insulin resistance. Chronic HFD feeding is not always associated with deficits in liver mitochondria respiration[176]. Mice with diet-induced or hepatic insulin signaling deficiency-mediated insulin resistance do

not show any changes in expression or activities of liver respiratory chain complexes[177]. In fact, recent evidence has even suggested that pharmacological or genetic impairment in mitochondrial function may actually protect against hepatic insulin resistance by dampening ROS production and oxidative damage[178].Therefore, it is still unclear whether mitochondrial dysfunction is a cause or consequence of insulin resistance in muscle and liver[124].

1.4 Mitochondrial permeability transition pore

1.4.1 Characterization of the mitochondrial permeability transition pore

The mitochondrial permeability transition pore (mPTP) was first described in 1979 by Haworth and Hunter[179] as a non-specific pore in the inner mitochondrial membrane responsible for calcium-mediated swelling of mitochondria. Subsequent work showed that this non-specific pore had a diameter of roughly 2.3nm[180] and allowed passage of substrates less than 1.5kDa[181] between the mitochondrial matrix and cytoplasm of cells. These initial findings ignited an explosion of research focused on defining the pharmacology of this mitochondrial pore (Figure 7). Mitochondrial permeabilization mediated by the mPTP is activated by mitochondrial depolarization[182], uncoupling[183], free phosphate[179], palmitate[183], matrix calcium overload[184,185], the pro-oxidants phenylarsine oxide[186] and *t*-butylhydroperoxide[187] and ROS (e.g. $O_2^{\cdot}$) [179,188,189]. mPTP opening is inhibited by divalent cations (e.g. Mg^{2+})[183], low pH (<7.0)[190], negative (hyperpolarized) mitochondrial membrane potential[182], adenine nucleotides (ATP and ADP)[183,189], anti-oxidants[191] and the pharmacological agents cyclosporin A (CsA) and bongkrekic acid (BKA)[184]. Recent evidence has suggested that ubiquinone analogs may either activate or inhibit mPTP opening by modulating electron flow through ETC Complex I[179]. Thus, several physiological factors dictate the mitochondrial permeabilization phenomenon attributed to the mPTP.

Prolonged opening of the mPTP has several important consequences for cellular function (Figure 7). In response to activating cues, opening of the pore dissipates the proton gradient across the inner mitochondrial membrane[179,192]. This essentially depolarizes the mitochondrial membrane potential and uncouples proton influx from ATP

production via OXPHOS. Mitochondrial ATP production is halted and ATP synthase operates in reverse, consuming glycolysis-derived ATP in an effort to restore mitochondrial membrane potential. The resulting ATP depletion causes bioenergetic collapse. In addition, opening of the mPTP allows equilibration of all low molecular weight substrates, including ions and metabolites between the mitochondrial matrix and cytoplasm. Equilibration abolishes compartmentalization of metabolites and any ion gradients, as accumulated matrix calcium is released from mitochondria. Since larger proteins are retained within the matrix, free passage of small molecules across the inner membrane also causes mitochondrial swelling. Based on these observations, CsA-sensitive mitochondrial calcium release and mitochondrial swelling have both become reliable measures of mPTP activity[193]. Pressure exerted by the expanding matrix on the outer membrane eventually causes rupture of the outer membrane, which releases cytochrome c and other pro-apoptotic proteins. Eventually, either apoptotic or necrotic cell death ensues[179,192].

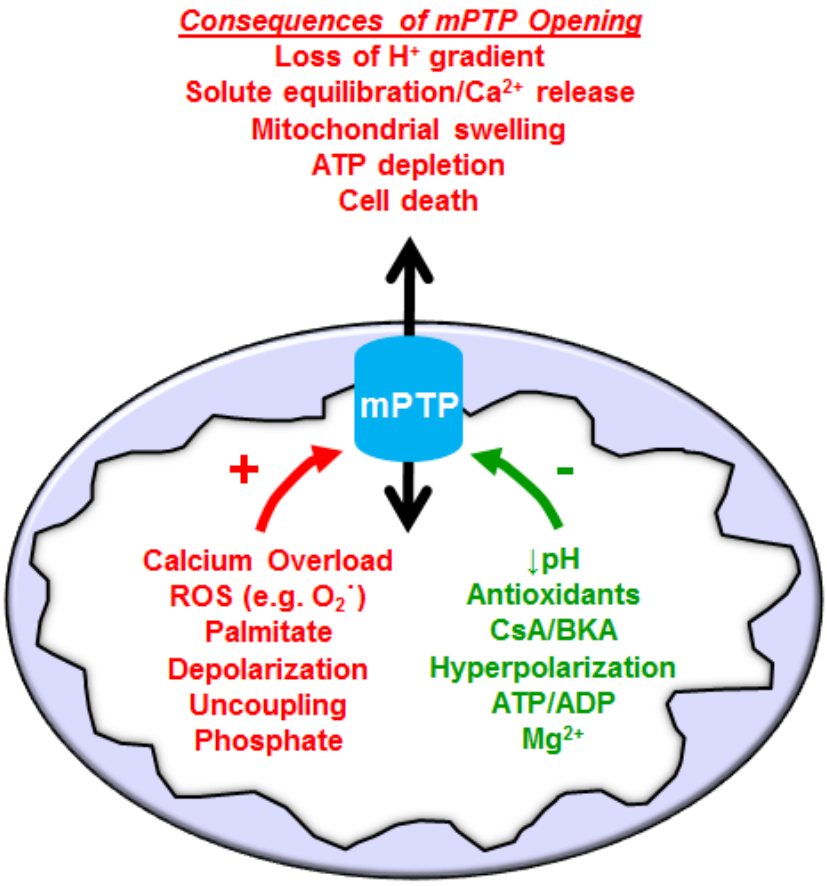

Figure 7. Molecular regulation and metabolic consequences of mPTP opening. Factors denoted in green reduce the probability of mPTP activation. Factors in red, especially mitochondrial calcium overload and high ROS levels, stimulate mPTP opening. Prolonged mPTP opening can ultimately result in ATP depletion, bioenergetic failure, and cell death.

Despite the advances in understanding the regulation and consequences of mPTP opening, the molecular structure of the mPTP has largely remained elusive. For a considerable amount of time, theoretical mPTP models consisted of a nebulous grouping of proteins with no solid evidence for the pore-forming component(s). In the late 1980s, Kottke[194], Beutner[195] and their respective colleagues found specialized regions where protein-protein interactions formed close appositions between the inner and outer mitochondrial membranes, and these regions contained CsA-sensitive channels displaying permeability characteristics of the mPTP. Further work done by Halestrap[188,196] and Beutner[195] formed the basis for a working mPTP model that spanned both mitochondrial membranes and included various combinations of the voltage-dependent anion channel (VDAC), the adenine nucleotide translocase (ANT), the mitochondrial phosphate carrier and the matrix protein cyclophilin D (CypD) as core constituents. In this model, CypD bound to ANT/mitochondrial phosphate carrier dimers in response to mitochondrial calcium overload and/or oxidative stress, inducing a conformational change in ANT that favored pore opening[179]. Binding of phosphate to the mitochondrial phosphate carrier enhanced CypD-induced conformational changes in the mPTP. Other groups added a number of peripheral regulatory factors including but not limited to pro- and anti-apoptotic members of the Bcl2 family[197], peripheral benzodiazepine receptor[198], Sirt3[199,200], STAT3[201], GSK3β[202], hexokinases[203] and connexin 43[204]. However, genetic ablation of many of these putative pore components such as VDAC[205] and ANT[206] suggested that these proteins were not necessary for mPTP function. CypD seemed to be the only verified regulator of mPTP opening, leaving the mPTP as more of a theoretical complex than a real biophysical structure.

CypD is a 22 kDa (207 amino acids) mitochondrial matrix peptidyl-prolyl *cis-trans* isomerase encoded by the *Ppif* gene[207]. CypD is one of 17 cyclophilins in humans, all of which have a similar secondary structure composition of eight β-strands, two α-helices and a 310 helix[208]. As a part of their protein structure, all cyclophilins share a conserved 109 amino acid cyclophilin domain that mediates isomerase activity[209]. The immunosuppressant CsA targets cyclophilins and inhibits their isomerase activity. The resulting CsA/cyclophilin complex inactivates the phosphatase calcineurin and inhibits inflammatory gene expression mediated by the transcription factor NFAT. Inhibition of CypD enzymatic activity by CsA or through genetic disruption of the catalytic domain has highlighted the importance of isomerase activity for the stimulatory actions of CypD on mPTP opening[210].

CypD is the mitochondrial isoform of the cyclophilin family and is localized to the mitochondrion by an N-terminal mitochondrial targeting sequence[207]. This sequence is cleaved before entry into mitochondria, yielding the mature 18kDa CypD isoform in the matrix[207]. CypD is expressed in a wide range of tissues, especially in insulin-sensitive tissues such as skeletal muscle and liver. Not much is known in terms of transcriptional regulation of CypD, but some evidence exists for translocation of CypD to mitochondrial membranes in the heart[211]. However, pharmacological inhibition and post-translational modifications are more validated modes of altering CypD function. Several groups have demonstrated that binding of CsA to CypD not only inhibits CypD activity but also attenuates mPTP opening. It is important to note that CsA does not completely abolish mPTP opening, but instead desensitizes the pore to calcium-induced opening[212]. CypD is also the target of endogenous modifications downstream of several metabolic signaling

pathways. GSK3β may phosphorylate CypD[213], but conclusive evidence that this CypD phosphorylation modulates mPTP opening is lacking. The mitochondrial deacetylase Sirt3 deacetylates CypD at Lys145 and 166, which can result in mPTP inhibition[199,200]. Finally, S-nitrosylation of Cys203 of CypD attenuates mPTP-induced mitochondrial swelling and ROS-mediated cell death, most likely by protecting this cysteine residue from oxidation[214]. CypD also binds to a number of proteins that are (or were) considered to be part of the mPTP, including ANT, VDAC, mitochondrial phosphate carrier and ATP synthase[207]. The CypD-ATP synthase interaction seemed to be the most fruitful and sparked the development of a new structural model of the mPTP.

Recent work pioneered by Giorgio and Bernardi[215,216] has provided compelling evidence for a novel, stripped-down structure of the mPTP that involves ATP synthase and CypD. CypD binds the lateral stalk of ATP synthase and partially inhibits the enzyme in a CsA-sensitive manner[215]. Subsequent studies narrowed the CypD binding site to the OSCP subunit of the ATP synthase stalk, and knockdown of OSCP increased the calcium threshold for mPTP opening[216]. Reconstitution of purified ATP synthase dimers into membrane bilayers produced a calcium-activated conductance reminiscent of the mPTP that was inhibited by Mg^{2+} and ADP, but not affected by CsA or the ANT inhibitor BKA. These findings established the basis of a new working mPTP model[212], in which dimers of ATP synthase constitute the pore while CypD binds to the OSCP subunit of ATP synthase in a calcium-dependent manner to induce pore opening (Figure 8). In healthy mitochondria, ATP synthase binds Mg^{2+}-ADP/ATP and functions normally in the absence of matrix calcium levels high enough to trigger pore opening. Binding of CypD in response to high matrix calcium or oxidative stress induces a conformational change in

the ATP synthase dimers that allows calcium to replace the inhibitory Mg^{2+} ions, which triggers mPTP opening. Solute exchange is hypothesized to occur at the junction of the two c rings (Figure 8). Despite convincing evidence for this updated mPTP model, a few questions arise. Although ATP synthase dimers are mostly located deep within cristae away from the mitochondrial outer membrane[217,218], the outer membrane exerts a sensitizing effect on the mPTP[198]. It is still not exactly clear how ATP synthase can revert from its normal ATP synthesizing activity to form a non-specific pore and how other potential regulatory components in the outer membrane may fit into this model. Thus, it is likely that ATP synthase dimers and CypD comprise the vital mPTP core, while other non-essential components such as VDAC and ANT can still regulate pore activity.

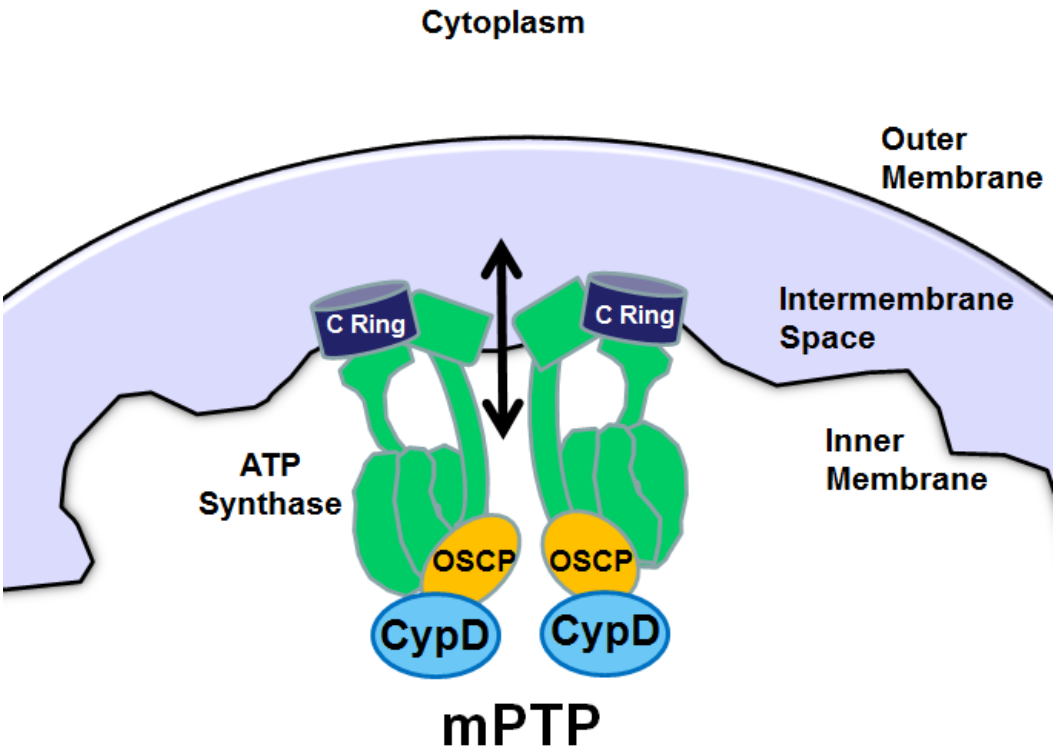

Figure 8. An updated model of mPTP structure.

Recent evidence has supported a new model of the mPTP consisting of ATP synthase dimers and CypD. In response to stimulatory cues as described in Figure 7, CypD can bind to the OSCP subunit of ATP synthase and induce a conformational change that favors establishment of a non-specific pore. Passage of solutes is hypothesized to occur at the apposition of the c rings of ATP synthase. This figure is based on Figure 1 from a recent review by Bernardi[212].

1.4.2 Physiological function

Despite a significant portion of research focused on structure and function of the mPTP, few studies have elucidated a physiological role for the pore. Observations that the mPTP can "flicker" in between open and closed states showing very rapid and brief opening[184] suggested that this molecular entity may also play a homeostatic role. Indeed, work by Altschuld et al.[219] showed that CsA blocked calcium efflux in cardiomyocytes, which was complemented by studies proposing a calcium-induced mitochondrial calcium release via low-conductance mPTP opening[220,221]. These results support a role for the mPTP as a mitochondrial calcium release valve. Interestingly, ablation of CypD increases mitochondrial matrix calcium, which activates calcium dependent dehydrogenases in the mitochondrion and promotes utilization of carbohydrates instead of fatty acids in the heart[222]. Loss of CypD may also accelerate bodyweight gain in mice in association with greater accumulation of adipose tissue[223], implicating CypD and the mPTP as regulators of energy substrate metabolism.

1.4.3 Pathophysiological role in metabolic diseases

Much of the work characterizing the mPTP has been done in the context of pathophysiology. Given the consequences of prolonged mPTP opening, it is not surprising that this event can contribute to cell death observed in many diseases. Genetic ablation of CypD improves cognitive function in a mouse model of Alzheimer's disease, due in part to attenuation of amyloid-beta protein- and oxidative stress-induced neuronal cell death[224]. Furthermore, pharmacological inhibition of the mPTP preserved dopaminergic neurons in a chemical toxin-induced model of Parkinson's Disease[225], suggesting that mPTP opening is a critical mediator of neurological disease.

Opening of the mPTP is a major mechanism underlying reperfusion-induced mitochondrial dysfunction and cardiomyocyte death during ischemia-reperfusion injury[226,227,228]. Ischemic conditions increase mitochondrial ROS and calcium and diminish ATP, all of which prime the mPTP for opening upon further increases in ROS and calcium during reperfusion[226]. mPTP opening during reperfusion is controlled by a GSK3β/hexokinase 2 (HK2) signaling axis. HK2 localization to mitochondria helps maintain ATP levels and suppresses pore opening[229], but GSK3β-mediated phosphorylation of VDAC releases HK2 from mitochondria, favoring mPTP activation[230]. Importantly, preventing mPTP opening with CsA and other inhibitors limits myocardial infarction and maintains cardiac function[228].

Interestingly, diabetic hearts show greater oxidation of ANT and increased sensitivity to mPTP opening[185]. This same study demonstrated that pharmacological blockade of the mPTP reduces reperfusion-induced cardiac infarct size[185]. A similar protective effect of mPTP inhibition was observed in the hearts of mice with streptozotocin-induced diabetes[231]. In a genetic model of diabetes, deletion of CypD preserves β-cell mass and improves insulin secretion and glucose tolerance in HFD-fed mice[232]. However, as mentioned in the previous section, one group showed that ablation of CypD may also result in obesity[223]. These results imply that mPTP opening is associated with metabolic diseases including diabetes, but its exact role in regulating insulin-stimulated energy substrate utilization remains unresolved.

CHAPTER 2: MATERIALS AND METHODS

2.1 Cell culture and reagents

Maintenance and differentiation of L6 rat skeletal muscle cells expressing HA-tagged GLUT4 was performed as described[13,138]. Differentiation of myoblasts into myotubes was induced by culturing cells in MEM-α containing 2% (v/v) horse serum and 1% (v/v) penicillin–streptomycin (pen/strep). L6 myotubes and primary hepatocytes were treated with specified drugs, hormones or lipids for the durations and concentrations noted in the figure legends.

Ferutinin, bongkrekic acid (BKA), cyclosporin A (CsA), antimycin A, C2-ceramide, dexamethasone, glucagon and bovine serum albumin (BSA) were purchased from Sigma Aldrich (St. Louis, MO). Free fatty acid-free BSA was purchased from ThermoFisher (Waltham, MA). Amplex Red was purchased from Invitrogen (Carlsbad, CA). Insulin was obtained from EMD Millipore (Billerica, MA). Lysophosphatidic acid (LPA) was obtained from Dr. Jill Slack-Davis (UVa Department of Microbiology, Immunology, and Cancer Biology). Palmitate, oleate and linoleate were obtained from Dr. Thurl Harris (UVa, Department of Pharmacology).

2.2 GLUT4 translocation assays

GLUT4 translocation assays were performed as previously described[138] in L6 myotubes treated with either 150μM palmitic acid conjugated to BSA or ethanol (control) in DMEM. Palmitate–BSA complexes were made by combining BSA (20% BSA stock) and palmitic acid (200mM palmitic acid stock) in DMEM while vortexing at low speed at 50 °C. The palmitate:BSA or ethanol:BSA (vehicle control) solutions were heated at 50 °C in a water bath for 20min, then cooled to 37 °C for 15min and diluted in DMEM to

the final concentrations indicated. The diluted solutions were sterile filtered through a 0.45μm PVDF membrane prior to treatment of myotubes.

2.3 Measurement of ATP content of cultured cells

ATP levels in antimycin A-treated L6 myotubes expressing HA-GLUT4 were determined following instructions provided by the manufacturer (Roche Applied Science).

2.4 Isolation and culture of primary mouse hepatocytes

Primary mouse hepatocytes from LPP1 KO and WT control mice were isolated by collagenase perfusion as previously described[233]. Briefly, the perfused liver was excised and immediately placed in ice-cold sterile 1x PBS. The liver was rinsed and placed into cold plating medium (DMEM supplemented with 25mM glucose, 10% FBS, 4mM L-glutamine, 1μM dexamethasone, 100nM insulin and 1% pen/strep). The liver lobes were gently scored with sterile fine-point forceps, and the liver was repeatedly shaken in the plating medium to release hepatocytes into the medium. The hepatocyte suspension was filtered through a 70μm cell strainer (Corning Life Sciences) into a 50mL tube and centrifuged at 50xg for 3min at 4° C. The supernatant was aspirated, and the cell pellet was resuspended in 10mL of cold plating medium and mixed with 10mL of 90% Percoll (Sigma) in sterile PBS. The resuspended cells in Percoll were centrifuged at 100xg 6min at 4° C, and the supernatant was aspirated. The cells were washed by resuspending in 20mL of cold plating medium and centrifuging at 50xg for 3min at 4° C. The supernatant was aspirated and the pellet was fully resuspended in 25-35mL of warm plating medium. Viable hepatocytes were counted by taking 50μL of resuspended cells and mixing with 50μL of Trypan blue. Viability was assessed by Trypan blue exclusion and was ≥ 90%

for each isolation. Primary hepatocytes were seeded in collagen-coated 6-or 12-well plates in plating medium at 1.5 x 10^5 cells/mL. Four hours after seeding, hepatocytes were washed 1x with PBS and switched to serum-free medium (DMEM with 5mM glucose, 0.2% BSA and 1% pen/strep) prior to HGP experiments. For RNA isolation, hepatocytes were incubated in either serum-free medium or serum-containing medium (DMEM with 5mM glucose, 10% fetal bovine serum and 1% pen/strep) prior to harvest.

2.5 Hepatic glucose production assays

Hepatic glucose production (HGP) assays were performed as previously described in primary mouse hepatocytes[234] with minor modifications. Primary hepatocytes were seeded in 12-well plates at 1.5 x 10^5 cells/well and cultured at 37 °C 5% CO_2 for 16hrs in serum-free medium. After serum starvation, hepatocytes were washed twice with sterile PBS, and incubated in 400μL/well of glucose production buffer (serum-, glucose-, and phenol red-free DMEM with 3.7 g/L sodium bicarbonate, 0.6% BSA, 10mM HEPES, 2mM sodium pyruvate, and 20mM lactic acid, pH 7.4) and incubated at 37 °C for 13hrs in the absence or presence of hormones and/or LPA. For experiments measuring HGP in the presence of LPA, cells were incubated with serum-free and glucose production buffer containing free-fatty acid-free BSA. Cells were immediately placed on ice, and the medium from each well was harvested and centrifuged at 700rpm for 5min. Glucose released into the medium was detected using an Amplex Red/Glucose Oxidase kit (Invitrogen) and quantified spectrophotometrically at 560nm with an Infinite M200 plate reader (Tecan). Glucose levels in the medium were normalized to total cellular protein content in each well.

2.6. Fatty acid treatment of primary hepatocytes

Primary hepatocytes were serum-starved for 13hrs and treated for 3hrs in presence of vehicle (BSA:ethanol) or a 1:2:1 mixture of palmitate:oleate:linoleate (POL) diluted in DMEM. To make the vehicle and POL media, free fatty acid-free BSA was diluted to a concentration of 1% in serum-free DMEM with 5mM glucose and 1% (v/v) pen/strep and divided into 50mL tubes. Concentrated POL stock was made by combining palmitate, oleate and linoleate stock solutions in a tube, drying down the mixture under N_2 gas and reconstituting the lipids in 95% ethanol. Ninety-five percent ethanol (final concentration: 0.5%) or POL stock (final concentrations: palmitate 125μM, oleate 250μM and linoleate 125μM) were added to media in 50mL tubes while vortexing at low speed. Media were incubated in a 50 °C water bath for 30min, then at 37 °C for 30min. Vehicle and POL media were sterilized through 0.45μm sterile filters and stored at -20 °C prior to addition to cells the next day.

2. 7 Real-time quantitative reverse transcription PCR (qRT-PCR)

Measurement of gene expression by qRT-PCR was performed as previously outlined[233]. Briefly, total RNA was isolated using Trizol and used for cDNA synthesis (2μg liver RNA or 1-2μg cell RNA) by two-step RT-PCR with the High Capacity cDNA synthesis kit (Roche). Levels of mRNA were semi-quantified with Sensifast SYBR Green mix (Bioline) and gene-specific primers (Integrated DNA Technologies) and were normalized to the housekeeping gene *Ppia* (CypA). For specific primer sequences, see Table 1.

Table 1. Mouse primer sequences used in qRT-PCR analyses.

Gene	Forward (5' to 3')	Reverse (5' to 3')
Acadm	GCAGGTTTCAAGATCGCAATG	TGAAACTCCTTGGTGCTCCACT
Cpt1a	TTGGGCCGGTTGCTGAT	GTCTCAGGGCTAGAGAACTTGGAA
G6Pase	CCGGATCTACCTTGCTGCTCACTT	TAGCAGGTAGAATCCAAGCGCGAAAC
Nfe2l2	AGGACATGGAGCAAGTTTGG	TTCTTTTTCCAGCGAGGAGA
Pck1	CCACAGCTGCTGCAGAACAC	GAAGGGTCGCATGGCAAA
Ppap2a	TCACGGAACTACTCAACCAATC	AGCAGGAAGTAATACGCATCC
Ppargc1a	CCCTGCCATTGTTAAGAC	TGCTGCTGTTCCTGTTTT
Ppia	CGATGACGAGCCCTTGG	TCTGCTGTCTTTGGAACTTTGTC
Socs3	GCTCCAAAAGCGAGTACCAGC	AGTAGAATCCGCTCTCCTGCAG

2.8 Western blotting

Following drug, hormone or lipid treatment, cells were washed twice with ice-cold PBS and lysed with HEPES–EDTA–Sucrose lysis buffer (250mM sucrose, 20mM HEPES pH 7.4, and 1mM EDTA) containing 2% SDS. Whole cell lysates were cleared of insoluble material by centrifugation[13]. Powdered quadriceps (20mg) and livers (15-30mg) were homogenized in 20x volumes (~400 - 600μL) of RIPA buffer [150mM NaCl, 10mM NP-40, 0.5% sodium deoxycholate, 0.1% SDS, 50mM Tris pH 7.5] containing protease inhibitors (Roche) and phosphatase inhibitors (2mM Na-orthovanadate, 1mM Na-pyrophosphate, 10mM Na-fluoride, 250nM microcystin LR). Muscles were homogenized with a Polytron (Brinkman Instruments, Westbury, NY) and livers were homogenized with a hand held homogenizer (Kimble-Chase). Homogenates were sonicated, rotated at 4 °C for 1hr and centrifuged at 16,000x g at 4 °C for 10min. Lysates were diluted in 4x Laemmli buffer and denatured at 65 °C for 5 min or heated at 37 °C for 7min in order to measure OXPHOS Complex proteins. Cellular proteins (20- 60μg) were resolved on 8-10% SDS-polyacrylamide gels or AnykD pre-cast gels (Bio-Rad Laboratories, Hercules, CA) and electro-transferred for 1.5hrs or overnight onto nitrocellulose membranes. Equal protein loading was confirmed by Ponceau staining. Protein expression was detected with the following antibodies: phospho-Akt S473, total Akt, phospho-GSK3β S9, total GSK3β, HK2, total pyruvate dehydrogenase (PDH), glyceraldehyde 3-phosphate dehydrogenase (GAPDH), phospho-FOXO1 S256, phospho-CREB S133 and voltage-dependent anion channel (VDAC) (Cell Signaling, Beverly, MA), phospho-insulin receptor (IR)/insulin-like growth factor 1 receptor (IGF1R) Y1158/Y1162/Y1163 (Millipore, Billerica, MA), CypD (Mitosciences, Eugene, OR),

MitoProfile Total OXPHOS Rodent WB Antibody Cocktail (abcam, Cambridge, United Kingdom), phospho-STAT3 Y705and STAT3 (BD Biosciences, San Jose, CA), PEPCK and 14-3-3 (Santa Cruz Biotechnology, Dallas, Texas), phospho-PDH S293 E1α (Novus Biologicals, Littleton, CO), GLUT4 R82 (generously provided by Dr. Thurl Harris, University of Virginia Department of Pharmacology), myosin heavy chain (MHC) I (BA-F8) and MHC IIa (sc-71) (generous gifts from Dr. Zhen Yan, University of Virginia Robert M. Berne Cardiovascular Research Center). Primary antibodies were detected using goat anti-mouse IgG (DyLight 800 conjugate) or goat anti-rabbit IgG (DyLight 680 conjugate) polyclonal secondary antibodies (Rockland, Limerick, PA). Membranes were visualized, and protein band intensities quantified, using the LI-COR ODYSSEY System and software (LI-COR, Lincoln, NE, USA).

2.9 Animals

Food and water were provided ad libitum until the date of study and all animal care was in compliance with NIH guidelines and the University of Virginia Animal Care and Use Committee. The high fat diet (45% kcal as fat) was purchased from Research Diets (D12451). Normal chow diet was purchased from Harlan Teklad (diet 7912). Animals were maintained on a 12/12 light/dark schedule at 68–72 °F and housed 4–5 per cage. The whole-body CypD KO mice were obtained from Dr. Jeffery Molkentin[210]. Briefly, a neomycin-resistance gene-containing vector targeting the *Ppif* gene (encoding CypD) was introduced into Sv129 embryonic stem cells. After homologous recombination, the targeting vector replaced the first three coding exons of the *Ppif* gene. The embryonic stem cells carrying the mutated *Ppif* gene were used to create chimaeric mice that were crossed with C57BL/6 mice to eventually obtain CypD KO mice[210]. The

CypD KO line was maintained by Molkentin and colleagues on a mixed C57BL/6 and 129 background. Whole-body CypD KO mice at UVa were maintained on an inbred C57BL/6 background, and offspring of heterozygous breeder pairs were used for experiments. Tissue-specific CypD KO mice were bred and maintained in conjunction with Dr. Zhen Yan and kept on a C57BL/6 background. Muscle-specific CypD KO (MKO) mice were generated by crossing mice with two floxed CypD alleles (CypD floxed, $CypD^{Fl/Fl}$) with mice expressing Cre recombinase driven by the muscle creatine kinase (MCK) promoter, resulting in loss of CypD in both skeletal muscle and heart. Liver-specific CypD KO (LKO) mice were generated by crossing $CypD^{Fl/Fl}$ mice with mice expressing Cre under control of the albumin promoter. The $CypD^{Fl/Fl}$ mice on a C57BL/6 background were purchased from Jackson Labs and had been generated by introducing loxP sites flanking exons 3-5 in the *Ppif* gene. For both MKO and LKO studies, the corresponding littermate $CypD^{Fl/Fl}$ control mice were referred to as "WT" in the data figures. Generation of LPP1 KO mice, which lack LPP1 expression in all tissues except the brain, has been previously described[107]. LPP1 KO mice were maintained on a C57BL/6 background. Mice for this study were obtained from Drs. Kevin Lynch and Jill Slack-Davis (University of Virginia, Departments of Pharmacology and Microbiology, Immunology, and Cancer Biology, respectively).

Glucose and insulin tolerance tests were performed on mice that were fasted for 5–6 h prior to intraperitoneal injection of glucose (1.5–2 g/kg) or insulin (1 U/kg). Pyruvate tolerance tests were performed on mice fasted overnight (~16hrs) prior to intraperitoneal injection of pyruvate (2g/kg). Blood glucose levels were monitored at indicated time points using an Accu-check II glucometer (Roche Diagnostics). Clearance

of the glucose analog [^{3}H]-2-deoxyglucose (2-DOG) into glucose-6-phosphate and [U-^{14}C]-glucose into glycogen was measured in quadriceps muscles as described previously[138,235].

2.10 Serum and tissue analyses

Serum insulin was determined by ELISA kit (Crystal Chem, Downers Grove, IL) or by ELISA with the assistance of Dr. Chien Li (University of Virginia, Department of Pharmacology). Briefly, a 96 well plate was coated overnight at 4 °C with a mouse monoclonal anti-insulin antibody (E86210M, at 0.9μg/mL) and blocked for 1hr at room temperature. Insulin standards and mouse serum samples (10μL) were added to the plate and incubated with a guinea pig anti-insulin antibody (Linco) for 1hr at room temperature on an orbital shaker, then at 4 °C overnight. Wells were incubated with a biotin-conjugated donkey anti-guinea pig IgG secondary antibody (1:10,000) at room temperature for 1-2hrs, followed by addition of streptavidin-horseradish peroxidase (1:10,000, Zymed) for 30-60min at room temperature. Wells were incubated with Ultra-TMB for 30min, before addition of stop solution (0.18N H_2SO_4) and spectrophotometric measurement at 450 and 590nm. Triglycerides (Pointe Scientific, Canton, MI) and non-esterified fatty acids (WAKO diagnostics, Osaka Japan) were measured from serum or liver tissue by colorimetric assay. Liver cholesterol was quantified by colorimetric assay (Infinity Cholesterol Liquid Reagent, Thermo Scientific), according to manufacturer's instructions. Transmission electron microscopy (TEM) was performed at the UVa EM facility using finely diced tibialis cranialis muscle fixed in 4% glutaraldehyde and 2.5% paraformaldehyde for 3 days prior to post- fixation in osmium tetroxide. TEM images were taken using a JEOL 1230. Mitochondrial length in the TEM images was calculated

with ImageJ using a standard size scale (600 pixels = 1μm). At least 170 intermyofibrillar and ≥90 subsarcolemmal mitochondria from 2 animals per genotype were quantified. Only mitochondria fully contained within the borders of the TEM images were included in the analysis.

2.11 Measurement of sphingolipids, glycerolipids and phospholipid derivatives

Powdered quadriceps muscles (15mg) and liver (~10mg) were weighed and homogenized in ice-cold PBS using a Polytron (Brinkman Instruments, Westbury, NY) or hand held homogenizer (Kimble-Chase). Primary hepatocytes were harvested in ice-cold PBS and sonicated. Protein concentrations were determined by BCA assay. Equal volumes of muscle, liver or hepatocyte homogenates or mouse serum were diluted and mixed in 1mL acidified methanol (0.1N HCl) containing internal standard cocktails for sphingolipids (containing 0.5nmol each: C17-ceramide, C12-glucosylceramide, C8-dihydroceramide, and C12-sphingomyelin) and glycerolipids (0.1nmol each of C15-diacylglycerol and C17-lysophosphatidic acid). The homogenate was divided into two 500μL aliquots for extraction of sphingolipids and glycerolipids/phospholipid derivatives.

To measure sphingolipids, 250μL of chloroform was added to the homogenate, and the homogenate was incubated overnight at 48 °C. After cooling to room temperature, 200μL of 0.1M KOH in methanol was added, and the samples were incubated at 37 °C for 2hrs. Lipids were neutralized with 17μL of glacial acetic acid and centrifuged at 5000 xg for 10min to pellet debris. One milliliter of chloroform and 2mL of millipure H_2O were added to the supernatant, vortexed, and centrifuged at 1500 xg for 15min to separate the organic and aqueous phases. The organic phase was dried under

nitrogen prior to resuspension in mobile phase solvent containing 97% acetonitrile, 2% methanol, and 1% formic acid (v/v/v) supplemented with 5mM ammonium formate. Samples were subjected to normal phase LC/MS/ MS using a using a triple quadrupole mass spectrometer (Applied Biosystems 4000 Q-Trap) coupled to a Shimadzu LC-20AD LC system equipped with a Supelcosil LC NH2 column (50cm x 2.1mm, 3μm) and a multiple reaction monitoring scheme for naturally occurring species of ceramide, glucosylceramide, and sphingomyelin. Data acquisition was performed as we have described[236], and quantification was carried out by measuring peak areas for each analyte using Analyst 1.5.1 software. Recovery was assessed using internal standards, and values were normalized to tissue weight and dilution.

To measure glycerolipids and phospholipid derivatives, 250μL of chloroform was added to 500μL homogenate, and the homogenate was incubated on ice for 60min. Chloroform (250μL) and 0.2M NaOH in H_2O (250μL) was added to the samples. The samples were vortexed, centrifuged for 5min at 1000 xg and the organic phase was extracted and dried under nitrogen. Dried lipids were resuspended in mobile phase solvent (69% methanol, 31% H_2O, 10mM ammonium acetate) for LC/MS/ MS with appropriate Reverse Phase chromatographic columns. Diacylglycerols (DAGs), phosphatidylcholines (PCs) and phosphatidylethanolamines (PEs) were analyzed in positive mode after separation in a Discovery (Supelco) C18 column (50mm x 2.1 mm, 5μm bead size). Mobile phase A consisted of 69% methanol, 31% H2O, 10mM ammonium acetate; and mobile phase B consisted of 1:1 ethanol:isopropanol (v/v) supplemented with 10mM ammonium acetate. The solvent gradient was as follows: 1min 100% solvent A, a linear gradient to reach 100% solvent B at 9min, 1min 100% solvent

B, 2min 100% solvent A. Total flow was 0.75mL/min. DAGs were analyzed by monitoring product ions generated by neutral loss of ammoniated acyl groups [RCOOH + NH_3] from DAGs ammonium adducts $[M + NH_4]^+$ as previously described[237]. PCs were analyzed by the production of the m/z 184 phosphocholine ion, whereas PEs were analyzed by monitoring the product ions obtained after the loss of a m/z 141.1 neutral fragment[238]. Phosphatidic acids (PAs), LPAs, and phosphatidylserines (PSs) were analyzed in negative mode after separation in a Nucleodur (Macherey Nagel) C8 column (125mm x 2mm, 5μm bead size). Mobile phase A consisted of 75% methanol, 25% H_2O, 0.1% formic acid, and 1mM ammonium acetate. Mobile phase B consisted of 80% methanol, 20% chloroform, 0.1% formic acid, and 1mM ammonium acetate. The solvent gradient was as follows: 1min 100% solvent A, 1min 65% solvent B, a linear gradient to reach 77% solvent B at 7min, 3min 100% solvent B, 2min 100% solvent A. Total flow was 0.33mL/min. LPAs were analyzed by the production of the m/z 153 glycerophosphate ion, PAs were analyzed by the production of an ion corresponding to the loss of an acyl chain (the most intense ion was used), and PSs were analyzed by monitoring the product ions obtained after the loss of a m/z 87.0 neutral fragment[239]. Optimal settings (DP, EP, CE, and CXP voltages; Ion Spray voltage, and gas flows) were obtained by infusion of selected authentic phospholipids. Quantification was carried out by measuring peak areas for each analyte using Analyst 1.5.1. Recovery was assessed using appropriate internal standards. LPAs, PAs, PCs, PEs, and PSs were normalized to C17-LPA, and DAGs were normalized to C15-DAG. Total values were normalized to tissue weight, dilution factor and protein concentration (for tissue and cell samples).

2.12 Measurements of oxidative damage

Thiobarbituric Acid Reactive Substances (TBARS) were quantified spectrophotometrically in quadriceps muscles using a kit (Cayman Chemical), according to the instructions provided by the manufacturer. Malondialdehyde (MDA)-modified proteins were assessed in quadriceps muscles via Western blotting with a rabbit polyclonal antibody against MDA (Academy Biomedical Company, Inc.). Protein carbonyls in gastrocnemius muscles were measured spectrophotometrically using a kit (Cayman Chemical), with minor modifications to the manufacturer's instructions. Briefly, powdered gastrocnemius muscles (~20-25mg) were homogenized (2 x 30sec bursts) in 20x volumes of buffer containing 50mM 2[N-morpholino]ethanesulfonic acid, 1mM EDTA, pH 6.7 at 4 °C, supplemented with fresh protease inhibitors. After centrifugation to remove insoluble material, a NanoDrop 2000c spectrophotometer (Thermo Scientific) was used to measure A280/A260 in order to estimate nucleic acid content in samples. To reduce contaminating nucleic acids, the supernatant was incubated with 0.1% (w/v) polyethyleneimine for 30min at 4 °C and centrifuged at 6000 xg 10min at 4° C. Protein carbonyls were detected in the supernatant at 370nm.

2.13 Calcium retention capacity

Isolated mitochondria were obtained from gastrocnemius muscles. Muscle tissues were placed in 5mL of ice-cold isolation buffer (in mM: 150 sucrose, 75 KCl, 50 Tris-base, 1 KH_2PO_4, 5 $MgCl_2$, 1 EGTA, 0.2% BSA, pH 7.4) with 5mg/mL of nagarse (Sigma P8038) for 1min. Tissue was homogenized using a polytron homogenizer. Isolation buffer (15mL) was further added and centrifuged at 700 xg for 10min at 4 °C. The supernatant was then centrifuged at 10,000 xg for 10min at 4 °C. The pellet obtained was

resuspended in 15mL of suspension buffer (in mM: 250 sucrose, 10 Tris-base, 0.1 EGTA, pH 7.4) and centrifuged at 8000 xg for 10min at 4 °C. The mitochondrial pellet was then resuspended in 50μL of suspension buffer. DC Protein Assay Kit (BioRad, USA) was used to measure protein concentration in the buffer. Mitochondria (15μg) were suspended into a total volume of 100μL using mitochondrial challenge buffer (in mM: 250 sucrose, 10 MOPS, 0.05 EGTA, 10 Pi-Tris, pH 7.4) with the addition of 50mM of Na-succinate (Sigma S2378) and 10μM rotenone (Sigma R8875). Calcium Green 5N (1μM; Invitrogen C3737) was added and fluorescence was measured using an excitation/emission wavelength of 506/532 nm, respectively, in a FLUOstar omega plate reader (BMG Labtech). Calcium chloride (83nmol/mg protein) was added at regular pulses as indicated.

2.14 Mitochondrial enzyme activity

Immunoblotting and measurements of enzyme activities of proteins involved in mitochondrial function and lipid metabolism were conducted as described previously[172,240,241], with minor modifications. Briefly, powdered quadriceps muscles (20-40 mg) from CypD KO and WT mice were homogenized in 50mM Tris-HCl, 1mM EDTA, 0.1% Triton X-100, pH 7.4, using a Polytron (Brinkman Instruments, Westbury, NY) and centrifuged at 7,000 rpm at 4°C for 10min. Protein content in homogenates was measured via BCA assay. Enzyme activities were assessed using a Spectra Max M5 plate reader (Molecular Devices). All assays were conducted in 96-well plates with a 300μL final reaction volume. Reactions were initiated by adding 50μL of initiator solution to wells containing 250μL of reaction buffer and muscle homogenate preincubated at 30°C for 5min. Enzyme activities were calculated based on linear absorbance change and were

normalized to protein content and dilution factor. Absorbance change from a control blank sample containing tissue homogenate was subtracted out of each assay. Conditions for individual enzyme assays were as follows:

Cytochrome C Oxidase assay. The reaction buffer was comprised of 100mM KH_2PO_4, pH 7.4. Prior to beginning assay, 0.6mM cytochrome C was prepared in reaction buffer. Sodium dithionite was added to cytochrome C until the mixture turned pink, and air was bubbled through the mixture for approximately 2min to remove excess dithionite. Wells were loaded with 10µL of homogenate and 240µL of reaction buffer. The reaction was initiated by addition of 50µL of cytochrome C. Absorbance change at 550nm was followed for 5min.

Citrate Synthase assay. The reaction buffer was 100mM Tris-HCl, 1mM $MgCl_2$, 1mM EDTA, pH 8.2. Acetyl-CoA (3.6mM) and a separate solution of 14mM oxaloacetic acid were prepared in reaction buffer. Prior to beginning assay, 1.0mM 5,5'-dithiobis(2-nitrobenzoic acid) was added to the reaction buffer. Wells were loaded with 10µL of homogenate, 25µL of acetyl-CoA and 215µL of reaction buffer containing DTNB. The reaction was initiated by addition of 50µL of oxaloacetic acid. Absorbance change was followed at 412nm for 5min.

β-hydroxyacyl-CoA Dehydrogenase (βHAD) assay. The reaction buffer was 50mM imidazole, 1.2mM EDTA, 0.3mM NADH, pH 7.4 prepared fresh on the day of the assay. Acetoacetyl-CoA (0.6mM) was prepared in reaction buffer fresh on the day of the assay.

Wells were loaded with 10µL of homogenate and 240µL of reaction buffer. The reaction was initiated with 50µL of acetoacetyl-CoA. Absorbance change was followed at 340nm for 5min.

Medium Chain Acyl-CoA Dehydrogenase (MCAD) assay. The reaction buffer was 100mM KH_2PO_4, 1mM EDTA, 0.5mM sodium tetrathionate, 200µM ferrocenium hexafluorophosphate, pH 7.2. Octanoyl-CoA (0.5mM) was prepared in 100mM KH_2PO_4, 1mM EDTA, pH 7.2. Wells were loaded with 30µL of homogenate and 220µL of reaction buffer. The assay was initiated with 50µL octanoyl-CoA. Absorbance change was followed at 300nm for 5min.

Phosphofructokinase assay. The reaction buffer was 50mM imidazole, 6mM $MgCl_2$, 60mM KCl, 5mM ATP, 0.4mM NADH, 8U/mL aldolase, and 2U/mL GAPDH/Triose, pH 7.4. Fructose-6-phosphate (30mM) was prepared in reaction buffer. Wells were loaded with 10µL of muscle homogenate, 240µL of reaction buffer, and the assay was initiated with 50µL fructose-6-phosphate. Absorbance change was followed at 340nm for 5min.

Acyl-CoA Oxidase assay. The reaction buffer was 25mM KH_2PO_4, 40mM aminotriazole, 0.08mg/mL horseradish peroxidase, 0.05mM Amplex Red, pH 7.4. Palmitoyl-CoA (0.3mM) was prepared in 25mM KH_2PO_4, pH 7.4. Wells were loaded with 40µL homogenate, 210µL reaction buffer, and the assay was initiated with 50µL palmitoyl-CoA. Absorbance change was followed at 571nm for 5min.

NADH Dehydrogenase assay. The reaction buffer was 25mM KH_2PO_4, 2.5mM KCN, 6.25mM $MgCl_2$, 2.5μM antimycin A, 0.6mM NADH, pH 7.0. Dicholoroindophenol (2.0mM) was prepared in 25mM KH_2PO_4, pH 7.0. Wells were loaded with 10μL homogenate, 240μL of reaction buffer, and the assay was initiated with 50μL dicholoroindophenol. Absorbance change was followed at 340nm for 5min.

Succinate Dehydrogenase assay. The reaction buffer was 50mM KH_2PO_4, 20mM succinic acid, 2.5mM KCN, 2.5μM antimycin A, 0.45mM phenazine methosulfate, pH 7.0. Prior to beginning the assay, 0.1mg/mL of 50mM KH_2PO_4 was prepared. Wells were loaded with 10μL homogenate, 240μL reaction buffer, and the assay was initiated with 50μL dicholoroindophenol. Absorbance change was followed at 600nm for 5min.

2.15 Mitochondrial respiration

Respiration was measured at 37° C in isolated quadriceps mitochondria with a Seahorse XF24 Analyzer, following the protocol outlined by Rogers et al.[242] with minor modifications. Pellets of isolated mitochondria from CypD KO and WT mice fed a HFD for 14 weeks were resuspended in 500μL of 1X Mitochondrial Assay Solution (MAS) containing 70mM sucrose, 220mM mannitol, 10mM KH_2PO_4, 5mM $MgCl_2$, 2mM HEPES, 1mM EGTA, and 0.2% (w/v) of fatty acid-free BSA (pH 7.2 at 37 °C), and protein concentrations were determined via BCA assay with 1X MAS as a blank. Substrates for respiration experiments were 10mM pyruvate and 2mM malate, which were made in MAS (MAS + substrate). Mitochondria were diluted in 1X MAS + substrate to 2.5μg/50μL, and 2.5μg of mitochondria or 50μL of 1X MAS + substrate

(blank controls) were added to wells of a Seahorse XF24 Cell Culture Microplate. Mitochondria were adhered to the culture plate by centrifuging at 2000 xg 20min at 4 °C, and compounds to be injected were diluted in 1X MAS + substrate.

To the adhered mitochondria, 450µL/well of ice cold 1X MAS + substrate was added, and the mitochondria were warmed in a CO_2-free incubator for 20min at 37 °C before measuring respiration. Coupled respiration by mitochondria was measured in the presence of substrate following sequential additions of ADP (5mM final concentration), oligomycin (5µM final concentration), FCCP (7µM final concentration) and antimycin A (4µM final concentration). Basal respiration, State 3, State 4_o, and maximal respiration were measured, allowing for the calculation of respiratory control ratios (RCR) determined by State 3/State 4_o.

2.16 Blue native-PAGE

Blue Native-PAGE was conducted according to the protocol described by[243,244] with minor modifications. Briefly, mitochondria were isolated from quadriceps, manually homogenized with a spatula, and solubilized in 50mM NaCl, 50mM Imidazole/HCl, 2mM 6-aminohexanoic acid, 1mM EDTA (pH 7 at 4 °C) with digitonin (6g digitonin/g protein). Coomassie blue G-250 (8g detergent/g dye) was added to solubilized mitochondrial proteins. Equal amounts of Coomassie-labeled mitochondrial proteins (100µg) were separated on non-denaturing 4-15% polyacrylamide gradient gels (BioRad Mini-PROTEAN TGX) alongside a standard cocktail of native proteins of known size (NativeMARK Unstained Protein Standard, Life Technologies) at 4 °C at 100V for 15min, then 15mA (102V) for 25min. After replacing cathode buffers, native gels were run at 15mA at 4 °C for an additional 100min. Blue native gels were fixed in 10% acetic

acid/50% methanol on a rocker at room temperature for 30min and stained in 0.05% (w/v) Coomassie blue G-250 in 10% acetic acid/40% methanol for 1hr. Gels were then destained in 10% acetic acid/40% methanol for 30min, and further destained in 5% acetic acid/20% methanol overnight on a rocker at room temperature. The intensity of bands in the gel representing individual ETC/OXPHOS complexes or supramolecular assemblies was visualized with a Fuji Film LAS-4000 and quantified with ImageJ. ETC complex content was normalized to Complex V.

2.17 Statistics

Data were expressed as means ± standard error of the mean (SEM) of at least 3 independent experiments or animals per group. p-values were calculated by two-tailed, unpaired t-test, one-way ANOVA with either Fisher's PLSD or Tukey's post-hoc test or two-way ANOVA with Sidak's post-hoc test. Statistical significance was set at $p < 0.05$.

CHAPTER 3: OPENING OF THE MITOCHONDRIAL PERMEABILITY TRANSITION PORE LINKS MITOCHONDRIAL DYSFUNCTION TO INSULIN RESISTANCE IN SKELETAL MUSCLE

3.1 Introduction

Skeletal muscle tissue has an important role in whole body glucose homeostasis by increasing glucose clearance from the blood in response to insulin. Therefore, insulin resistance in skeletal muscle is a contributing factor to glucose intolerance and type 2 diabetes. Risk factors for skeletal muscle insulin resistance include aging and obesity; however, the molecular mechanisms are unclear. Current evidence links aging and obesity to insulin resistance in skeletal muscle via correlations with mitochondrial dysfunction, aberrant lipid accumulation, and oxidative stress[138,245,246,247,248,249]. For example, physiological studies in both humans and rodents demonstrate that acute lipid infusion or chronic consumption of a high fat diet (HFD) is sufficient to promote skeletal muscle insulin resistance concomitant with lipid accumulation in muscle and/or mitochondrial dysfunction[158,250,251,252]. Furthermore, skeletal muscle of young insulin resistant pre-diabetic patients that are non-obese also demonstrates mitochondrial dysfunction and aberrant lipid accumulation[152]. These data led the authors to speculate that mitochondrial inefficiency may promote lipotoxic lipid accumulation to drive skeletal muscle insulin resistance. Together, these studies and others[169] have identified an association between mitochondrial dysfunction and insulin resistance, but cause–effect relationships remain to be proven[169]. Further work is required to determine the molecular mechanisms linking skeletal muscle mitochondria to insulin sensitivity.

We have previously demonstrated that acute induction of mitochondrial superoxide ($O_2^{\cdot}$) in skeletal muscle myotubes with the mitochondrial electron transport chain (ETC) inhibitor antimycin A was sufficient to cause insulin resistance[138]. This mechanism of insulin resistance was prevented by overexpression of mitochondrial

manganese SOD (SOD2), treatment with mitochondrial $O_2^{\cdot}$ scavengers, and inhibition of the ETC with stigmatellin at a site upstream of antimycin A. Collectively, this experiment demonstrated that mitochondrial $O_2^{\cdot}$, but not altered ATP production, is sufficient to drive insulin resistance in skeletal muscle. However, it also revealed a gap in knowledge concerning the mechanism whereby membrane impermeable mitochondrial $O_2^{\cdot}$ triggers insulin resistance, a process that occurs in the cytoplasm and at the plasma membrane (PM)[253,254]. To explore this mechanism we investigated a role for the mitochondrial permeability transition pore (mPTP). The mPTP has been classically described as a multi-protein complex that spans both mitochondrial membranes and allows the passage of molecules less than 1500Da between the cytoplasm and mitochondrial matrix. Importantly, the mPTP is triggered to open by mitochondrial $O_2^{\cdot}$ and other factors linked to insulin resistance including mitochondrial calcium overload, [188,189,255,256]. Under normal physiological conditions, transient opening of the mPTP releases ions and metabolites from the mitochondrial matrix in order to maintain proper homeostasis[179,188,189,207,257]. To investigate whether opening of the mPTP is required for insulin resistance, we targeted the mitochondrial matrix peptidyl-prolyl *cis-trans* isomerase cyclophilin D (CypD). CypD regulates mPTP opening by directly binding to pore constituent proteins, and inhibition of CypD decreases the probability of mPTP opening[179,207,256]. Based on these data, we investigated whether the genetic or pharmacological inhibition of CypD would protect from insulin resistance.

3.2 Results

3.2.1 CypD KO mice are resistant to diet-induced glucose intolerance and demonstrate improved skeletal muscle glucose uptake.

To test the role of the mPTP in diet-induced insulin resistance, we fed whole-body CypD knockout (KO) mice and wild type (WT) littermate controls a low fat chow diet (LFD) or HFD for a period of up to 11 weeks. Glucose tolerance tests (GTTs) were performed at weeks 1, 4, and 11 of HFD feeding. As shown in Figure 9A-D, WT mice had time-dependent impairment in glucose clearance when challenged with an intraperitoneal bolus of glucose, whereas CypD KO mice were largely protected from glucose intolerance. The improved glucose tolerance was not due to differences in adiposity (Figure 9E), body weight (Figure 9F and Figure 10), or food intake (2.98 ± 0.10 and 2.88 ± 0.06 g/mouse/night for WT and CypD KO, respectively). Also, serum insulin, free fatty acid (FFA), and triglyceride levels were not statistically different between genotypes in either the fed or fasted states (Figure 9G-I). Therefore, these parameters were not underlying the improved glucose clearance observed in the CypD KO mice.

To determine the tissue type(s) that accounted for the increased glucose clearance, CypD KO and WT control mice fed a HFD for 11 weeks were administered a glucose bolus containing [U-^{14}C]-glucose and [^{3}H]-2-deoxyglucose (2-DOG) (Figure 11). The clearance of [^{3}H]-2-DOG from the circulation was significantly higher in the CypD KO mice compared to WT controls (Figure 11A-B). Analysis of tissue [^{3}H]-2-DOG–phosphate identified a 1.75-fold increase in glucose uptake in CypD KO quadriceps muscle (Figure 11C, $p < 0.01$) compared to WT controls, with a trend towards reduced glucose uptake in adipose tissue (Figure 11D, $p = 0.12$). Skeletal muscle tissue of CypD

KO mice also utilized more glucose for glycogen storage compared to WT controls, as determined by a 2.1-fold increase in the incorporation of [U-^{14}C]-glucose into glycogen (Figure 11E, $p < 0.05$). In contrast, hepatic glycogen synthesis was not significantly different between CypD KO and WT mice, although CypD KO mice showed a trend towards reduced liver glycogen (Figure 11F, $p = 0.24$). These data suggest that skeletal muscle may play an important role in whole body glucose clearance in CypD KO mice.

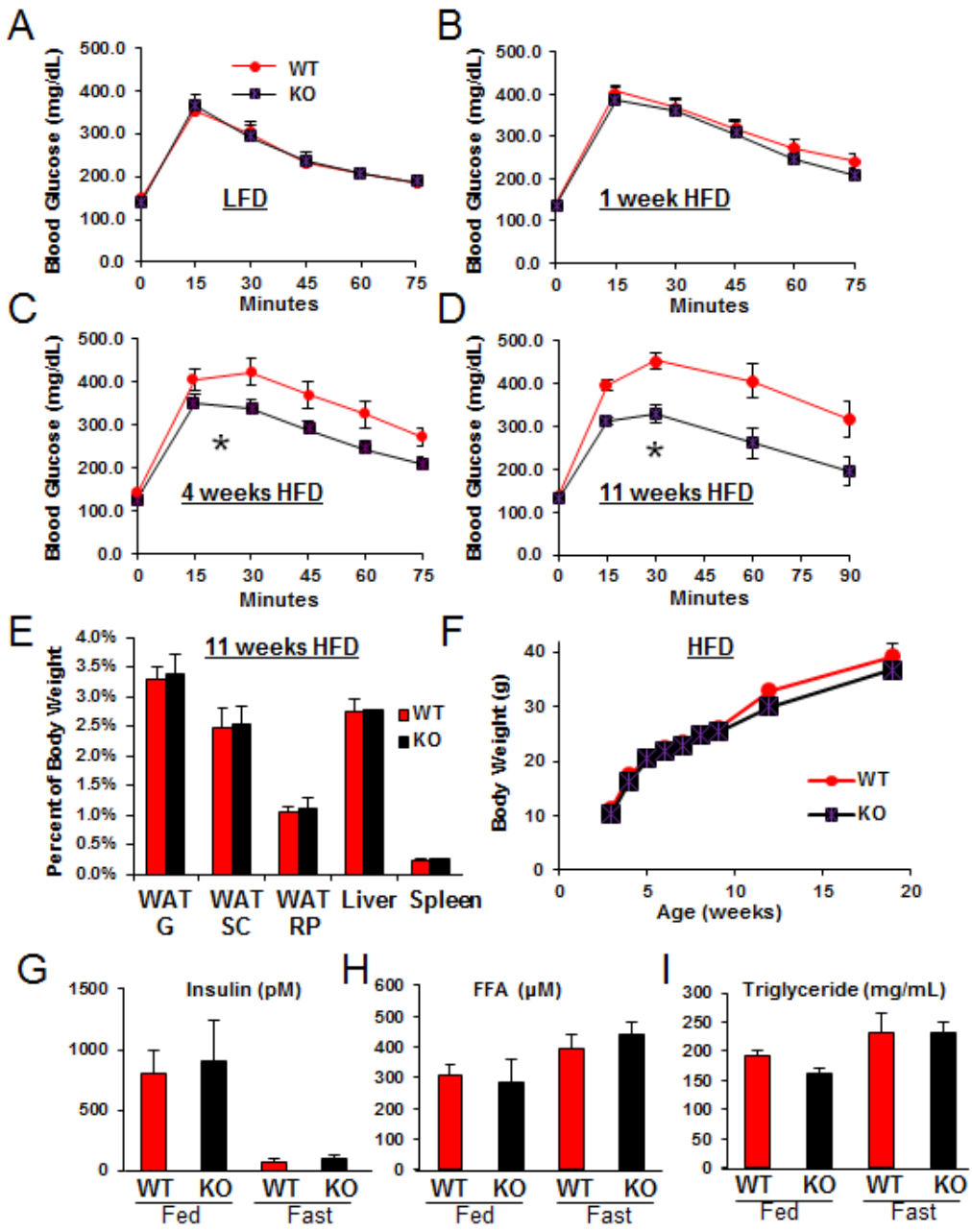

Figure 9. CypD KO mice are protected from HFD-induced glucose intolerance.

(A-D) CypD knockout (KO) mice and wild type (WT) control littermates were fed a LFD until 8 weeks of age when they were switched to a 45% high fat diet (HFD) for up to 11 weeks. Glucose tolerance was tested at weeks 0 (LFD), 1, 4, and 11 of HFD (2 g/kg glucose in (A) and 1.5 g/kg in (B-D)); * represents a significant difference in integrated

AUC ($p < 0.05$). (E-F) Gonadal (G), subcutaneous (SC), and retroperitoneal (RP) white adipose tissue (WAT) mass, liver mass, and total body mass were not statistically different between genotypes when fed a HFD diet for up to 11 weeks. Circulating insulin (G), free fatty acid (FFA) (H), and triglyceride (I) levels were similar between genotypes in either the fed or fasted states. Data are presented as means ± standard error of the mean (SEM). n = 8-16 for A-F and n = 4-7 for G-I.

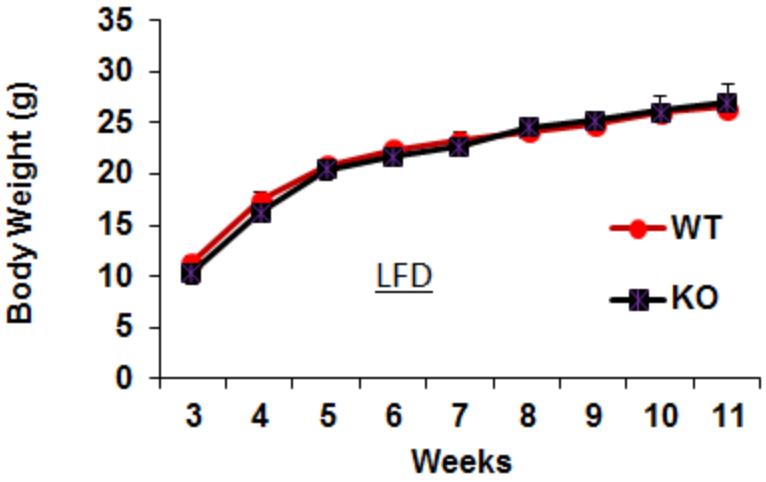

Figure 10. Body weights of CypD KO and WT littermate control mice fed a LFD. Body weights of mice fed a LFD for 11 weeks. Body weights were measured weekly for mice housed 3-5 per cage and did not differ between genotypes. Results are displayed as means ± SEM. n = 8-16 per genotype.

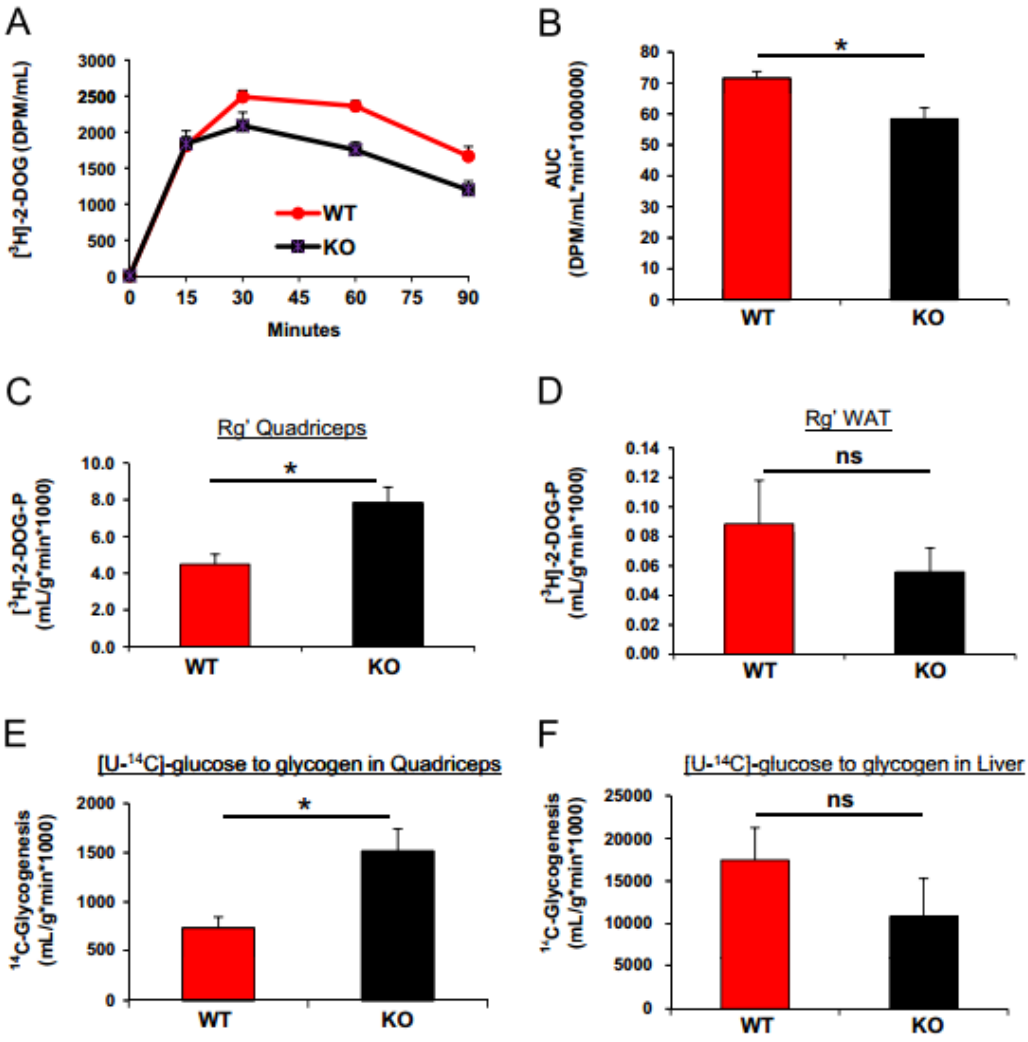

Figure 11. Improved skeletal muscle glucose clearance in CypD KO mice fed HFD for 11 weeks.

(A) [^{3}H]-2-DOG tracer appearance and disappearance curves for each genotype. (B) The calculated AUC for each genotype. (C-D) The estimated rate of glucose transport (Rg') into quadriceps muscle and gonadal WAT as determined by phosphorylated-[^{3}H]-2-DOG normalized to tracer availability over time and tissue mass. (E-F) [U-^{14}C]-glucose storage as glycogen in quadriceps muscle and liver. Data are represented as means ± SEM. n = 9 WT and 8 KO. *$p < 0.05$. ns, not significant.

3.2.2 Enhanced skeletal muscle glucose utilization in CypD KO mice is independent of insulin signaling and lipid accumulation.

To further investigate the mechanism underlying improved glucose tolerance (increased glucose uptake and storage) in skeletal muscle from CypD KO mice, we evaluated the expression of proteins that regulate insulin signaling and glucose metabolism in muscles from mice harvested 90min after administration of radioactive glucose analogs. After 11 weeks of HFD, the phosphorylation of Akt (S473) and GSK3β (S9), and the expression of GLUT4 and hexokinase 2 (HK2) were not altered in skeletal muscles from CypD KO mice compared with WT mice (Figure 12A-D and Figure 13).

Lipid accumulation in skeletal muscles can lead to lipotoxicity and is associated with insulin resistance. We therefore measured lipid accumulation in skeletal muscle from HFD-fed mice injected with glucose. Mice were harvested 90 minutes after glucose injection (1.5 g/kg), as this time point correlates with the period during which we observe the improved glucose uptake and metabolism (Figure 11). However, there were no observable differences in the accumulation of sphingolipids, including ceramides (Figure 14), phosphatidic acid (PA) or diacylglycerol (DAG) species (Figure 15), or phospholipid derivatives (Figure 16) in skeletal muscle from CypD KO and WT mice. In sum, these data indicate that the mechanism whereby CypD ablation protects from diet-induced glucose intolerance is likely downstream or independent of metabolic enzyme expression, signal transduction defects and lipotoxicity.

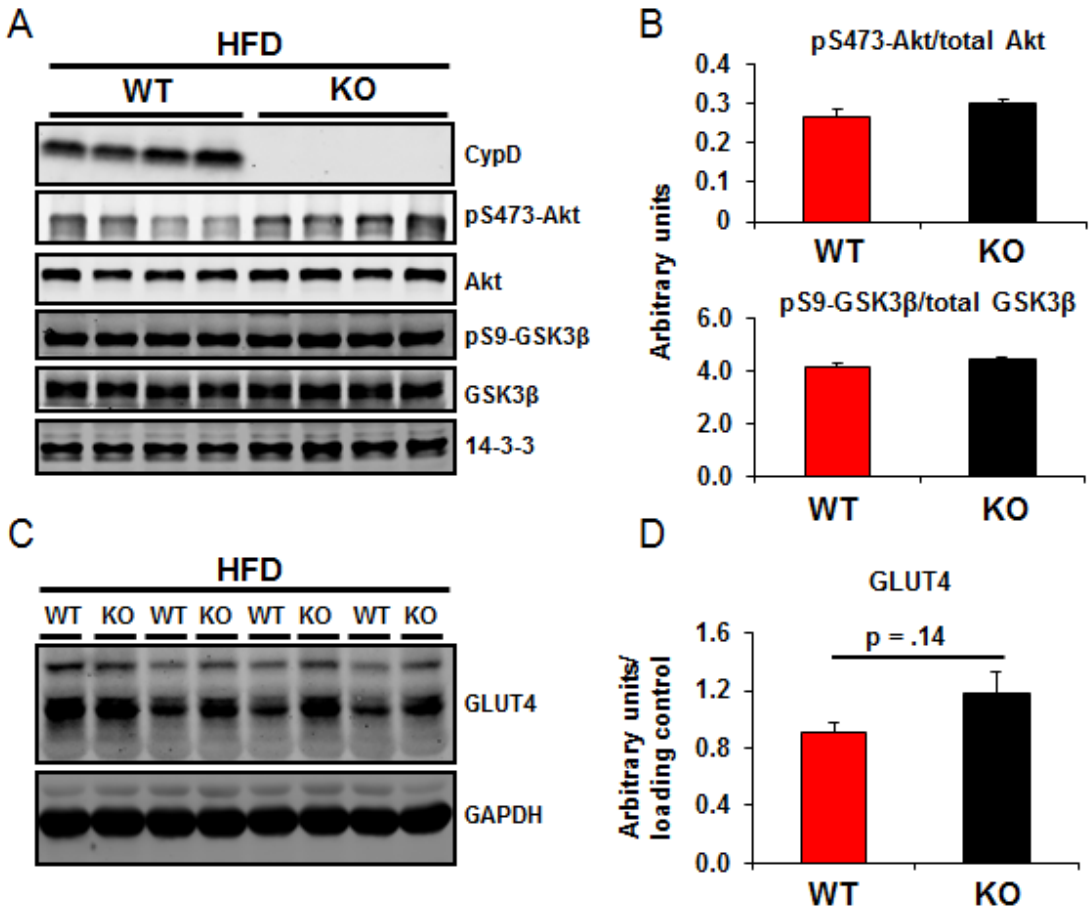

Figure 12. Insulin signaling and GLUT4 protein expression in skeletal muscle from mice fed a HFD for 11 weeks.

(A) Western blots for CypD, phospho-S473 Akt, total Akt, phospho-S9 GSK3β and total GSK3β in mixed quadriceps muscles. Expression of 14-3-3 was used as a loading control. (B) Quantification of phospho/total Akt and phospho/total GSK3β immunoblots. (C) Western blot of GLUT4 protein expression in quadriceps muscle. GAPDH served as a loading control. (D) Quantification of normalized GLUT4 expression. Results are displayed as means ± SEM. $n \geq 3$.

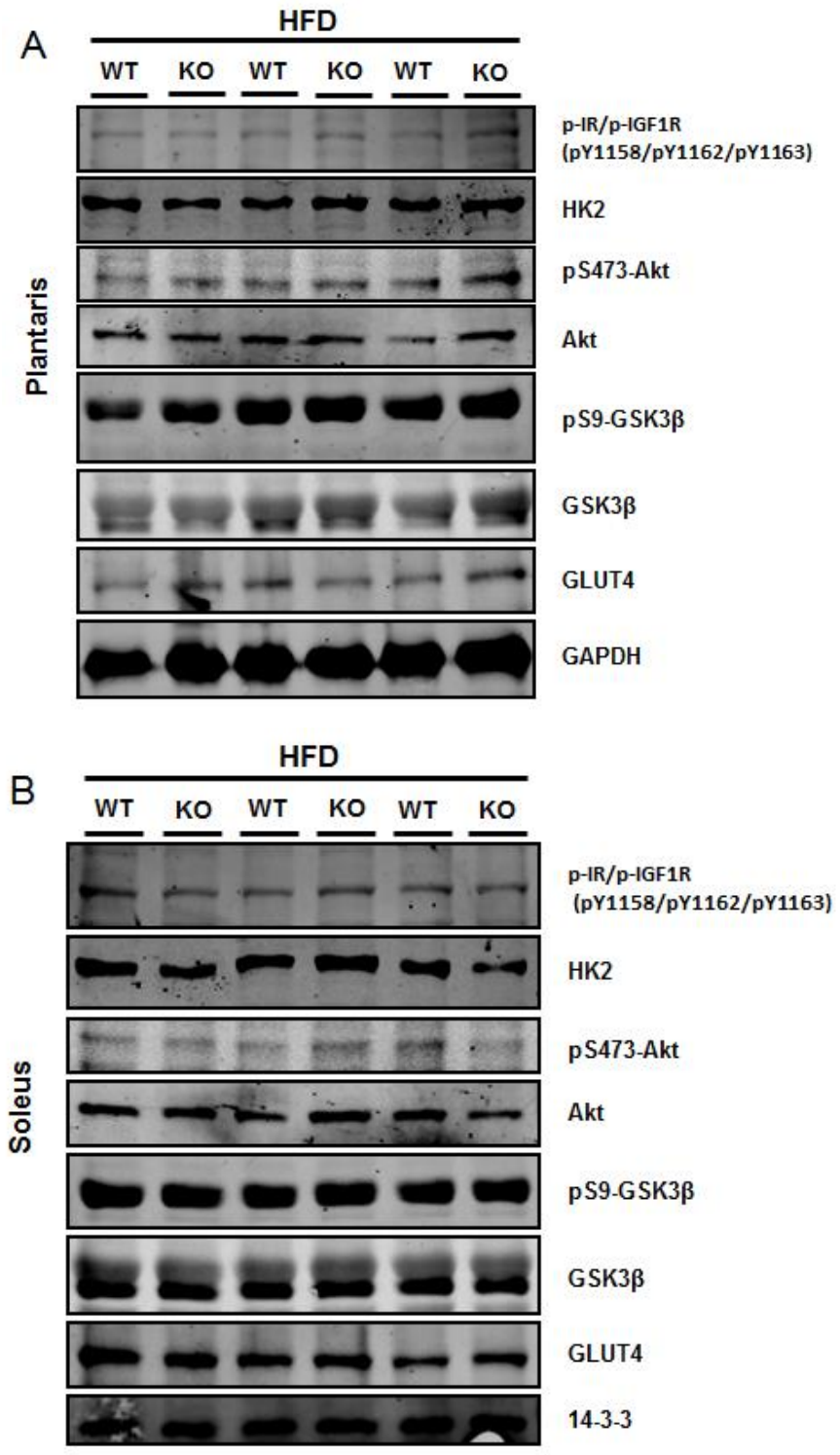

Figure 13. Insulin signaling in oxidative and mixed fiber muscles from WT and CypD KO mice fed a HFD for 14 weeks.

Representative Western blots of proteins involved in glucose metabolism and insulin signaling to GLUT4 in (A) plantaris and (B) soleus muscles. GAPDH and 14-3-3 were used as loading controls for plantaris and soleus blots, respectively. n = 3 per genotype.

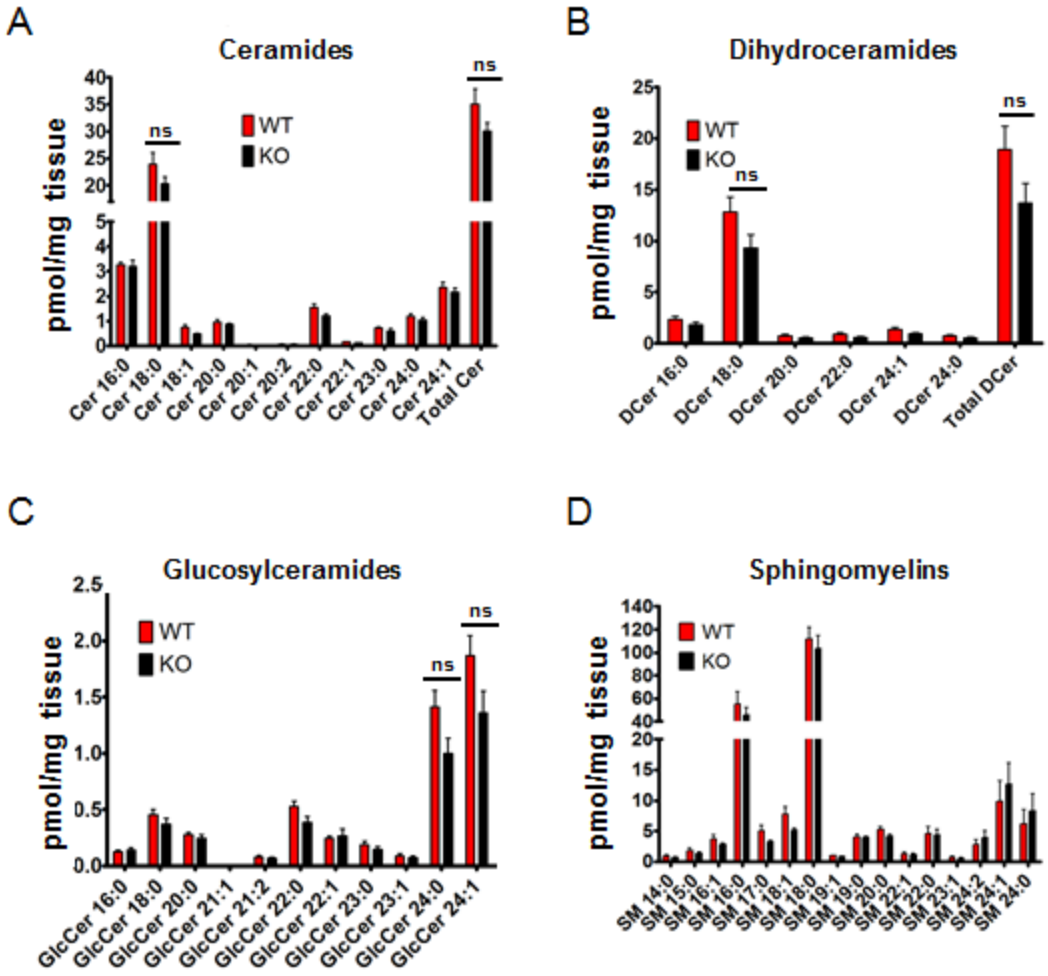

Figure 14. Sphingolipid analysis of muscle from WT and CypD KO mice fed HFD for 11 weeks.

No significant differences were observed in quadriceps (A) ceramide, (B) dihydroceramide, (C) glucosylceramide, or (D) sphingomyelin species. ns, not significant. n = 4 WT, 5 KO.

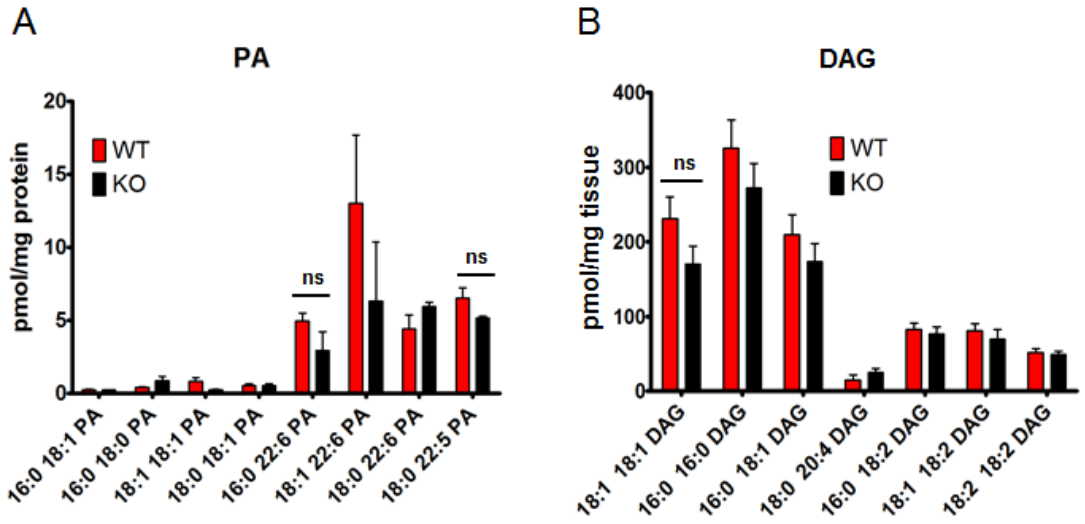

Figure 15. Skeletal muscle glycerolipids from CypD KO and WT control mice on HFD.

(A) Phosphatidic acid (PA) and (B) diacylglycerol (DAG) species in quadriceps muscle. ns, not significant. n = 4 WT, 5 KO.

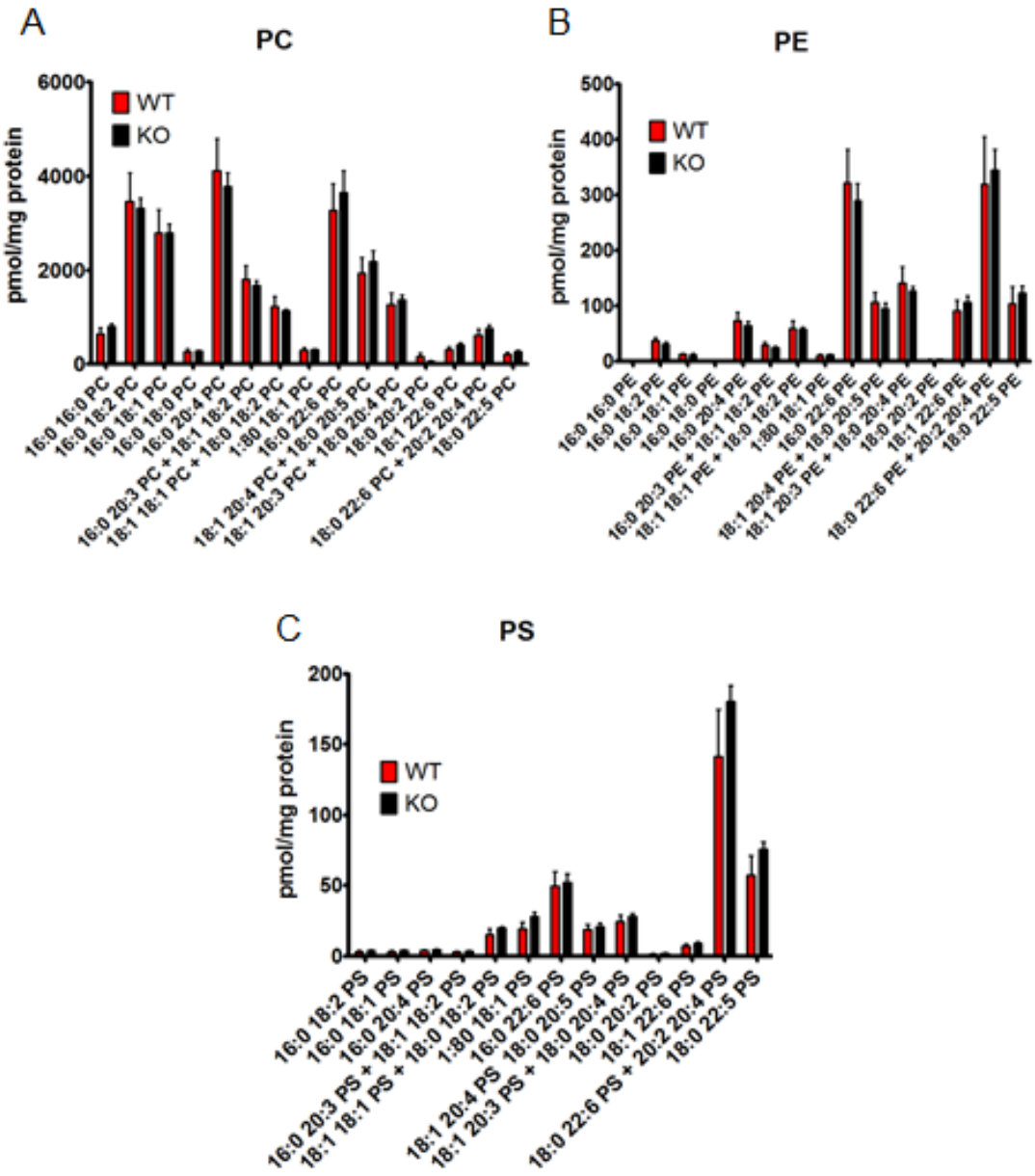

Figure 16. Skeletal muscle phospholipids from WT and CypD KO mice fed HFD. No significant differences were observed in quadriceps (A) phosphatidylcholine (PC), (B) phosphatidylethanolamine (PE), or (C) phosphatidylserine (PS) species. ns, not significant. n = 4 WT, 5 KO.

3.2.3 Ablation of CypD does not alter the oxidative phenotype of skeletal muscle.

The proportion of oxidative skeletal muscle fibers is indicative of insulin sensitivity in humans, as insulin resistant subjects have fewer type I oxidative muscle fibers and more type II glycolytic fibers[258]. However, we found that the ratio of type I oxidative fibers to type II glycolytic fibers was similar between genotypes (Figure 17, Figure 18). Furthermore, the level of Thiobarbituric Acid Reactive Substances (TBARS) and protein carbonyls, which are indicative of skeletal muscle oxidative damage, were not different between CypD KO and WT mice on HFD (Figure 19). Therefore, the enhanced skeletal muscle glucose metabolism in the absence of CypD was independent of changes in skeletal muscle fiber composition and oxidative damage.

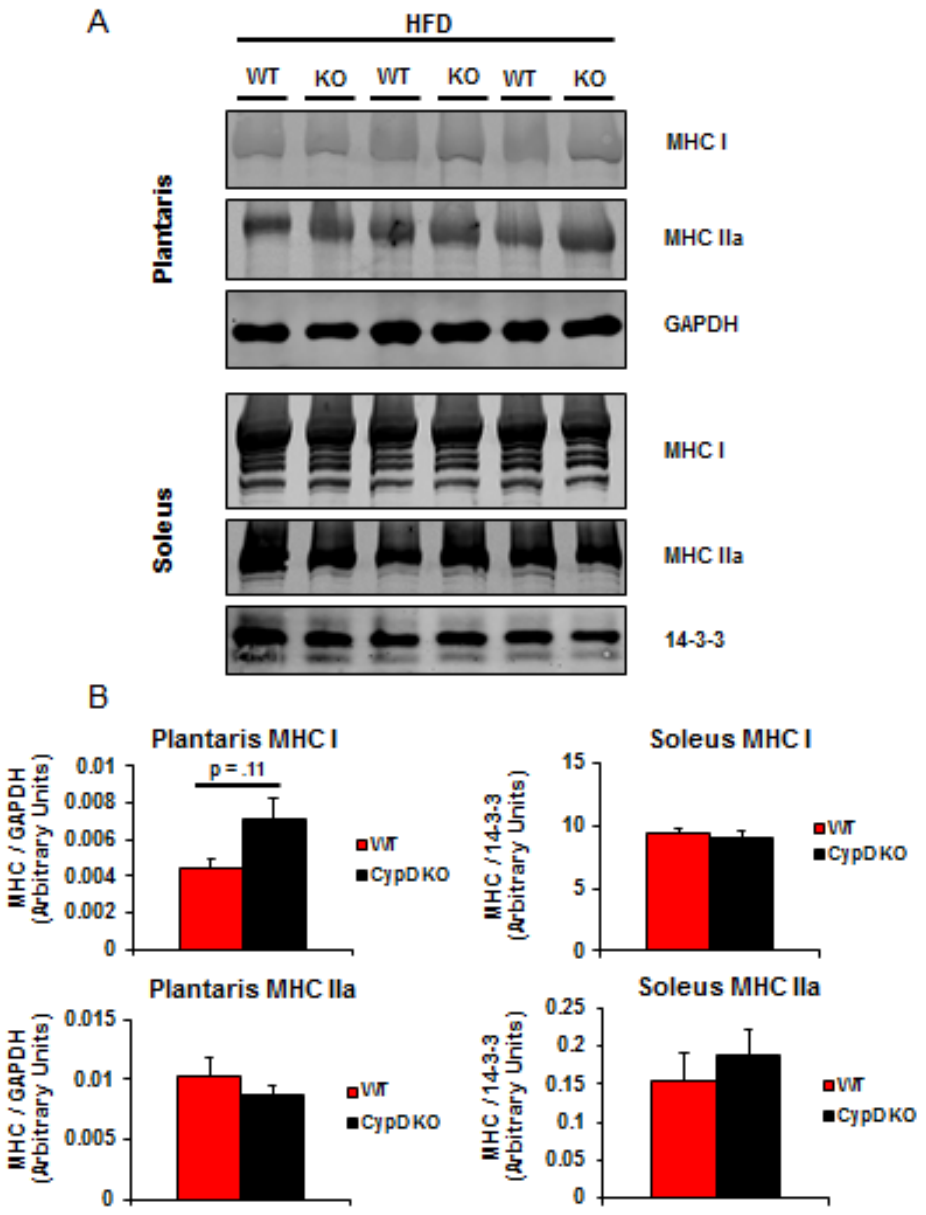

Figure 17. Analysis of skeletal muscle fiber type in plantaris and soleus muscles of HFD-fed mice.

(A) Representative Western blots of type I oxidative fiber marker MHC I and type IIa intermediate fiber marker MHC IIa in plantaris or soleus muscles from CypD KO or WT control mice. GAPDH and 14-3-3 were loading controls for plantaris and soleus,

respectively. (B) Quantification of MHC I and MHC IIa expression relative to respective loading controls. Results are displayed as means ± SEM. n = 3 per genotype.

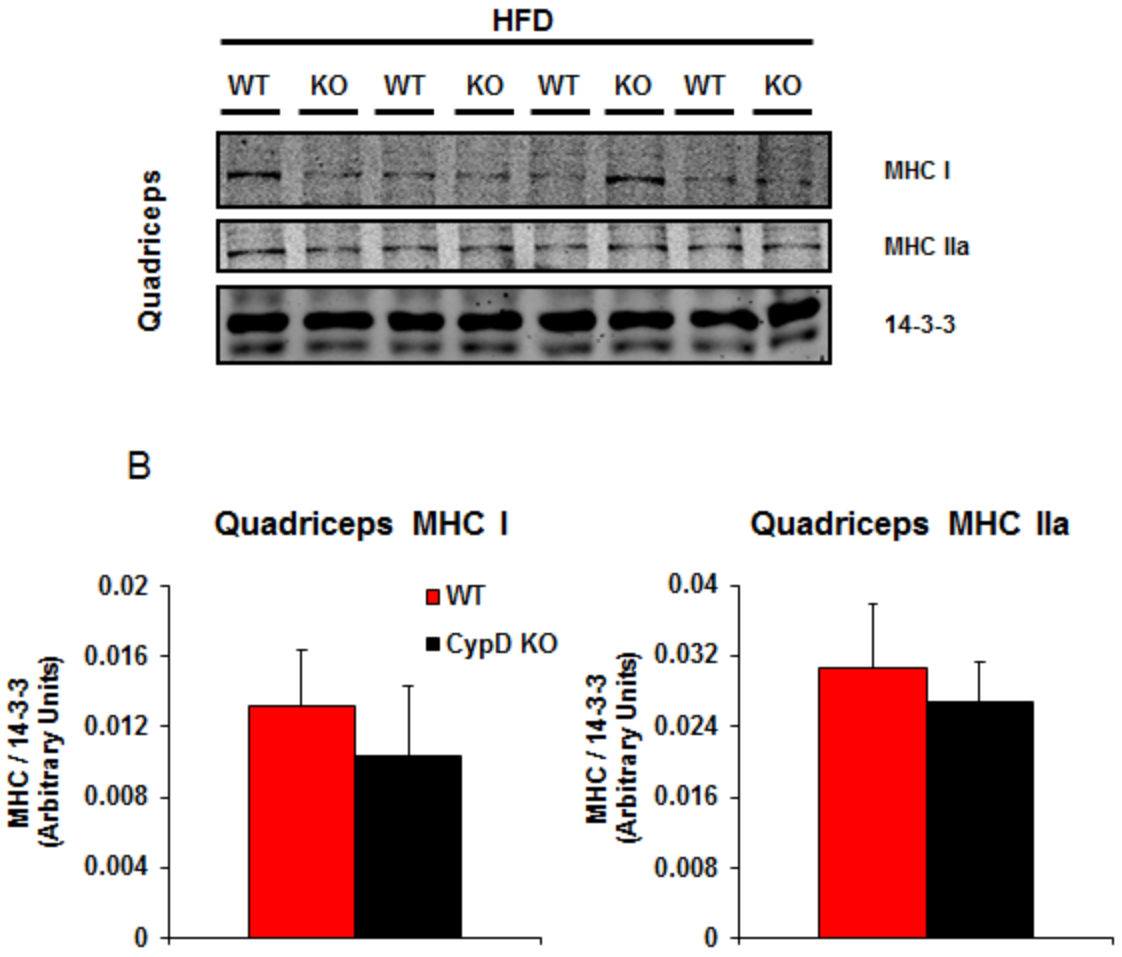

Figure 18. Analysis of skeletal muscle fiber type in quadriceps muscles from mice on HFD.

(A) Representative Western blots of MHC I and MHC IIa in quadriceps muscles of CypD KO and WT control mice. 14-3-3 served as a loading control. (B) Quantification of MHC I and MHC IIa relative to the 14-3-3 loading control. Results are displayed as means ± SEM. n = 3 per genotype.

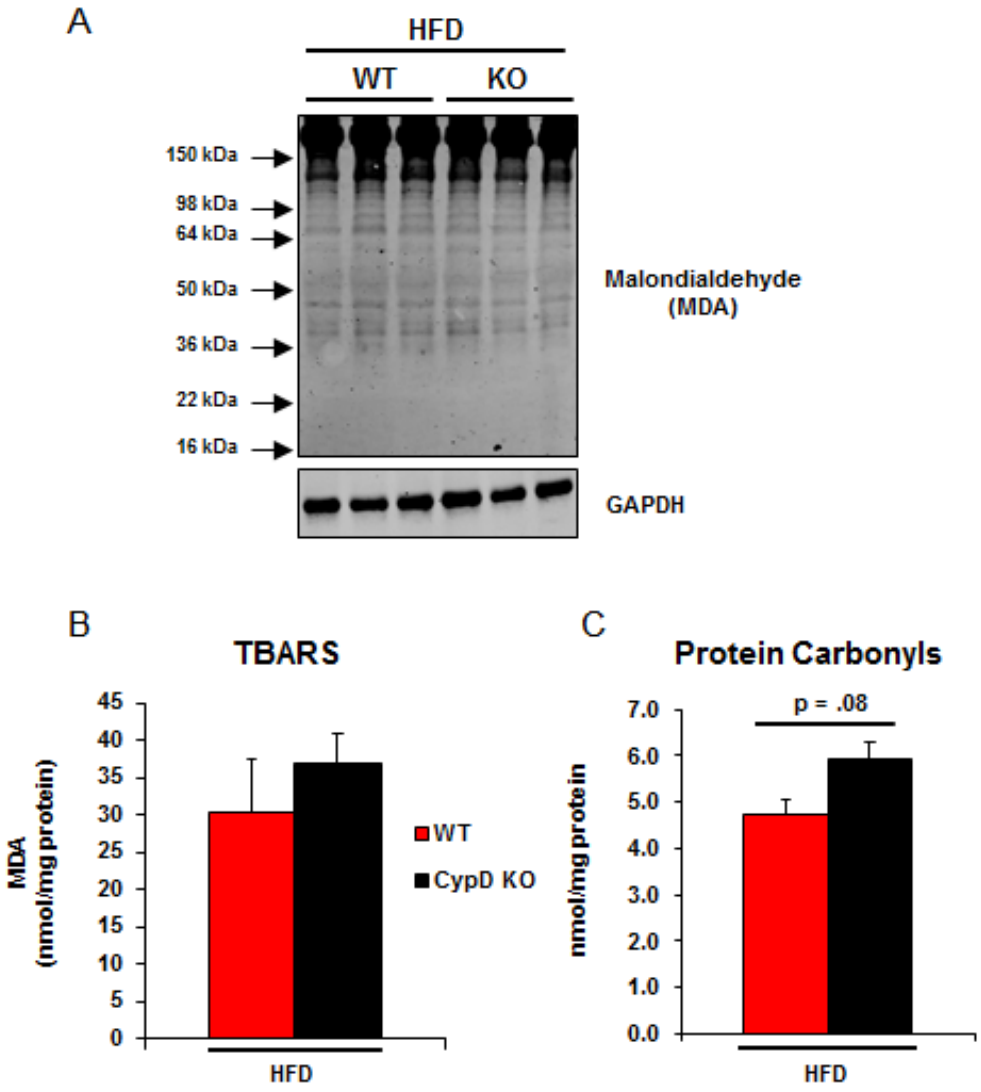

Figure 19. Skeletal muscle oxidative damage in HFD-fed CypD KO and WT control mice.

(A) Representative Western blot of malondialdehyde (MDA)-modified proteins in quadriceps. GAPDH was used as a loading control. (B) Spectrophotometric measurement of TBARS in quadriceps muscles. (C) Spectrophotometric quantification of protein carbonyl content in gastrocnemius muscles from HFD-fed mice. Results are displayed as means ± SEM. For A,C, n = 3 per genotype; for B, n = 5 for WT and n = 6 for KO.

3.2.4 Improved mitochondrial morphology and calcium retention capacity in CypD KO muscle.

Mitochondrial swelling is reported in skeletal muscles of insulin resistant mice fed a HFD[158]. To determine whether mitochondrial swelling was altered in skeletal muscle lacking CypD, we analyzed mitochondrial morphology by transmission electron microscopy (TEM). Consistent with previous reports[158], we observed that the mitochondria within skeletal muscle fibers of WT mice fed a HFD were vacuolated and swollen in both intermyofibrillar and subsarcolemmal muscle regions. In contrast, CypD KO skeletal muscle did not show any mitochondrial swelling or accumulation of damaged organelles (Figure 20A-D). However, these morphological differences in skeletal muscle mitochondria between WT and CypD KO mice were not accompanied by changes in mitochondria size (Figure 20E). In contrast, HFD feeding was associated with a decrease in skeletal muscle mitochondrial calcium retention capacity in WT mice (Figure 20F), an effect that was rescued by deletion of CypD (Figure 20G). Despite the improved calcium storage capacity, loss of CypD did not affect regulation or activity of the calcium-dependent mitochondrial enzyme pyruvate dehydrogenase (PDH) (Figure 21). These results indicate that CypD ablation may improve skeletal muscle glucose uptake by preserving mitochondrial morphology and calcium handling in insulin resistant skeletal muscle without changing substrate flux through PDH.

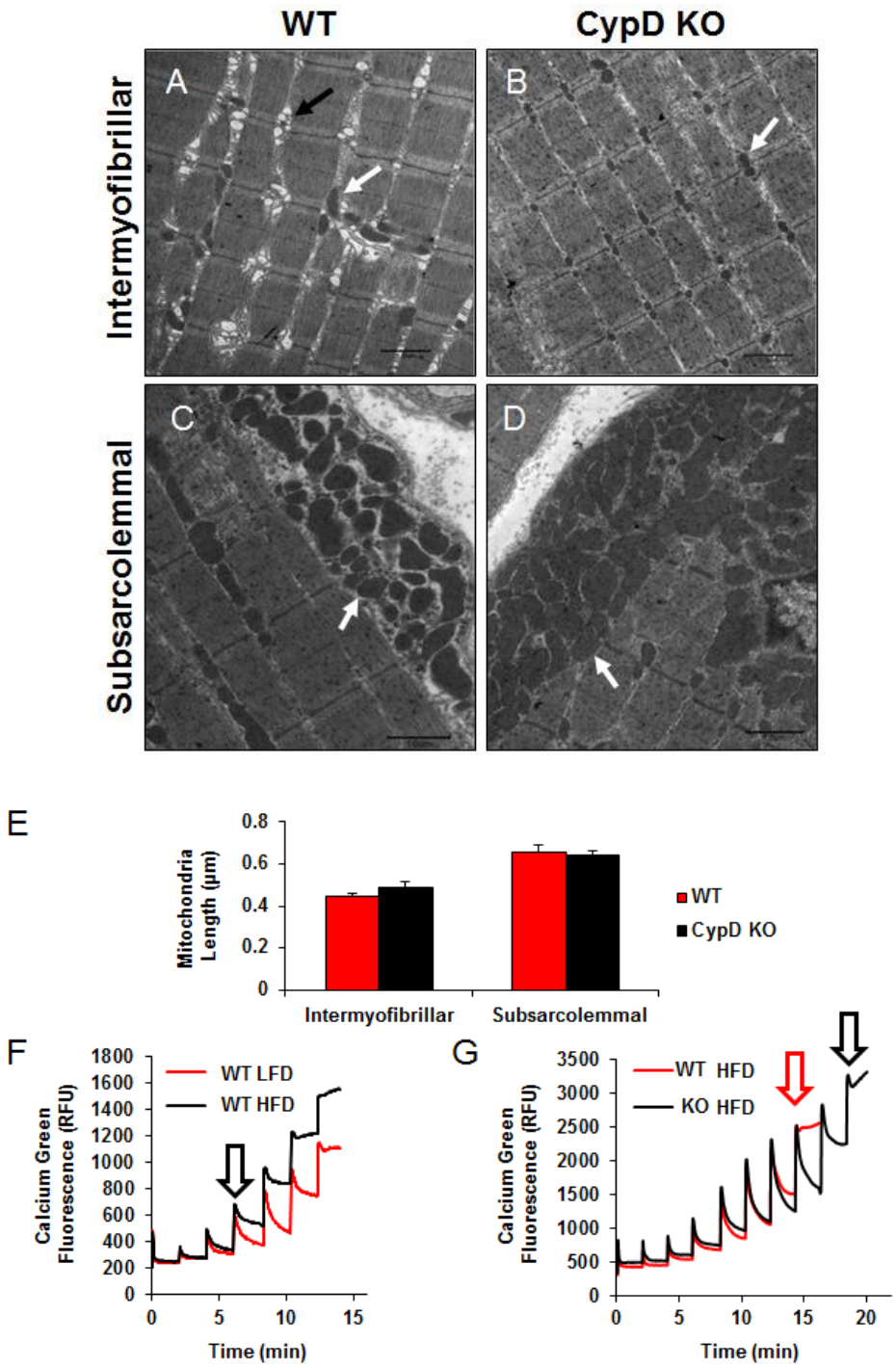

Figure 20. Skeletal muscle morphology and mitochondrial calcium retention capacity in WT and CypD KO mice.

(A-D) Representative TEM images (10,000x magnification) of intermyofibrillar and subsarcolemmal mitochondria in tibialis cranialis muscle from WT and CypD KO mice fed a HFD for 29 weeks. Black arrow denotes vacuolar structures, and white arrows indicate mitochondria. Scale bar equals 1μm. (E) Quantification of mitochondrial length in tibialis cranialis muscles. Lengths from ≥ 170 mitochondria per genotype (intermyofibrillar) or ≥ 90 mitochondria per genotype (subsarcolemmal) were quantified in TEM images using ImageJ. (F) Representative trace from three calcium retention capacity assays of mitochondria isolated from gastrocnemius muscles of WT mice fed a LFD or HFD for 10 weeks. (G) Representative trace from three calcium retention capacity assays comparing WT and CypD KO mice fed HFD for 10 weeks. Arrows indicate calcium-induced mPTP opening.

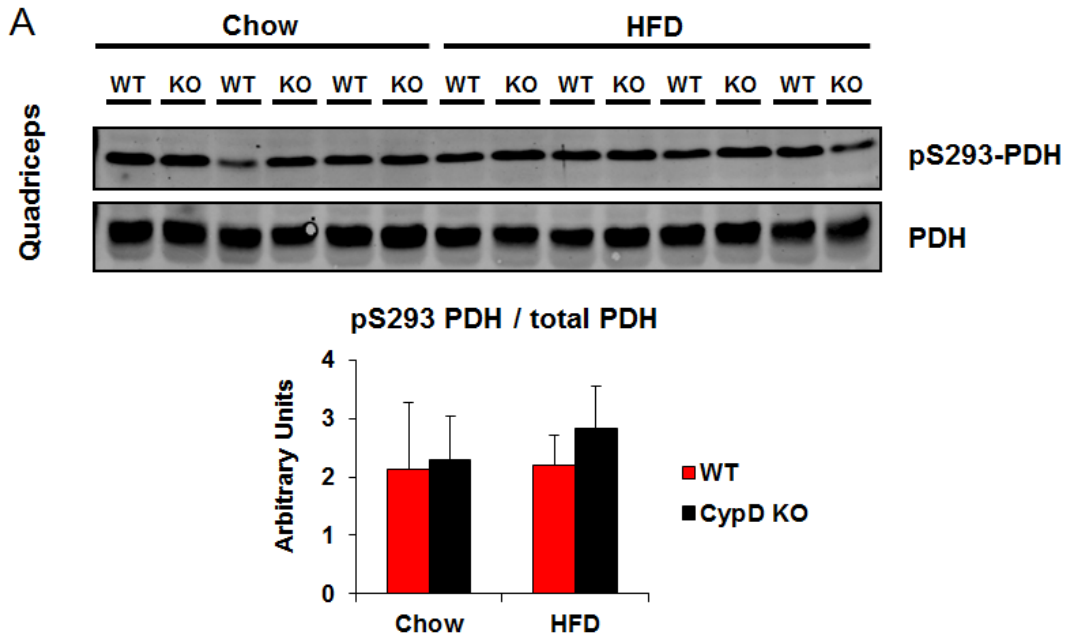

B

	Chow		HFD		
	WT	CypD KO	WT	CypD KO	2-Way ANOVA[#]
PDH_a	11.3 ± 1.7	11.6 ± 2.1	10.6 ± 0.9	10.3 ± 0.5	p = .99[a], p = .97[b]
PDH_t	15.9 ± 2.2	17.6 ± 3.8	15.8 ± 1.1	17.1 ± 0.6	p = .83[a], p = .86[b]
PDH_a / PDH_t	70.9 ± 2.0%	67.0 ± 2.0%	67.4 ± 4.3%	60.0 ± 3.2%	p = .70[a], p = .24[b]

[#]WT vs. CypD KO fed [a]Chow, [b]HFD by 2-WAY ANOVA and Sidak test for multiple comparisons

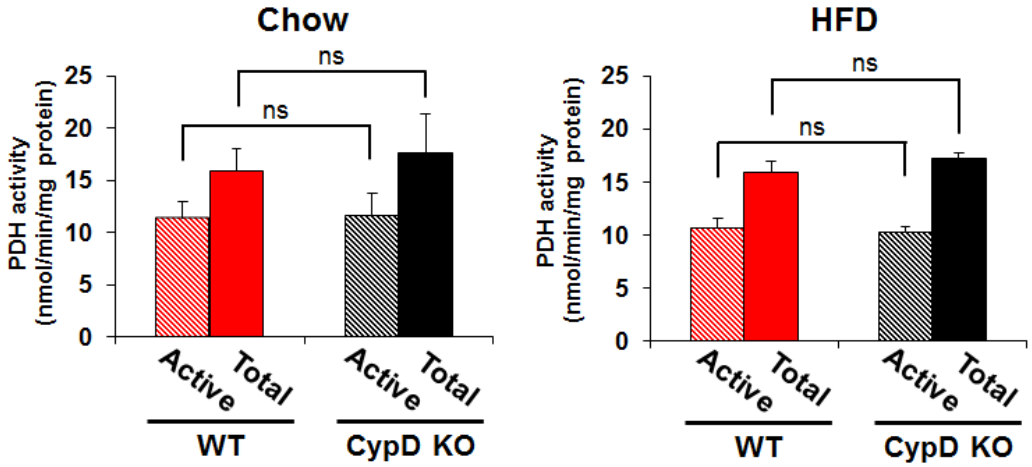

Figure 21. Skeletal muscle PDH phosphorylation and activity in CypD KO and WT control mice fed either a normal Chow or HFD.

(A) Representative Western blots of PDH phosphorylation at S293 and total PDH content in quadriceps muscles. Levels of pS293-PDH were normalized to total PDH expression. (B) Spectrophotometric measurement of active (PDHa) and total (PDHt) PDH activity in quadriceps muscles. Ratios of active to total PDH activity (PDHa/PDHt) were calculated to estimate the fraction of skeletal muscle PDH complexes in the activated form. Results are displayed as means ± SEM. n = 3 per genotype, #WT vs. CypD KO fed [a]Chow, [b]HFD by two-way ANOVA and Sidak test for multiple comparisons. ns, not significant.

3.2.5 Loss of CypD does not affect oxidative enzyme capacity or mitochondrial bioenergetics in skeletal muscle.

Insulin resistant skeletal muscle often shows defects in energy substrate oxidation and/or mitochondrial oxidative phosphorylation (OXPHOS)[150,152]. However, deletion of CypD had no effect on activity of the TCA cycle enzyme citrate synthase or on the β-oxidation enzymes medium chain acyl-CoA dehydrogenase (MCAD) and β-hydroxyacyl-CoA dehydrogenase (β-HAD) in skeletal muscle (Figure 22A-C). Similarly, enzyme activities of ETC complexes I, II, and IV were comparable in skeletal muscle from CypD KO and WT mice (Figure 22D-F). Mitochondria isolated from quadriceps muscles of CypD KO and WT mice also showed similar native ETC complex content and supramolecular assembly (Figure 23) and bioenergetic function (Figure 24).

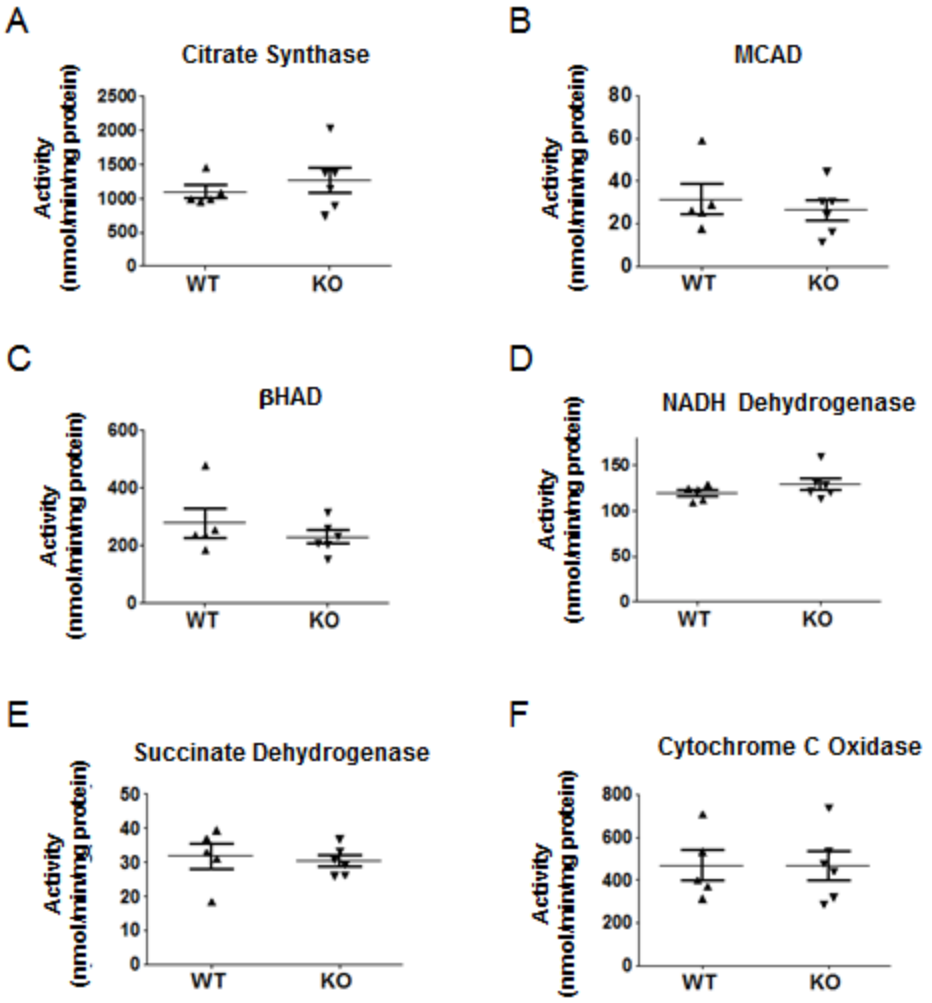

Figure 22. Mitochondrial enzyme activities in quadriceps muscles of mice fed HFD. Spectrophotometric measurement of activities of citrate synthase (A), medium chain acyl-CoA dehydrogenase (MCAD) (B), β-hydroxyacyl-CoA dehydrogenase (β-HAD) (C), complex I (NADH Dehydrogenase) (D), complex II (Succinate Dehydrogenase) (E) and complex IV (Cytochrome C Oxidase) (F). No statistically significant differences were observed in the activities of these enzymes. n = 5 WT and 6 KO.

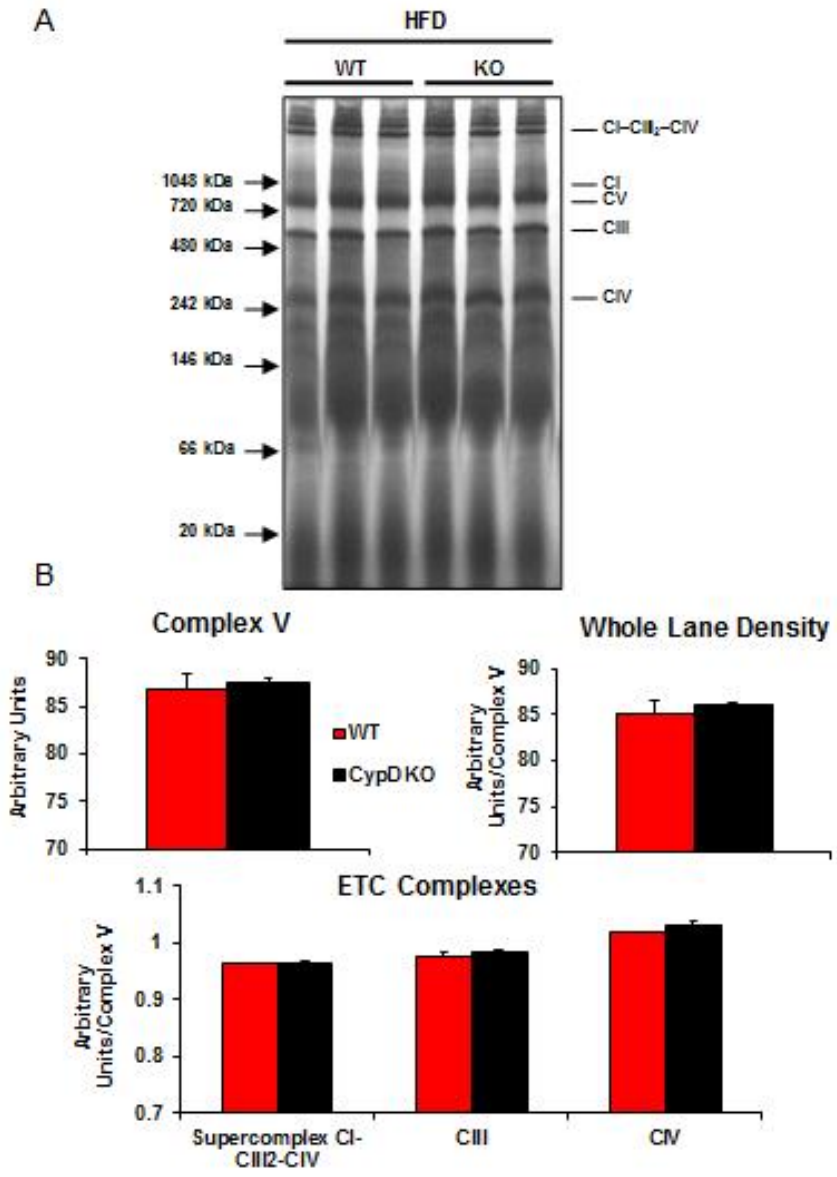

Figure 23. Blue Native-PAGE analysis of native OXPHOS complexes in mitochondria isolated from WT and CypD KO mice fed a HFD for 14 weeks.

(A) Representative blue native gel of digitonin-solubilized isolated quadriceps mitochondria. Coomassie blue G-250-labeled mitochondrial proteins (100µg/lane) were separated on non-denaturing 4-15% polyacrylamide gradient gels alongside a standard cocktail of native proteins of known size. (B) Quantification of the intensity of bands representing individual ETC/OXPHOS complexes or supramolecular assemblies,

including CI–$CIII_2$–CIV, the major respiratory supercomplex in mammalian mitochondria[243]. ETC complex content was normalized to Complex V and shown as means ± SEM. n = 3 per genotype.

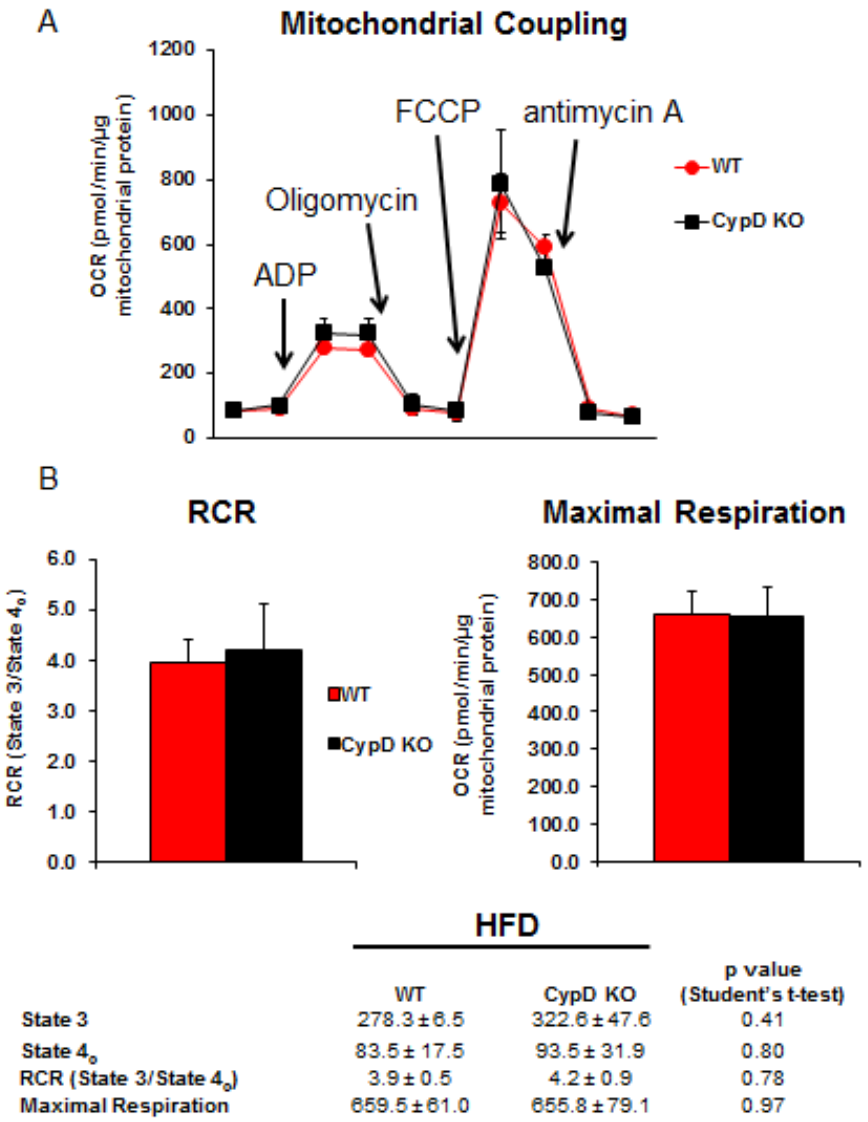

	HFD		
	WT	CypD KO	p value (Student's t-test)
State 3	278.3 ± 6.5	322.6 ± 47.6	0.41
State 4_o	83.5 ± 17.5	93.5 ± 31.9	0.80
RCR (State 3/State 4_o)	3.9 ± 0.5	4.2 ± 0.9	0.78
Maximal Respiration	659.5 ± 61.0	655.8 ± 79.1	0.97

Figure 24. Mitochondrial bioenergetics in quadriceps muscles from HFD-fed mice. (A) Representative trace of oxygen consumption rates (OCR) from quadriceps mitochondria (2.5µg/well) isolated from CypD KO and WT control mice using a Seahorse XF24. Coupled respiration was measured in the presence of substrate (Basal respiration), ADP (5mM; State 3), oligomycin (5µM; State 4_o), FCCP (7µM; maximal respiration) and antimycin A (4µM; mitochondria-specific respiration). (B) Quantification of mitochondrial respiration. Respiratory control ratios (RCRs; State

3/State 4_o) were calculated for each genotype. Results are displayed as means ± SEM. n = 3 per genotype.

3.2.6 Inhibition of mPTP opening prevents multiple models of insulin resistance in vitro.

We next sought to determine if mPTP opening was sufficient or necessary to induce insulin resistance, as determined by inhibition of insulin-stimulated GLUT4 trafficking to the PM, an endpoint of the insulin signaling pathway. We tested two well-documented mechanisms of mPTP opening including mitochondrial calcium overload[259] and mitochondrial $O_2^{\cdot}$ production[189] in cultured L6 myotubes. Mitochondrial calcium overload was induced by 30 minute treatment with the ionophore ferutinin[260,261]. Ferutinin treatment caused dose-dependent inhibition of insulin-stimulated GLUT4 trafficking to the PM that was reversible with either of the mPTP inhibitors cyclosporin A (CsA) or bongkrekic acid (BKA) (Figure 25A). CsA inhibits CypD and calcineurin, whereas BKA inhibits another mPTP regulatory component, the adenine nucleotide translocator (ANT). Since CsA is a dual inhibitor of both CypD and calcineurin, we confirmed that the calcineurin inhibitor FK506 did not protect myotubes from ferutinin-induced mPTP opening and insulin resistance (Figure 25B). Ferutinin-induced insulin resistance did not affect insulin signaling through Akt, nor was signaling altered by CsA or BKA (Figure 25C).

We have previously demonstrated that the mitochondrial complex III inhibitor antimycin A is sufficient to promote mitochondrial $O_2^{\cdot}$ production and cause insulin resistance[138]. Antimycin A attenuated insulin-stimulated GLUT4 mobilization in a dose dependent manner (Figure 26A) without significantly altering cellular ATP content (Figure 26B). Furthermore, antimycin A-induced insulin resistance requires mPTP opening, as CsA fully protected L6 myotubes from defects in GLUT4 trafficking caused by antimycin A (Figure 26C). Previously, we have validated that antimycin A-induced

insulin resistance is due to $O_2^{\cdot}$ rather than mitochondrial inhibition because it is reversible by overexpression of MnSOD[138]. To confirm the requirement of the mPTP for $O_2^{\cdot}$-induced insulin resistance, we also tested C2-ceramide, which is an inducer of mitochondrial $O_2^{\cdot}$[262] and promotes insulin resistance[263]. As shown in Figure 26C, CsA also completely prevented insulin resistance caused by C2-ceramide.

Finally, we and others have demonstrated that low-dose (150μM) palmitate induces insulin resistance in L6 myotubes at the level of GLUT4 trafficking to the PM, without disrupting insulin signaling[13,138],. Here we show that palmitate treatment reduced mitochondrial calcium retention capacity (Figure 27A) and impaired insulin-stimulated GLUT4 trafficking to the PM (Figure 27B). Treatment of myotubes with CsA improved mitochondrial calcium retention capacity and prevented palmitate-induced insulin resistance at the level of GLUT4 translocation (Figure 27A-B). These data identify that CypD-dependent opening of the mPTP is required for multiple models of skeletal muscle insulin resistance *in vitro* and *in vivo* as outlined in Figure 28.

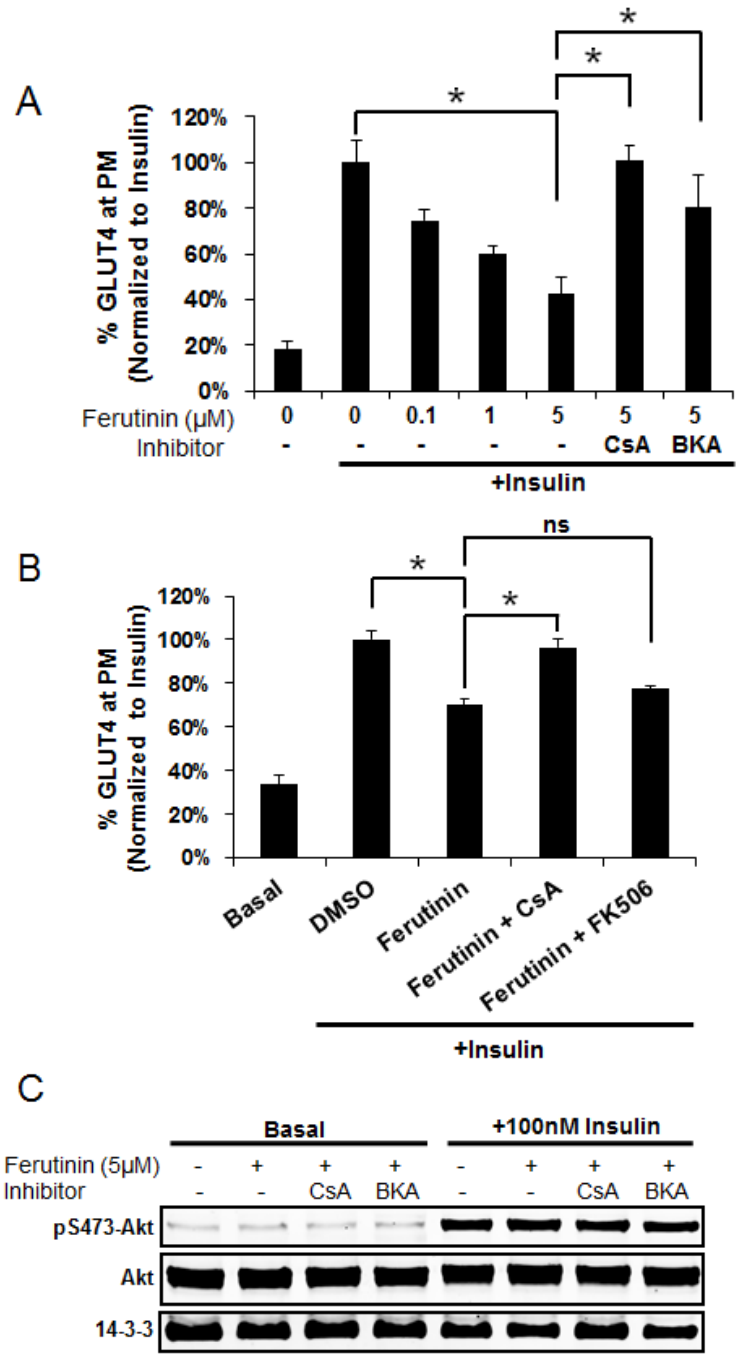

Figure 25. mPTP opening drives insulin resistance *in vitro*.

(A) Insulin-stimulated GLUT4 translocation was analyzed in L6 myotubes treated for 30 minutes with increasing concentrations of ferutinin (0.1μM, 1μM, and 5μM) in the absence or presence of a 10 minute pretreatment with mPTP inhibitors CsA (1μg/mL) or

BKA (10μM). (B) Insulin-stimulated GLUT4 translocation in control and ferutinin-induced insulin resistant L6 myotubes in the absence or presence of CsA or the calcineurin inhibitor FK506. (C) Akt phosphorylation in basal or insulin-stimulated L6 myotubes treated with or without 5μM ferutinin in the absence or presence of 1μg/mL CsA or 10μM BKA. Representative Western blots from three individual experiments are shown. For A, n = 3 and for B, n = 6. Results are displayed as means ± SEM, *$p < 0.05$. ns, not significant.

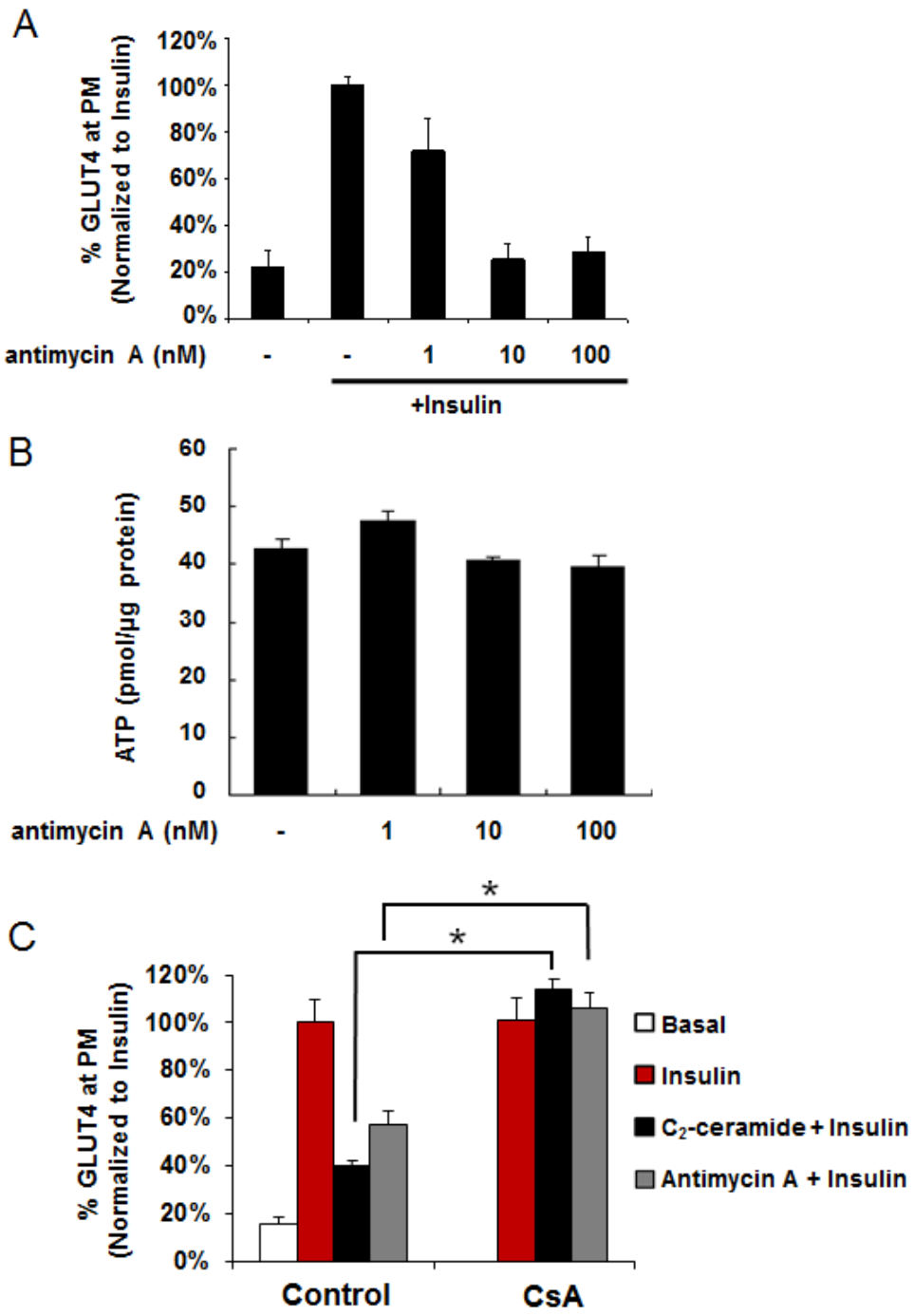

Figure 26. Inhibition of mPTP opening ameliorates $O_2^{\cdot}$–induced insulin resistance. (A) Insulin-stimulated GLUT4 trafficking and (B) ATP levels in L6 myotubes treated for 30 minutes with increasing concentrations of antimycin A prior to acute insulin treatment for 20 minutes. (C) GLUT4 translocation assay after a 30 minute treatment with 100nM

C2-ceramide or 50nM antimycin A, with or without a 10 minute pretreatment with 1μg/mL CsA. Results are displayed as means ± SEM. n = 3. *p < .05.

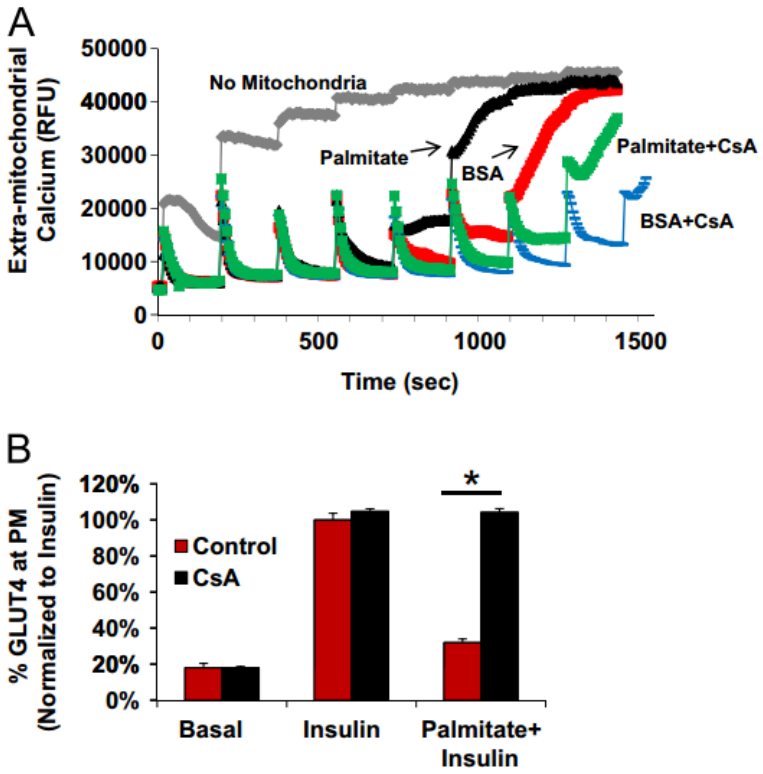

Figure 27. Palmitate-induced insulin resistance requires mPTP opening.

(A) Calcium retention capacity was measured in mitochondria isolated from L6 myotubes treated for 16hrs with 150μM palmitate or control (BSA) in the absence or presence of CsA treatment (1μg/mL). CsA improves mitochondrial calcium retention capacity in both palmitate- and BSA-treated cells. Representative traces are shown from one of three experiments that showed similar results. (B) Insulin-stimulated GLUT4 translocation to the PM was measured in control and palmitate-treated L6 myotubes in the absence or presence of CsA. Results are displayed as means ± SEM. n = 3, *$p < 0.05$.

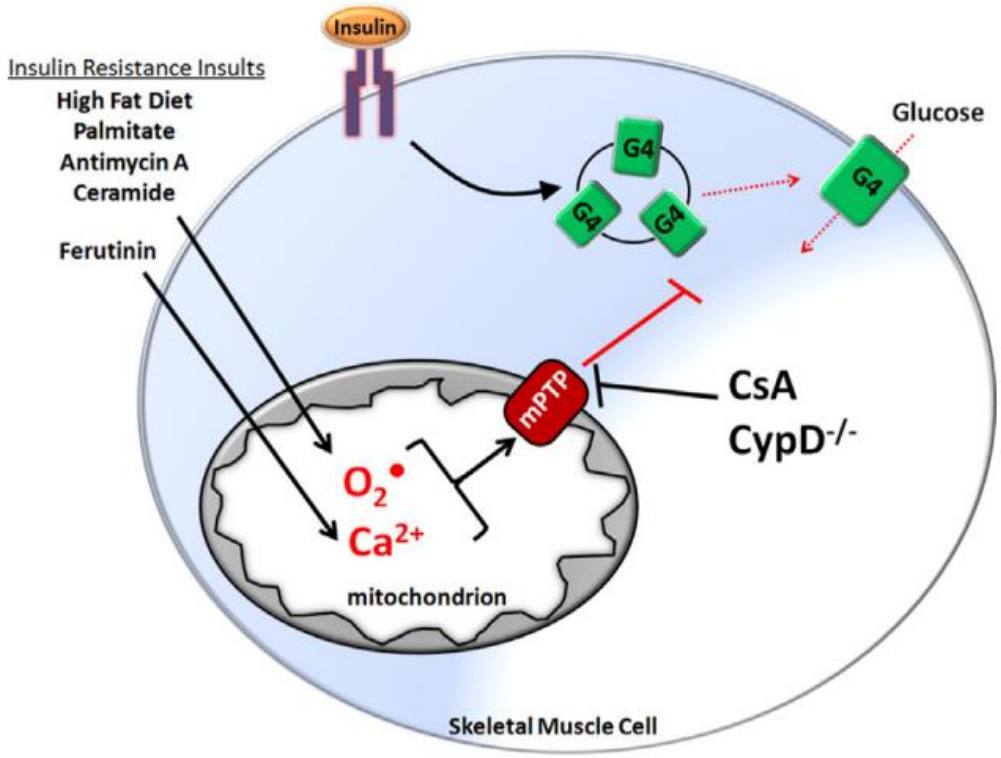

Figure 28. Opening of the mPTP promotes insulin resistance in skeletal muscle. Insults that promote excessive mitochondrial $O_2^{\cdot}$ and/or mitochondrial calcium overload converge on the mPTP to induce skeletal muscle insulin resistance, which is rescued by pharmacological or genetic inhibition of the mPTP regulatory protein CypD.

3.2.7 CypD regulates whole-body nutrient metabolism in a tissue-specific manner.

Based on the increased skeletal muscle glucose utilization in CypD KO mice, we investigated whether muscle-specific deletion of CypD would be sufficient to prevent diet-induced insulin resistance. To address this question, we generated mice lacking CypD in all muscles (MKO) (Figure 29A-B) and measured parameters of glucose metabolism. CypD MKO show similar glucose tolerance to control mice when fed LFD (Figure 29C). Interestingly, after HFD challenge, muscle-specific deletion of CypD does not alter whole-body glucose clearance compared to controls (Figure 29D). Thus, muscle-specific deletion of CypD does not prevent diet-induced defects in glucose metabolism, which may suggest compensatory adjustment by other CypD-expressing tissues.

CypD is highly expressed in the liver (Figure 29B), and whole-body CypD KO mice showed a trend toward reduced hepatic glycogen storage (Figure 11), raising the possibility that CypD may play an important role in regulating liver glucose metabolism. To investigate the role of CypD in hepatic glucose utilization, we generated liver-specific CypD KO (LKO) mice (Figure 30A-B). When fed HFD, mice lacking CypD in the liver show greater adiposity (Figure 30C) and exacerbated hepatic lipid accumulation (Figure 30D). Excessive storage of lipids in the liver is associated with hepatic insulin resistance and blunted suppression of HGP[87]. Deletion of liver CypD impaired glucose tolerance (Figure 31A) and promoted HGP (Figure 31B) in HFD-fed mice. Despite increasing HGP, loss of liver CypD did not alter expression of the gluconeogenic genes PEPCK and G6Pase or the pro-gluconeogenic transcription factor PGC1α (Figure 31C). Overall, these

results highlight a novel, tissue-specific regulatory function for CypD in insulin sensitivity and nutrient metabolism.

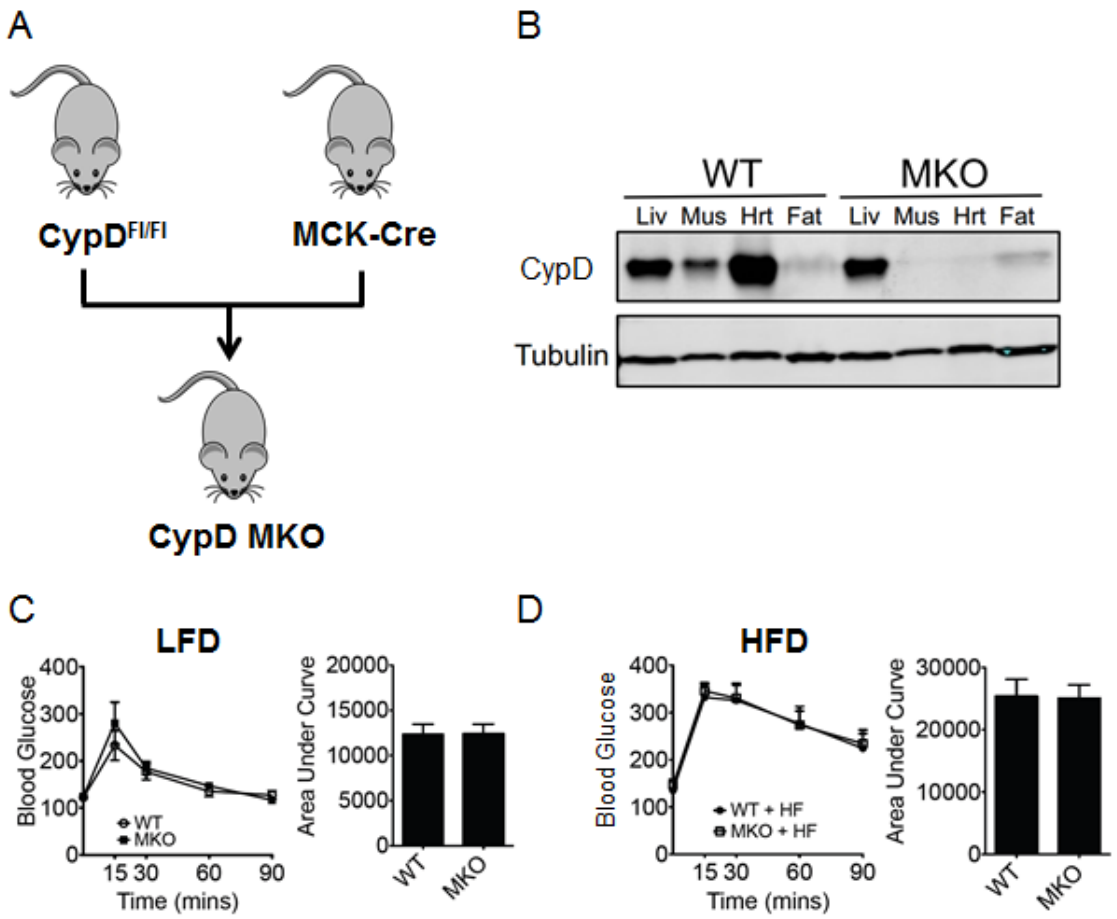

Figure 29. Muscle-specific deletion of CypD does not alter glucose tolerance in HFD-fed mice.

(A) CypD MKO mice were generated by crossing $CypD^{Fl/Fl}$ mice with muscle-specific Cre-expressing mice. The $CypD^{Fl/Fl}$ control mice are referred to as "WT" in panels B-D. (B) Western blot showing loss of CypD specifically in muscle tissues of CypD MKO mice. (C-D) GTTs in WT and CypD MKO mice fed a LFD (C) or HFD (D). Data are represented as means ± SEM. For C, n = 11 WT and 12 MKO and for D, n = 12 WT and 10 MKO.

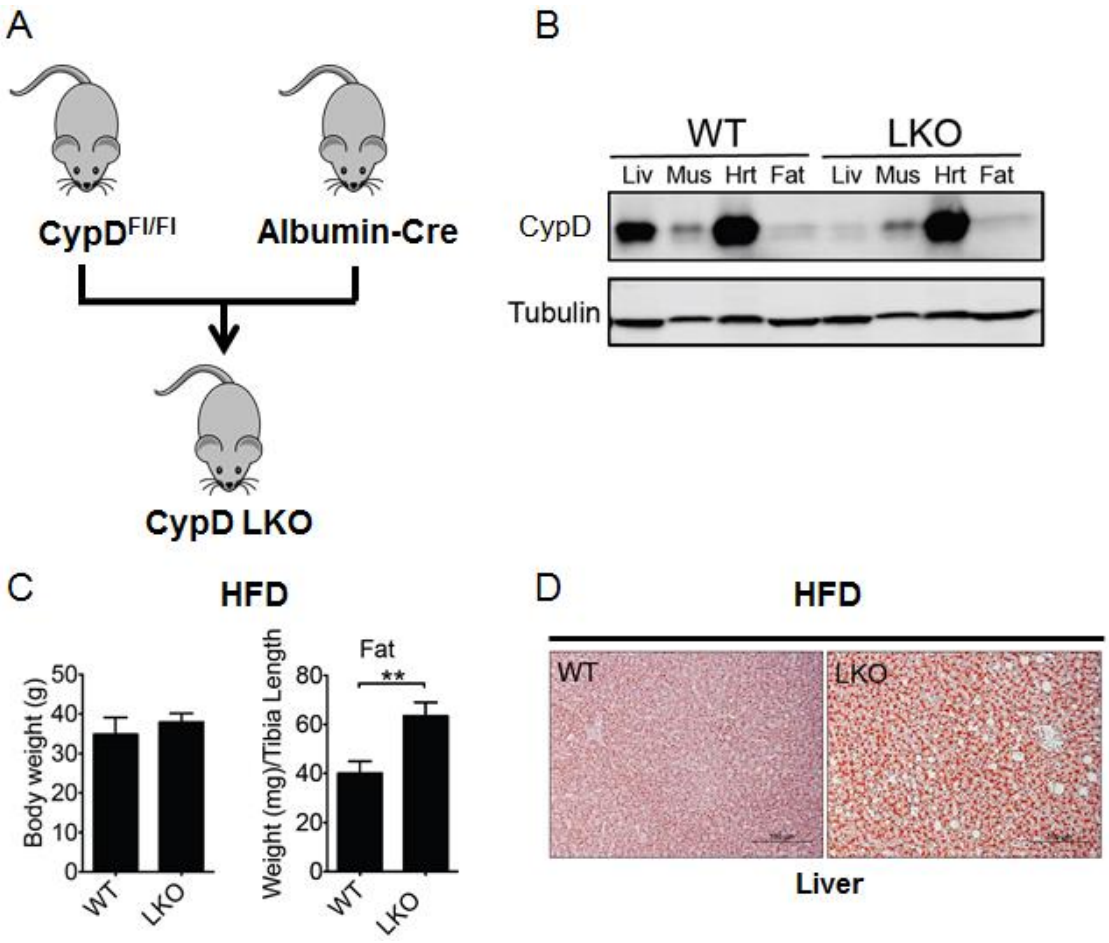

Figure 30. Liver-specific deletion of CypD exacerbates hepatic lipid accumulation in HFD-fed mice.

(A) CypD LKO mice were generated by crossing $CypD^{Fl/Fl}$ mice with liver-specific Cre-expressing mice. The $CypD^{Fl/Fl}$ control mice are referred to as "WT" in panels B-D and in Figure 31. (B) Western blot showing loss of CypD specifically in liver tissues of CypD LKO mice. (C) Total body weights and adipose tissue weights of WT and CypD LKO mice fed HFD. (D) Representative image of hepatic neutral lipid content assessed by Oil-Red O staining in livers from HFD-fed WT and CypD LKO mice. Data are represented as means ± SEM. For C and D, n = 9 WT and 11 LKO. **$p < .05$.

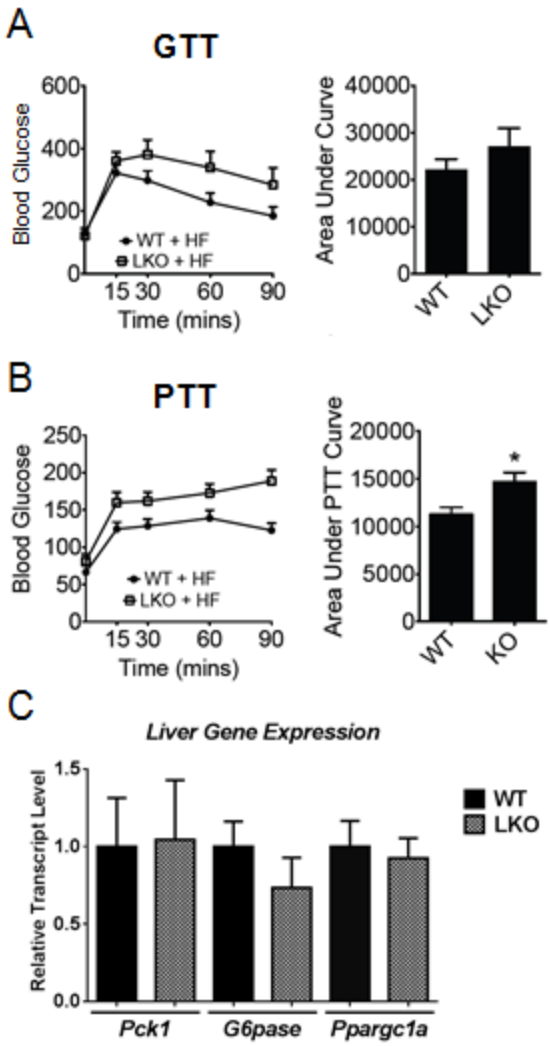

Figure 31. CypD LKO mice show exaggerated HGP.

(A) GTTs and pyruvate tolerance tests (PTTs) (B) in mice fed HFD. (C) Expression of gluconeogenic genes in livers of WT and CypD LKO mice on HFD. Data are represented as means ± SEM. For A, n = 5 WT and 6 LKO; for B, n = 9 WT and 11 LKO; for C, n = 4 WT and 6 LKO. *p < .05.

3.3 Discussion

Abnormal mitochondrial structure and/or function are correlated with insulin resistance in skeletal muscle. In the present study, we investigated whether the mPTP represents a link between mitochondrial dysfunction and insulin resistance. The rationale for investigating the mPTP included: (1) the close proximity of the mPTP to the source of mitochondrial $O_2^{\cdot}$ production in the mitochondrial inner membrane; (2) opening of the mPTP can be rapid and reversible, and is triggered by insults that are associated with insulin resistance including mitochondrial $O_2^{\cdot}$ and mitochondrial calcium overload; and (3) mPTP opening serves as a potential means of communication between mitochondrial stress and insulin-stimulated GLUT4 translocation to the PM and glucose uptake into the cytoplasm. We identified that genetic deletion of CypD in all tissues, which decreases the probability of mPTP opening[179,207,256,257], protected mice from HFD-induced glucose intolerance and increased glucose uptake in skeletal muscle. The increased glucose uptake in skeletal muscle was associated with preserved mitochondrial morphology and improved mitochondrial calcium handling. In cultured muscle cells, we found that mitochondrial $O_2^{\cdot}$, mitochondrial calcium overload, and palmitate all require mPTP opening for induction of insulin resistance. Tissue-specific ablation of CypD also demonstrated an important role for the mPTP in regulating glucose and lipid handling in liver. These results position the mPTP at a critical intersection between alterations in mitochondrial function, skeletal muscle insulin resistance and liver energy substrate metabolism.

It is intriguing that the improved glucose tolerance in HFD-fed CypD KO mice was associated with significantly higher glucose uptake and metabolism in skeletal

muscle, with substantial but not significant decreases in adipose glucose uptake and liver glycogen storage. This tissue-specific phenotype may be the result of structural and physiological differences in the mPTP complex in skeletal muscle, compared to liver, adipose and other tissues. For example, insulin-sensitive tissues display a wide range of CypD expression, with heart and liver containing a relatively high amount of CypD, in contrast to the low expression in adipose tissue and brain. In addition, skeletal muscle expresses the mPTP component ANT1, whereas the liver lacks ANT1, predominantly expresses ANT2 and has lower levels of ANT3 and ANT4[264]. The tissue-specific isoforms of ANT also have distinct mitochondrial localization within the inner membrane[264] and contain subtle structural variations that may affect interactions between pore components. Supporting this notion, ANT1 is reported to have a higher binding affinity for CypD than ANT2[264], and this CypD–ANT interaction promotes mPTP opening[179,207,256,257]. Another tissue-specific difference in mPTP composition involves HK2, which is expressed in skeletal muscle, but not in the liver. HK2 binds to VDAC in the mitochondrial outer membrane and stabilizes the structure to block mPTP opening[265,266], providing a molecular connection between glucose uptake and mPTP activity in skeletal muscle.

This structural heterogeneity is known to dictate mPTP activity in response to metabolic stress, as the mPTP shows tissue-specific sensitivity to opening[267]. Our results suggest that this variation in mPTP sensitivity may contribute to tissue-dependent metabolic regulation by CypD. In the context of HFD, whole-body deletion of CypD increased skeletal muscle glucose metabolism, but it is not clear whether this increase is a primary event or compensation for potential deficits in adipose or liver glucose

metabolism. The coordinated changes in glucose metabolism observed in the whole-body CypD KO mice may be the result of inter-tissue communication via a circulating factor, since loss of CypD can increase cytokine expression[268]. Whether this phenomenon is related to CypD regulation of mPTP function is not known. Furthermore, muscle-specific loss of CypD was not sufficient to protect against diet-induced glucose intolerance. It is possible that the CypD MKO mice may have increased skeletal muscle glucose uptake compared to WT controls, but changes in glucose disposal and output in adipose and liver, respectively, may mask this event and result in unchanged whole-body glucose clearance during a GTT. Thus, the CypD MKO results do not necessarily diminish the potential role of skeletal muscle mPTP in glucose uptake, but supports the involvement of other tissues such as the heart, since these mice also lack CypD in cardiac muscle. CypD is highly expressed in the heart, and Elrod and colleagues[222] have shown that CypD expression is important for determining the balance between fatty acid and glucose utilization in cardiomyocytes. In the liver, CypD ablation caused hepatic lipid accumulation and exacerbated HGP, but very little is known regarding CypD and the allocation of hepatic energy substrates. Therefore, variations in the composition and function of the mPTP may contribute to different pore dynamics and confer tissue-specific regulation of nutrient metabolism in insulin sensitive tissues.

Insulin resistance in muscle is frequently, but not always, associated with defects in the insulin signaling pathway. Our data demonstrate that mPTP opening promotes insulin resistance via a mechanism that does not involve alterations in the canonical insulin pathway. For example, induction of mPTP opening with insults that increase mitochondrial $O_2^{\cdot}$ and calcium caused insulin resistance at GLUT4 trafficking, but did

not affect the insulin signaling pathway. Similarly, inhibition of mPTP opening did not improve insulin signal transduction *in vitro* or *in vivo*. This disconnect between insulin-stimulated GLUT4 trafficking and signaling through the canonical insulin pathway (e.g. IRS/PI3K/Akt/AS160) has been described by our group previously[13,138], and is in agreement with other studies showing that lipid-induced impairment in the formation of GLUT4 vesicles[269] and their translocation to the PM[263] do not involve altered signaling through the canonical pathway. This phenomenon is also observed in humans, where impaired muscle glucose transport in insulin resistant individuals or type 2 diabetes patients is not associated with defects in Akt activation[14,270]. In agreement with these previous studies, the data presented herein indicate that the mechanism linking mPTP opening to insulin resistance does not involve the canonical insulin signaling pathway through Akt.

The precise molecular mechanism whereby mPTP opening triggers insulin resistance is unclear, but the broad spectrum of mitochondrial ions and metabolites that traverse the mitochondrial membranes during mPTP opening provides numerous possibilities. For example, calcium homeostasis is a critical function of mitochondria that is altered in insulin resistance. Normally, mitochondria serve as an intracellular calcium buffer to help maintain calcium homeostasis[271], with the mPTP opening transiently to act as a calcium release valve[207]. However, during periods of cellular stress, calcium accumulation in the mitochondrial matrix triggers high-conductance opening of the mPTP, which results in a loss of ionic gradients between the cytoplasm and mitochondrial matrix and an inability to retain matrix calcium[188,271]. Calcium retention capacity estimates the relative amount of calcium that mitochondria can store before

undergoing mPTP opening and thus is a measure of both mPTP opening and mitochondrial quality[193]. In this study, we observed that HFD reduces calcium retention capacity and sensitizes skeletal muscle mitochondria to mPTP opening, an effect that was reversed by deletion of CypD. However, apart from calcium[272], it is possible that blocking mPTP opening may sequester other ions such as iron[273,274] and metabolites such as fumarate[275] or acylcarnitines[276,277] that are associated with impaired insulin-stimulated glucose metabolism, and thus help maintain maximal insulin action in skeletal muscle. A consequence of high-conductance mPTP opening is the loss of mitochondrial membrane potential, which triggers ATP synthase to function in reverse and hydrolyze cytosolic ATP in an effort to restore potential[147]. It is possible that inhibition of mPTP opening maintains mitochondrial membrane potential and avoids the consumption of cytosolic ATP in insulin resistant muscle, allowing the use of this ATP for the energetically costly process of GLUT4 trafficking and glucose uptake. Although the most recognized function of CypD is to promote mPTP opening, CypD normally facilitates the proper folding of many mitochondrial proteins[278].Thus, it is possible that the effects of CypD inhibition on GLUT4 translocation and glucose uptake may be attributed to both mPTP-dependent and -independent mechanisms. Identification of the precise molecules that may pass through the mPTP to antagonize insulin action and the specification of which events are due to CypD actions on the mPTP will require further elucidation.

It is thought that nutrient overload can alter mitochondrial shape[157], and insulin resistant skeletal muscle often contains swollen, misshapen mitochondria with damaged membranes[158,279]. In WT mice fed a HFD, we observe mitochondrial swelling and accumulation of damaged organelles in both intermyofibrillar and subsarcolemmal

muscle regions, similar to the results seen by Bonnard et al. in mice fed a HFD for 16 weeks[158]. Remarkably, CypD KO muscle mitochondria were not swollen and demonstrated minimal evidence of damaged organelles compared to WT muscle. Our data therefore support findings of other groups which document that inhibition of CypD prevents mitochondrial swelling[210,280]. However, the molecular significance of mPTP-mediated swelling and regulation of muscle fiber morphology in the context of insulin resistance remains to be resolved.

In summary, our data show that opening of the mPTP is required for insulin resistance in skeletal muscle. This finding is important because it demonstrates a mechanism whereby mitochondrial dysfunction is causally linked to insulin resistance. Despite the question regarding whether mitochondrial dysfunction is a cause or consequence of insulin resistance[169], our current data suggest that in the early onset of diet-induced insulin resistance in skeletal muscle that mitochondrial dysfunction precedes impairment in insulin action. However, we acknowledge that our data do not rule out the possibility that insulin resistance may also occur upstream of mitochondrial dysfunction in different experimental conditions or genetic models. For example, the muscle insulin receptor knockout mouse has skeletal muscle mitochondrial dysfunction[173]. Since mPTP opening is indicative of mitochondrial stress, one interpretation of the current data is that mPTP-induced insulin resistance represents an effort by the cell to decrease nutrient influx and reduce mitochondrial stress. This could also be the case in liver, where impairing mPTP opening may have disrupted the physiological response of mitochondria to nutrient overload, resulting in lipid accumulation and higher HGP[281,282]. This theory that insulin resistance may be a protective mechanism was originally hypothesized by

Unger[283] and is supported by more recent studies[138,284,285,286]. Even though insulin resistance may be protective in an acute setting, chronic insulin resistance promotes metabolic disease. Although the tissue-specific roles of the mPTP remain to be elucidated, the development of a skeletal muscle-specific mPTP inhibitor may have beneficial effects on glucose clearance in diabetics. Supporting this concept is the fact that metformin, one of the most effective anti-diabetes drugs, is a weak mPTP inhibitor[287] and improves skeletal muscle mitochondrial function and insulin sensitivity[288,289].

CHAPTER 4: LIPID PHOSPHATE PHOSPHATASE 1 REGULATES HEPATIC GLUCOSE PRODUCTION AND LIVER MITOCHONDRIA HOMEOSTASIS DURING FASTING

4.1 Introduction

The liver plays a vital role in maintaining whole body glucose homeostasis by releasing glucose into the blood during fasting. With fasting, hepatic glucose production (HGP) increases to maintain blood glucose concentrations within the normal physiological range. Fasting-induced HGP is dependent upon the coordinated upregulation of genes involved in gluconeogenesis and activation of glycogenolysis, including phosphoenolpyruvate carboxykinase (PEPCK), encoded by *Pck1* and glucose-6-phosphatase (G6pase), encoded by *G6pc*, respectively[58]. This transcriptional program is controlled by a balance between the stimulatory hormone glucagon released from the pancreas during fasting and the inhibitory hormone insulin secreted postprandially[32,58]. One of the most common defects in patients with insulin resistance is inadequate suppression of HGP upon feeding, which contributes to hyperglycemia and the progression towards type 2 diabetes[51]. Thus, understanding the molecular mechanisms underlying the control of HGP is crucial for the development of new diabetes therapies.

There is evidence that bioactive lipids such as lysophosphatidic acid (LPA) can affect hepatocyte glucose metabolism. LPA and other bioactive lipids signal through cognate G protein coupled receptors (GPCRs) to modulate glucose utilization[79,92], but current studies have reported contradictory and inconsistent effects. Previous work has demonstrated that LPA can alter liver glucose metabolism through either the administration of LPA receptor inhibitors to mice or treatment of mice or cells with exogenous LPA. Acute injections of LPA lowered blood glucose levels in diabetic mice[92], an effect that may be attributed to LPA potentiation of insulin signaling through Akt and inactivation of GSK3β[100]. However, LPA may also counter this signaling

pathway by activating glycogen phosphorylase[99], raising questions concerning the effects of LPA on glycogen metabolism. Furthermore, chronic administration of the LPA receptor inhibitor Ki16425 to HFD-fed mice improved glucose tolerance, increased liver glycogen storage and reduced fasting levels of hepatic PEPCK and G6Pase[79]. These data suggest that blockade of LPA signaling has beneficial effects on whole body glucose homeostasis, at least in part by dampening the transcriptional program that promotes HGP. Therefore, the role of LPA in controlling hepatic glucose metabolism remains unclear. Expression of the LPA-generating enzyme autotaxin is increased in insulin resistance subjects[290], suggesting that enzymes controlling bioactive lipid signaling may be important regulatory nodes of hepatic glucose utilization in the context of nutrient stress.

Lipid phosphate phosphatase 1 (LPP1) is an integral membrane enzyme that catalyzes the hydrolysis of bioactive lipids. LPP1 acts primarily on LPA, converting it to monoacylglycerol (MAG), and this enzymatic action attenuates both LPA-mediated signaling through LPA receptors on the PM and intracellular LPA signaling[106,107,114]. However, few studies have explored the potential involvement of LPP1 in LPA-mediated effects on hepatic glucose metabolism. As a result, the role of the LPA-LPP1 signaling axis in the regulation of HGP is not known.

In order to investigate whether the LPA-LPP1 signaling axis is important for the control of HGP, we ablated LPP1 *in vivo*. Herein, we show that the LPP1 substrate LPA attenuates glucagon-mediated HGP in isolated hepatocytes and that loss of functional LPP1 in HFD-fed mice decreases gluconeogenic gene expression and HGP. Hepatocytes isolated from LPP1 KO mice show a trend towards lower glucose production under basal

conditions. Livers of fasted LPP1 KO mice show STAT3 activation, increased expression of mitochondrial respiratory subunits and upregulation of SOD2. This study uncovers a novel role for LPP1 in the regulation of HGP and liver mitochondria in the context of nutrient overload.

4.2 Results

4.2.1 LPA antagonizes glucagon-induced HGP in primary hepatocytes.

To investigate the role of LPA-LPP1 signaling in HGP, we first measured glucose release by isolated primary hepatocytes in the presence of the LPP1 substrate LPA. LPA is present in serum at levels between 300nM and10μM[75,291]. Treatment of WT hepatocytes with 2.5μM or 10μM LPA had no effect on basal glucose output, but decreased glucagon-induced HGP to levels not significantly different compared to vehicle-treated cells (Figure 32A). The signaling effects of LPA are curtailed by LPP1[106,114]. Consistent with a role for LPP1 in the degradation of LPA, hepatocytes from LPP1 KO mice accumulate more intracellular LPA after incubation with a physiological mixture of fatty acids (POL), without changes in PA or DAG (Figure 32B). These data suggest that the LPA-LPP1 signaling axis may influence hormonal stimulation of HGP in hepatocytes.

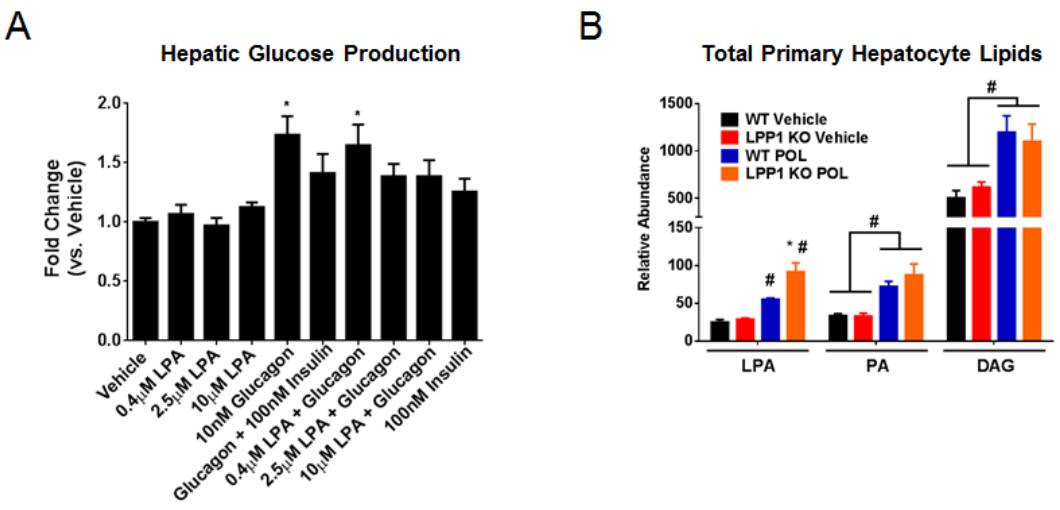

Figure 32. LPA attenuates glucagon-induced HGP in isolated primary hepatocytes. Primary hepatocytes were isolated from LPP1 KO and WT control mice as described in Materials and Methods, serum-starved for 16hrs and either incubated in glucose-free medium supplemented with 20mM lactic acid and 2mM sodium pyruvate for HGP measurement or harvested for lipid analysis by mass spectrometry. (A) Basal and glucagon-stimulated glucose production from WT hepatocytes after 13hrs in the absence or presence of LPA (0.4μM, 2.5μM or 10μM) or insulin (100nM); n = 5 separate experiments, from 3 independent hepatocyte isolations. (B) Lipidomics analyses of total lipids in 16hr serum-starved primary hepatocytes incubated for the last 3hrs in the presence of vehicle (BSA:ethanol) or a 1:2:1 palmitate oleate:linoleate (POL) mixture; n = 3 separate experiments from one hepatocyte isolation. For A, *$p < .05$ by one-way ANOVA compared to vehicle control. For B, $p < .05$ by two-way ANOVA between genotypes within the same treatment (*) or compared to the corresponding vehicle-treated control cells (#).

4.2.2 Ablation of LPP1 reduces HGP in vivo.

To determine whether loss of LPP1 affects HGP *in vivo*, we measured pyruvate-stimulated glucose output in overnight-fasted WT control mice and mice lacking LPP1 (Figure 33A). Despite LPP1 mRNA levels not being altered by fasting (Figure 33B), LPP1 KO mice fed a normal chow diet show a trend towards lower HGP compared with WT controls, as demonstrated by decreased blood glucose levels during the course of a PTT (Figure 33C). Since LPP1 expression is increased in the livers of diabetic mice (GEO Profiles, ID: 105483051) and exacerbated HGP is a common defect resulting from insulin resistance, we investigated whether loss of LPP1 could reduce HGP in the context of nutrient excess. We fed LPP1 KO and WT controls a HFD for up to 16 weeks and measured HGP via PTT. After 16 weeks of HFD, mice lacking functional LPP1 produced less glucose from pyruvate (Figure 33C-D) and had lower fasting blood glucose levels compared to their WT counterparts (Figure 33E). The blunted HGP was not associated with alterations in total body weight or tissue weights (Figure 34A-B). It is possible that the decreased HGP observed in LPP1 KO mice is due to increased circulating levels of, or enhanced sensitivity to, the HGP inhibitory hormone insulin. However, serum insulin levels (Figure 35A) and liver glycogen stores (Figure 35B) were similar between genotypes, both during fasting and after refeeding. Furthermore, ablation of LPP1 did not affect glucose or insulin tolerance (Figure 35C-F). Serum (Figure 36A) and liver (Figure 36B) triglycerides, liver cholesterol (Figure 36C) and liver LPAs (Figure 36D) were also comparable between LPP1 KO and WT control mice. Serum levels of unsaturated 20:4 LPA trended toward an increase in LPP1 KO mice (Figure 36E), but this change was not reflected in the total serum LPA levels (Figure 36F). Thus, aside from a small subset of

circulating LPAs, the blunted HGP in LPP1 KO mice is most likely not due to changes in these parameters.

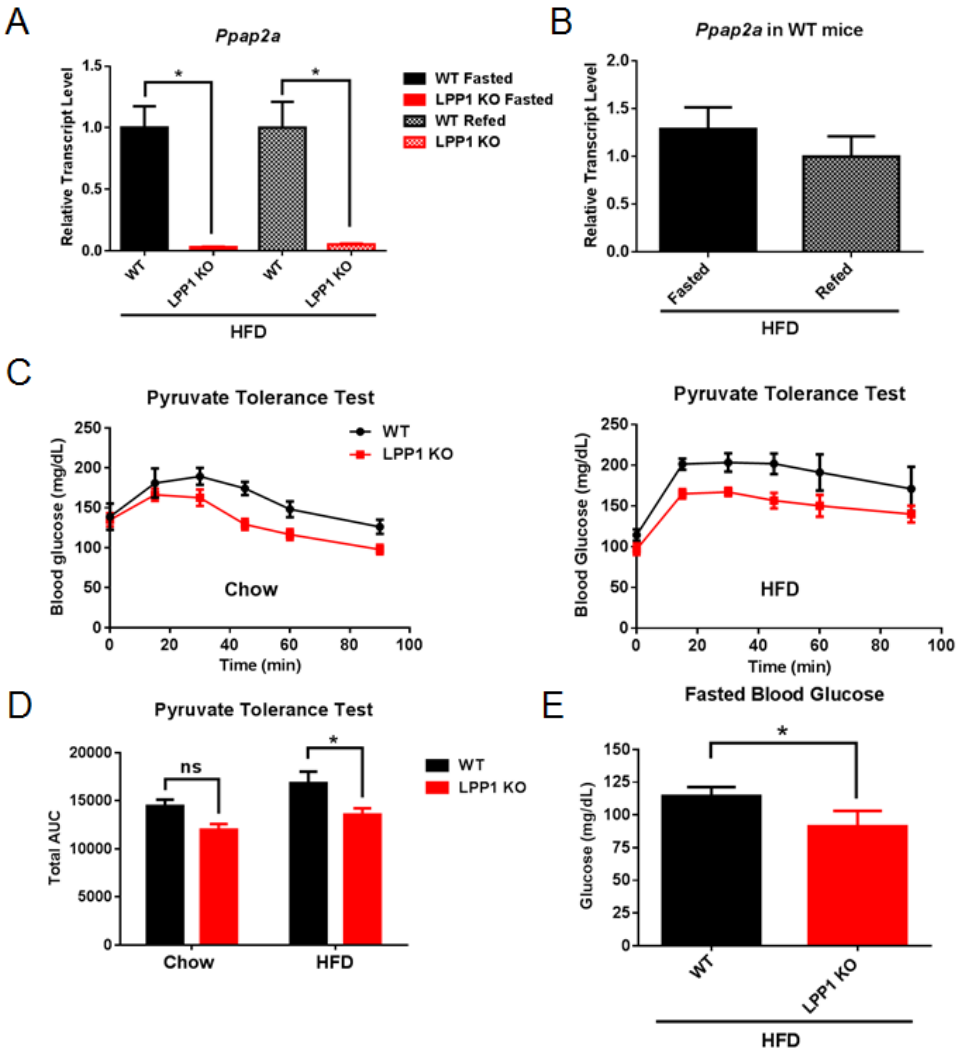

Figure 33. LPP1 deficiency reduces HGP *in vivo*.

(A-B) Expression of hepatic *Ppap2a* (LPP1) in HFD-fed mice in the fasted and refed states; n = 4-6 per genotype. (C) Pyruvate tolerance tests (PTTs) in overnight-fasted mice fed a chow or HFD diet for 15-17 weeks; for chow n = 6-10 per genotype and for HFD n = 7-8 per genotype. (D) Calculation of total AUC from PTTs shown in (C). (E) Blood glucose measurements in overnight-fasted LPP1 KO and WT control mice fed a HFD; n = 6-8 per genotype. All data are means ± SEM. For A and E, *p <. 05 by two-tailed, unpaired t-test. For D, *p < .05 by two-way ANOVA. ns, not significant.

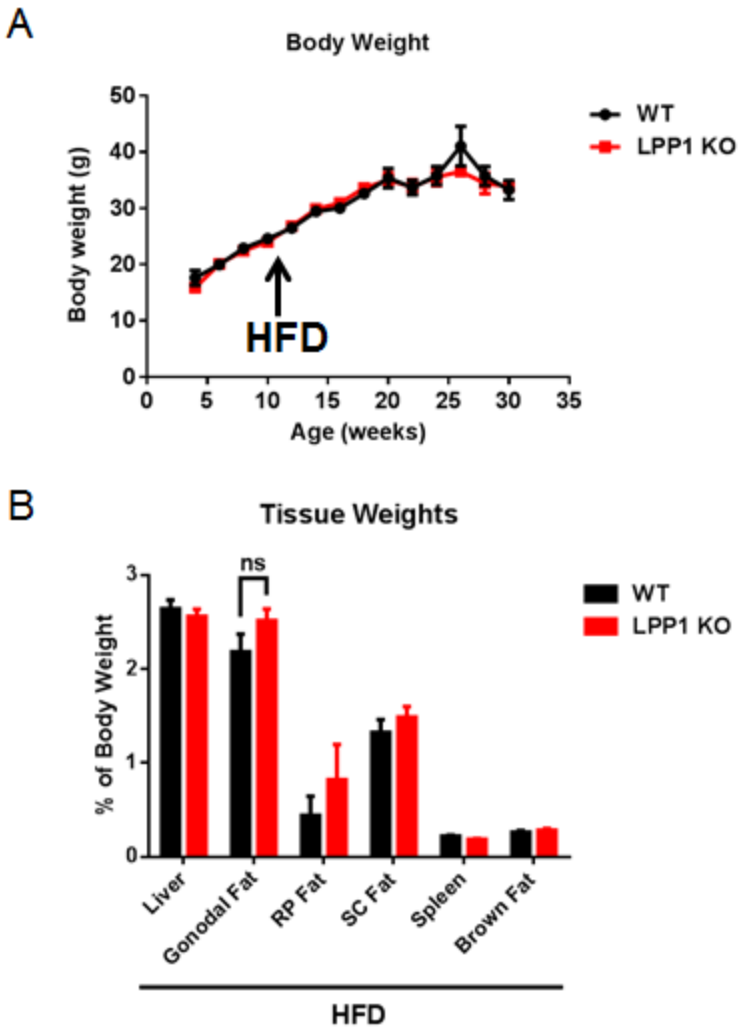

Figure 34. Body and tissue weights of LPP1 KO and WT control mice.

(A) Body weights of mice on chow diet and throughout the course of HFD feeding. Mice were fed a normal chow diet until approximately 10-12 weeks of age and were switched to a HFD for about 17 weeks. Body weights were monitored weekly and averaged, yielding weight values for each mouse for every two weeks; n = 16-21 per genotype. (B) Weights of tissues harvested from HFD-fed mice, expressed as percentage of total body weight for each mouse. RP (retroperitoneal) and SC (subcutaneous) fat; n = 4-20 per genotype. All data are means ± SEM. ns, not significant.

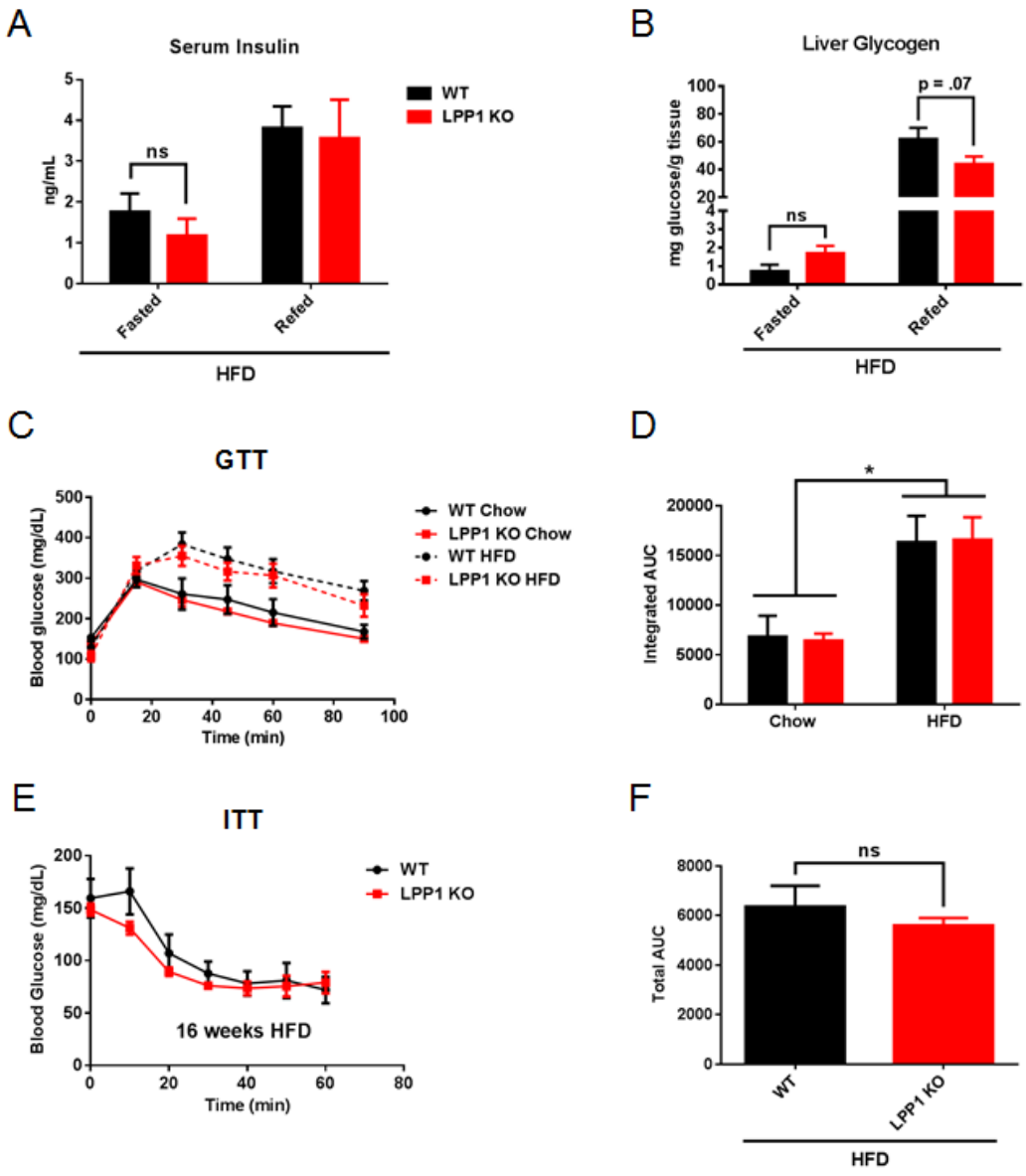

Figure 35. Serum insulin and insulin sensitivity in LPP1 KO and WT mice.

(A) Circulating insulin in the serum of fasted and refed mice on HFD; n = 6-7 per genotype. (B) Glycogen content in the livers of HFD-fed mice in the fasted and refed states; n = 4-5 per genotype. (C-D) GTTs administered to mice on chow diet or HFD for 15 weeks. Blood glucose levels (C) are shown after intraperitoneal injection with glucose, and the integrated AUC (D) was calculated; for chow n = 8-11 per genotype and for HFD n = 7-8 per genotype. (E-F) Insulin tolerance tests (ITTs) administered to mice on HFD

for 16 weeks. Blood glucose levels (E) were monitored over time after intraperitoneal injection with insulin, and the total AUC (F) was calculated; n = 4-5 per genotype. All data are means ± SEM. For D, *p < .05 by two-way ANOVA. ns, not significant.

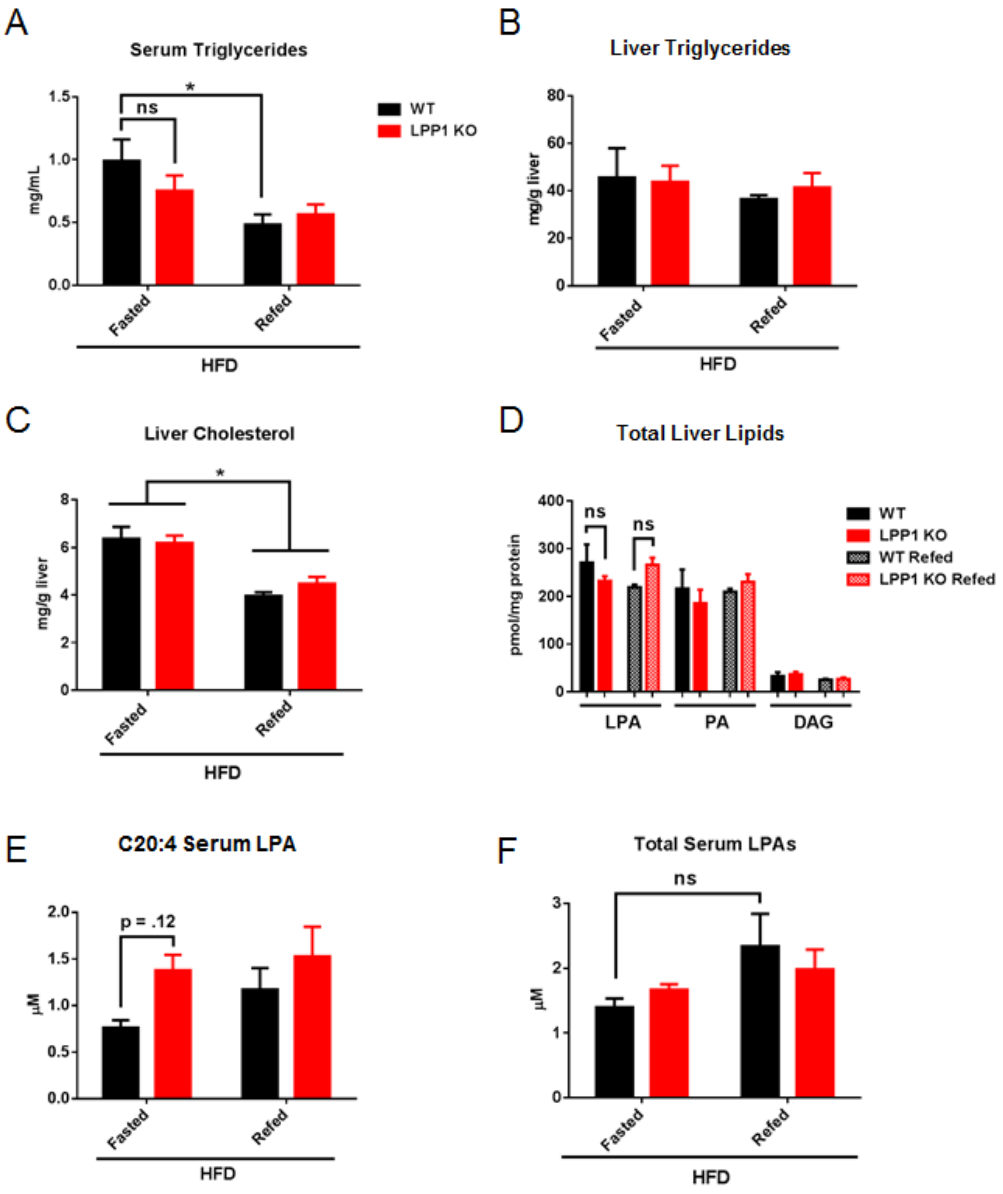

Figure 36. Liver and serum lipids of LPP1 KO and WT control mice on HFD.

(A-B) Triglycerides were quantified in the serum (A) and livers (B) of mice on HFD; for A, n = 9-13 per genotype and for B, n = 4-5 per genotype. (C) Liver cholesterol levels; n = 4-5 per genotype. (D-F) Lipidomics analyses in HFD-fed mice. Total levels of liver lysophosphatidic acids (LPAs), phosphatidic acids (PAs) and diacylglycerols (DAGs) (D) and C20:4 (E) or total serum LPAs (F) were measured by mass spectrometry; n = per 4-5

genotype. All data are means ± SEM. For A and C, *p < .05 by two-way ANOVA. ns, not significant.

4.2.3 Genetic ablation of LPP1 impairs fasting-induced PEPCK expression independent of CREB phosphorylation and insulin signaling.

The transcriptional program that promotes HGP during fasting ultimately leads to an increase in the expression of key gluconeogenic genes, including PEPCK and G6Pase in the liver [69]. Mice lacking LPP1 show significantly lower liver PEPCK mRNA and a trend towards decreased G6Pase in the fasted state (Figure 37A), compared with WT control mice on HFD. Loss of LPP1 also resulted in a modest reduction in PEPCK protein (Figure 37B). During fasting, the glucagon-PKA-CREB signaling axis is one of the major pathways that leads to the activation of gluconeogenic gene transcription in liver and induction of HGP[51]. Glucagon-mediated signaling through PKA culminates in the phosphorylation of CREB on Ser133, which activates the transcription factor and stimulates expression of its target genes, including PGC1α, PEPCK and G6Pase[51]. However, the impairment in fasting-activated gluconeogenic enzyme expression observed in the absence of LPP1 was not due to changes in CREB phosphorylation (Figure 37B), or transcriptional induction of PGC1α or the PGC1α target genes Cpt1a and MCAD (Figure 37A).

Insulin is a potent inhibitor of gluconeogenic gene expression and HGP and opposes the metabolic effects of glucagon in the liver[32]. Many of the inhibitory effects of insulin on HGP are mediated through the key downstream signaling intermediate Akt[51]. Loss of LPP1 did not affect liver insulin signaling through Akt (Figure 37C-D), nor change the inactivating phosphorylation (Ser256) of the pro-gluconeogenic transcription factor FOXO1 (Figure 37C-D), a major downstream target of the inhibitory actions of insulin. These data indicate that ablation of LPP1 *in vivo*, decreases gluconeogenic gene

expression in the liver and HGP in a manner that is independent of canonical insulin regulation of FOXO1 and the CREB-PGC1α transcriptional axis.

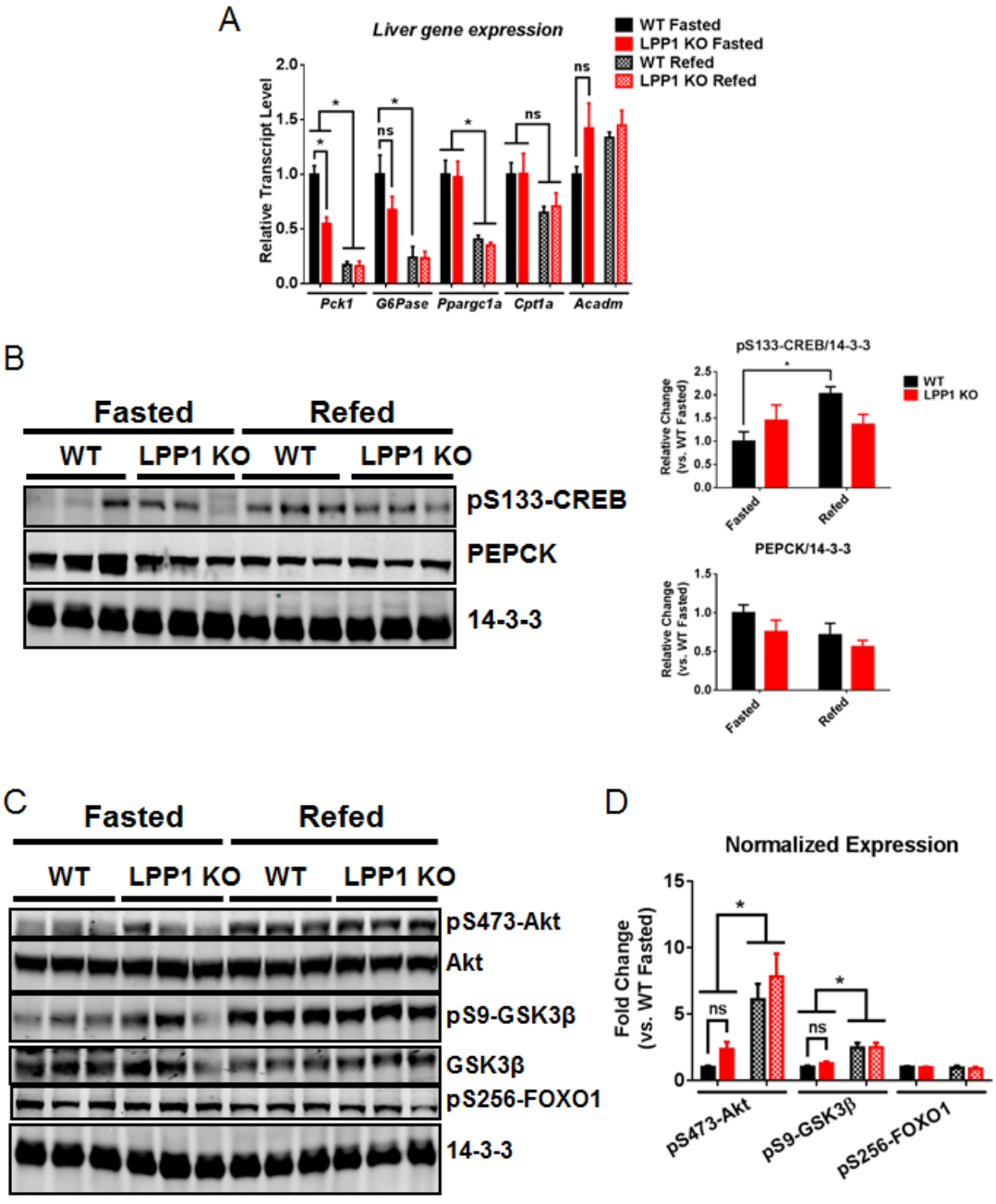

Figure 37. LPP1 KO mice show attenuated induction of PEPCK in response to fasting without changes in CREB phosphorylation or hepatic insulin signaling. (A) Expression of gluconeogenic genes and PGC1α target genes in livers of HFD-fed mice, measured via real-time qRT-PCR; n = 4-5 per genotype. (B) Representative Western blots of pS133-CREB and PEPCK in livers of mice on HFD with 14-3-3 as a

loading control. (C) Western blot analysis of insulin signaling pathway regulating gluconeogenic enzyme expression in the livers of mice fed a HFD, with 14-3-3 as a loading control. (D) Quantification of phospho-protein expression shown in (C), normalized to either total protein expression (pS473-Akt/Akt and pS9-GSK3β/GSK3β) or to 14-3-3 loading control (pS256-FOXO1). Data are expressed as fold change compared to fasted WT mice. All data are means ± SEM. For A, B and D, *p < .05 by two-way ANOVA . ns, not significant.

4.2.4 LPP1 KO mice show increased hepatic STAT3 activation during fasting.

The transcription factor STAT3 has been shown to inhibit HGP irrespective of insulin action and PGC1α[71]. STAT3 represses expression of liver PEPCK and G6pase[71,73] upon activating phosphorylation of the Y705 residue[71]. Therefore, we assessed tyrosine phosphorylation of STAT3 in livers of HFD-fed mice. In the fasted state, livers from LPP1 KO mice show higher phosphorylation of STAT3 at Y705, compared to WT mice (Figure 38A-B). Higher tyrosine phosphorylation of STAT3 in LPP1 KO livers was accompanied by increased expression of the STAT3 target gene *Socs3* (Figure 38C). Thus, the lower gluconeogenic gene expression in the absence of LPP1 may be due in part to STAT3-mediated transcriptional repression.

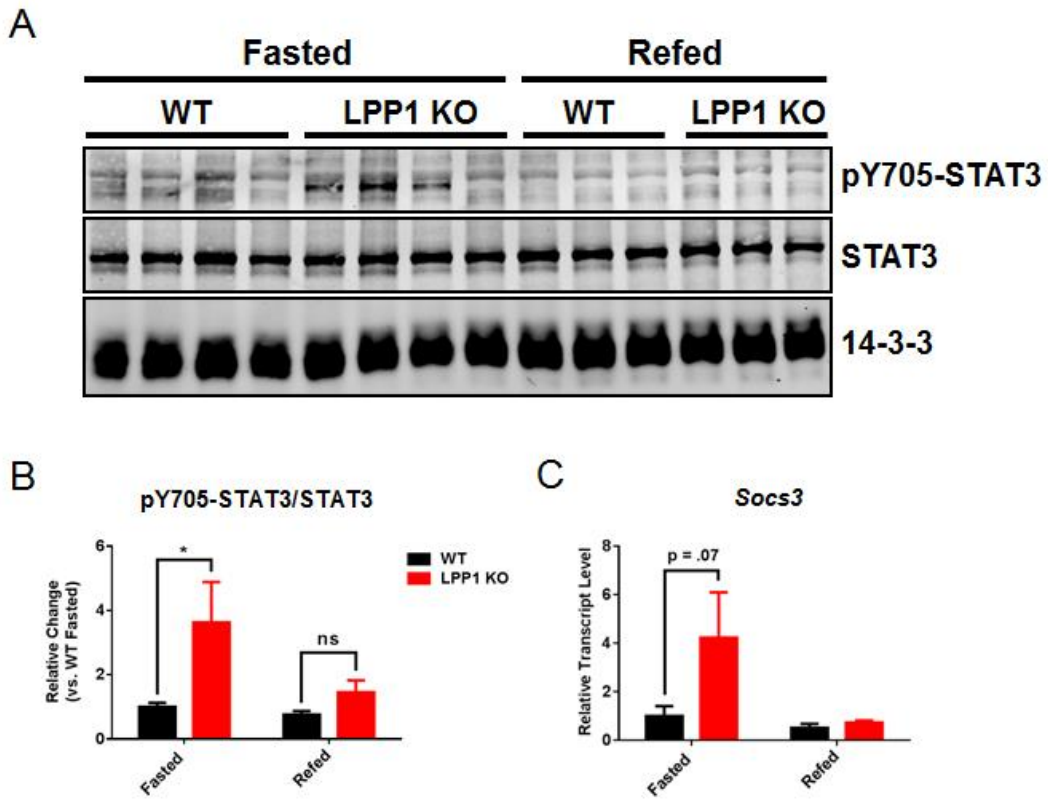

Figure 38. Lack of LPP1 increases liver STAT3 activation during fasting.

(A) Representative Western blots of pY705-STAT3 and total STAT3 in livers of WT and LPP1 KO on HFD, with 14-3-3 as a loading control. (B) Quantification of pY705-STAT3 normalized to total STAT3 levels; n = 4-5 per genotype. (C) Hepatic *Socs*3 gene expression in HFD-fed mice; n = 4-5 per genotype. All data are means ± SEM. *p < .05 by two-way ANOVA . ns, not significant.

4.2.5 Hepatocytes lacking functional LPP1 show a modest decrease in basal glucose production.

To determine whether the decreased HGP in mice lacking LPP1 was a cell autonomous phenomenon, we isolated primary hepatocytes from LPP1 KO and WT control mice and measured glucose output in the presence of the gluconeogenic substrates pyruvate and lactic acid. LPP1 KO hepatocytes showed a trend towards reduced basal glucose production (Vehicle) but released a similar amount of glucose compared to WT cells in response to glucagon (Figure 39A). Ablation of LPP1 did not alter expression of the gluconeogenic genes PEPCK and G6pase unless in the presence of serum (Figure 39B). Lack of LPP1 did not augment hepatocyte insulin signaling through Akt (Figure 39C) or the ability of insulin to suppress glucose production in hepatocytes (Figure 39D). These results indicate that loss of LPP1 in hepatocytes *per se* may contribute to the lower HGP in LPP1 KO mice, but the reduction in gluconeogenic genes probably occurs in response to a circulating factor *in vivo*.

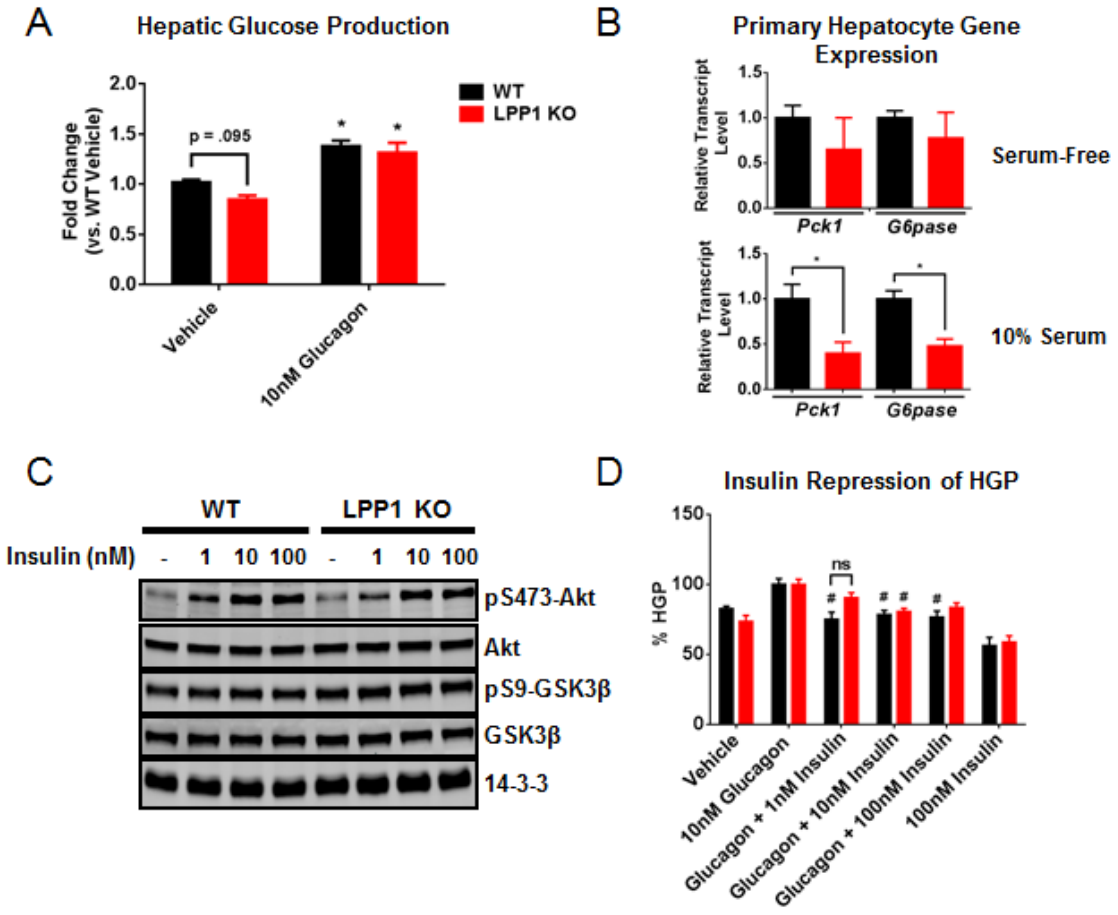

Figure 39. Hepatocytes lacking LPP1 show a modest reduction in basal glucose production.

Primary hepatocytes were isolated from LPP1 KO and WT control mice as described in Materials and Methods and serum-starved for 16hrs before incubation in glucose-free medium for glucose production measurement. For RNA, hepatocytes were incubated for 13hrs in the absence or presence of serum (10% fetal bovine serum), the serum-free or serum-rich media were refreshed and cells were harvested 3hrs later. (A) Glucose production from LPP1 KO and WT primary hepatocytes after a 13hr incubation in glucose-free DMEM in the absence or presence of 10nM glucagon; results from 3 independent experiments each from 4-5 separate paired hepatocyte isolations. (B) Gluconeogenic gene expression measured via real-time qRT-PCR in isolated hepatocytes

incubated in serum-free or serum-containing media; results of 5-7 independent experiments derived from two separate hepatocyte isolations. (C) Western blot analysis of insulin-stimulated phosphorylation of Akt at S473 and GSK3β at S9 in serum-starved LPP1 KO and WT control hepatocytes with 14-3-3 as a loading control; representative blot from 3 independent experiments. (D) Glucagon-induced glucose production from primary hepatocytes measured as noted in (A) in the absence or presence of insulin (1-100nM); n = 5-6 separate experiments, from 2 independent hepatocyte isolations. All data are means ± SEM. For A, *$p < .05$ by two-way ANOVA compared to the corresponding vehicle. For B, *$p < .05$ by two-tailed, unpaired t-test. For D, #$p < .05$ by two-way ANOVA compared to the corresponding glucagon control. ns, not significant.

4.2.6 Loss of LPP1 alters hepatic phospholipid content.

LPP1 could also potentially regulate hepatic phospholipid metabolism by controlling levels of the phospholipid precursors LPA, PA and DAG[113]. Loss of LPP1 significantly decreased levels of the phospholipids PE and PS in hepatocytes (Figure 40A). Despite unaltered LPA, PA or DAG (Figure 36D), livers from LPP1 KO mice showed decreased levels of PE and PC in the fasted state (Figure 40B). These data suggest that LPP1 plays a critical role in maintaining hepatic phospholipid levels, especially PE.

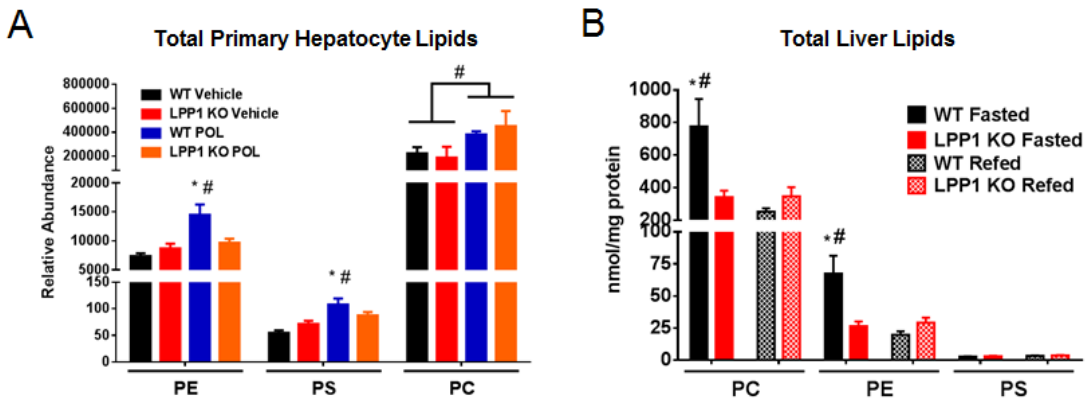

Figure 40. Loss of LPP1 disrupts hepatic phospholipid metabolism.

(A) Lipidomics analyses of total phospholipids in serum-starved primary hepatocytes incubated for 3hrs in the presence of vehicle (BSA:ethanol) or a 1:2:1 palmitate:oleate:linoleate (POL) mixture; n = 3 separate experiments from one hepatocyte isolation. (B) Lipidomics measurements of total phospholipids in livers from HFD-fed mice; n = 4-5 per genotype. All data are means ± SEM. For A, $p < .05$ by two-way ANOVA between genotypes within the same treatment (*) or compared to the corresponding vehicle-treated control cells (#). For B, $p < .05$ by two-way ANOVA between genotypes within the same nutritional state (*) or compared to the same genotype in the refed state (#).

4.2.7 Loss of LPP1 alters mitochondrial homeostasis in the livers of HFD-fed mice.

During fasting, HGP is mainly fueled by the synthesis of high energy phosphate molecules (e.g. ATP and GTP) by mitochondria[292], which is heavily dependent upon electron flow through ETC complexes and the coordinate generation of the electrochemical gradient across the inner mitochondrial membrane[147]. PE is a major mitochondrial inner membrane lipid[293] required for ETC complex stability[293,294], and STAT3 regulates mitochondrial respiration[295]. Therefore, to determine if ablation of LPP1 was associated with alterations in mitochondrial OXPHOS, we measured hepatic expression of protein subunits of ETC complexes I-IV and ATP synthase (Complex V). Compared to WT control mice on HFD, livers from fasted LPP1 KO mice showed higher expression of the Complex II subunit SDHB and subtle increases in the Complex III UQCRC2 subunit and the ATP synthase catalytic ATP5A subunit (Figure 41A-B). Higher expression of these subunits was most likely not due to increased mitochondrial mass, as evidenced by similar expression of the mitochondrial marker VDAC (Figure 41A-B). However, upregulation of Complexes II, III and V were not observed in isolated hepatocytes devoid of LPP1 (Figure 41C).

HFD increases mitochondrial ROS in murine liver[296], which is counteracted through induction of the oxidative stress-sensing transcription factor Nrf2[132,133] and the mitochondrial anti-oxidant enzyme SOD2[138]. During fasting, LPP1 ablation upregulated hepatic SOD2 levels (Figure 41D) and increased expression of *Nfe2l2,* which encodes Nrf2 (Figure 41E), suggesting an altered redox state in LPP1 KO liver mitochondria. Overall, these data uncover a new role for LPP1 in the regulation of liver mitochondria homeostasis and HGP during fasting.

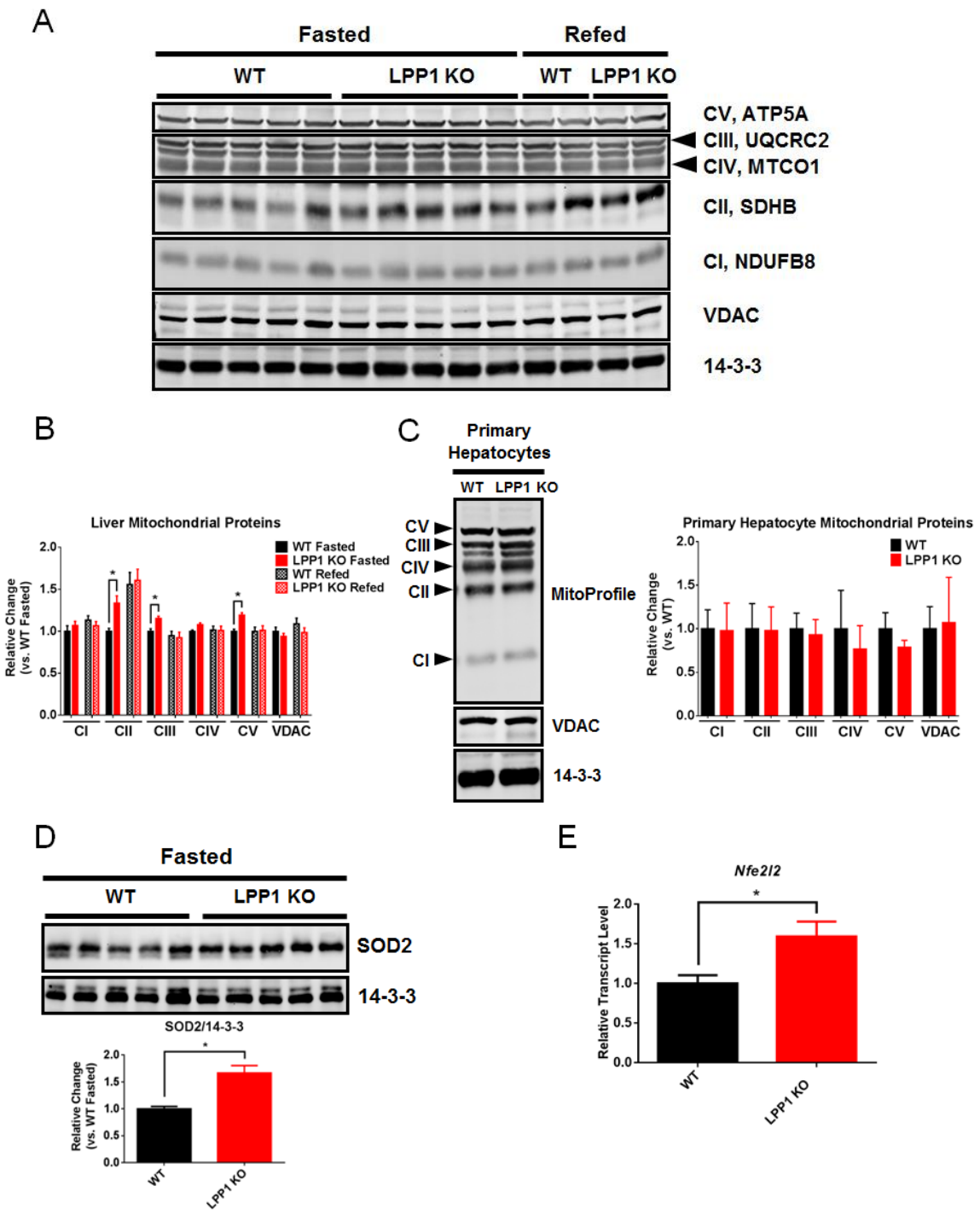

Figure 41. Expression of mitochondrial respiratory subunits and markers of antioxidant response in livers from HFD-fed mice and primary hepatocytes.

(A) Representative Western blots of liver samples from HFD-fed mice probed with an antibody against VDAC or the MitoProfile Total OXPHOS Rodent WB Antibody

Cocktail to measure expression of ATP Synthase (Complex V, ATP5A subunit) and ETC complexes I (NDUFB8 subunit), II (SDHB subunit), III (UQCRC2 subunit) and IV (MTCO1 subunit). Expression of 14-3-3 was used as a loading control. (B) Quantification of mitochondrial protein expression in (A), normalized to the loading control 14-3-3; n = 4-5 per genotype. (C) MitoProfile analysis and VDAC expression in serum-starved primary hepatocytes; representative blot from 3 independent hepatocyte isolations. (D) Representative Western blot and quantification of SOD2 expression normalized to 14-3-3 in livers from HFD-fed mice; n = 3 separate blots with 5 per genotype for quantification. (E) Hepatic *Nfe2l2* (Nrf2) expression in fasted mice on HFD; n = 4-5 per genotype. *p < .05 by two-way ANOVA (B), or by two-tailed, unpaired t-test (D-E).

4.3 Discussion

Hepatic glucose production (HGP) is a vital process that sustains energy supply to glucose-dependent organs such as the brain during fasting. However, excessive HGP which occurs as a result of insulin resistance can be detrimental, promoting hyperglycemia and type 2 diabetes. The liver is a metabolic hub that integrates both glucose and lipid flux, as demonstrated by the ability of several lipid species to alter HGP[44,101,297]. Bioactive lipids, including LPA are potent signaling molecules that influence liver growth and regeneration[298] and energy consumption[79], but it is not known if bioactive lipid signaling pathways are an important element in HGP regulation. The purpose of this study was to investigate the role of LPA and the LPA-degrading enzyme LPP1 in the regulation of HGP.

The LPP1 substrate LPA is known to affect glucose homeostasis, but the underlying mechanisms are not clear. In this study, we uncovered a novel regulatory role for LPA-LPP1 signaling in HGP and liver mitochondria homeostasis during fasting. Mice lacking LPP1 show lower expression of the gluconeogenic genes PEPCK and G6Pase and decreased pyruvate-stimulated HGP. These findings are consistent with the notion of LPA signaling intersecting with glucose metabolism pathways *in vivo*, as acute administration of LPA lowered blood glucose in mice in an LPA receptor-dependent manner[92]. Interestingly, LPA can also acutely impair glucose clearance in mice, and pharmacological blockade of LPA receptors improves glucose tolerance and insulin sensitivity in HFD-fed mice[79]. In contrast, we observed that ablation of LPP1 inhibited HGP during HFD without changes in insulin action or total levels of circulating LPA. Manipulating LPP1 expression may not be sufficient to significantly alter serum LPA

levels in mice on HFD, since LPA synthesis is already elevated during HFD[79], which may activate compensatory pathways to degrade LPA. Therefore, disrupting the LPA-LPP1 signaling axis at different nodes influences glucose metabolism, but yields variable outcomes. In the case of LPP1 inhibition in mice, the blunted HGP could arise from changes in signaling downstream of LPA.

STAT3 plays a critical role in coordinating hepatic glucose metabolism in the liver. Upon phosphorylation of Y705, STAT3 translocates to the nucleus and exerts transcriptional control over its target genes. Nuclear STAT3 induces SOCS3 and suppresses PEPCK and G6Pase[71] and inhibits HGP[73]. LPP1 KO mice show greater pY705-STAT3 after an overnight fast, the same condition under which we observed reduced HGP by PTT. In mice fed a normal diet, fasting decreases pY705-STAT3, whereas refeeding stimulates STAT3 tyrosine phosphorylation[73]. STAT3 inhibition of HGP is counteracted during fasting by Sirt1-mediated deacetylation of STAT3[73], implying that the STAT3-HGP pathway is regulated by nutrient status. However, it remains unknown exactly how LPP1 deletion leads to higher STAT3 phosphorylation and if this increased STAT3 activation is responsible for HGP inhibition in LPP1 KO mice.

It is intriguing that the attenuated gluconeogenesis phenotype manifested in isolated hepatocytes only in the basal state. Hepatocytes isolated from LPP1 KO mice showed a trend toward reduced glucose production in the absence of any hormones, yet retained the ability to induce HGP in response to glucagon and inhibited HGP in response to insulin to the same degree as WT cells. Thus, LPP1 expression in hepatocytes may govern baseline HGP without influencing the capacity to respond to hormones.

Interestingly, this reduction in basal HGP in serum-starved cells was not accompanied by decreased PEPCK or G6Pase gene expression, but may instead occur through posttranslational modifications of these proteins[299], changes in other gluconeogenic genes or alterations in other metabolic pathways. However, the mechanism underlying the decreased basal HGP in the absence of LPP1 is still unknown. Only when serum is added back to hepatocytes do LPP1 KO cells show decreased PEPCK and G6Pase expression. Thus, a serum-borne factor could be mediating the transcriptional repression of gluconeogenic genes observed in LPP1 KO mouse hepatocytes and livers and ultimately accentuate the modest reduction in HGP due to the loss of LPP1.

It is important to note that exogenous LPA at a concentration (2.5μM) akin to that measured in the serum of refed WT mice (Figure 36F), had no effect on basal glucose production but decreased glucagon-stimulated glucose production in WT primary hepatocytes. These results would suggest that exogenous LPA may be signaling through receptors on the PM to inhibit glucagon action. In contrast, Sankella et al.[101] have shown that PA promotes HGP in primary hepatocytes, but concluded that LPA does not have any effect. The discrepancy in LPA effects on HGP may be due to differences in duration of lipid exposure. Sankella and colleagues treated hepatocytes with LPA for 30min, while we incubated hepatocytes with LPA for 13hrs. Thus, LPA may synergize with other factors *in vivo* to suppress HGP, most likely not through acute alterations in signaling but through long-term transcriptional-dependent mechanisms. To this end, both IL-6[71] and IL-13[69] suppress gluconeogenic gene expression in a STAT3 phosphorylation-dependent manner in primary hepatocytes and in mice. In sum, the diminished gluconeogenic program in LPP1 KO mice is likely due to multiple mechanisms which may involve both

the lack of hepatic LPP1 expression and the interaction of circulating factors with glucagon action in hepatocytes.

Hepatocytes lacking LPP1 also display an altered lipid profile. In the presence of fatty acids, loss of LPP1 resulted in significantly lower steady state levels of the phospholipid PE, a finding that was recapitulated *in vivo* in the liver of fasted LPP1 KO mice. Our findings are in line with previous work showing hepatocytes with significantly lower LPP1 expression contain lower levels of several PE species[300]. Furthermore, the LPP1 substrate S1P promotes PLD-dependent conversion of PE to phosphoethanolamine[301]. PE is not only a major PM component, but also a critical inner mitochondrial membrane lipid required for sustaining mitochondrial function[293,302]. However, it remains to be seen whether the lower PE content of LPP1 KO livers is associated with decreased mitochondrial PE. Taken together, LPP1 is critical for hepatic phospholipid metabolism, especially maintaining PE content.

Mitochondrial respiration supplies much of the energy needed for fasting-induced HGP. The fasted phenotype in LPP1 KO mice was also associated with alterations in ETC/OXPHOS subunit expression. Loss of LPP1 increased Complexes II, III and V (ATP synthase) without changes in the mitochondrial marker VDAC, which may point to differences in mitochondrial respiratory function and/or TCA cycle flux independent of mitochondrial content. It is possible that ablation of LPP1 also leads to redirection of pyruvate away from HGP and into the TCA cycle, subsequently increasing ETC complex activity. In support of this notion, mice lacking the cytosolic form of PEPCK (encoded by *Pck1* gene) in the liver fail to produce glucose from lactate and amino acids leading to a buildup of TCA cycle intermediates[303]. Manipulating hepatic PE levels disrupts HGP by

rerouting pyruvate toward the TCA cycle and enhances both ETC/OXPHOS protein expression and mitochondrial respiration[297]. Finally, genetic activation of Nrf2 accelerates TCA cycle flux[133] and increases mitochondrial respiration[304]. The elevated Nrf2 and SOD2 levels in LPP1 KO mice may indicate an attempt to mitigate excessive mitochondrial oxidative stress from ETC-derived $O_2^{\cdot}$, which can target[305] and inhibit[306] ATP synthase. Of note, fibroblasts from patients with ATP synthase deficiency show significantly decreased LPP1 expression[307], demonstrating that a link between LPP1 and mitochondrial function exists in humans. While LPA is critical for mitochondrial fusion/fission[123], the mechanism by which LPP1 modulates mitochondrial function in mice is not known. Our evidence points to LPP1 as an important regulator of mitochondrial adaptation to nutrient oversupply in the liver.

In summary, this study introduces a new regulatory component of the metabolic adaptations occurring during fasting. Specifically, our data suggest a novel role for the LPA-LPP1 signaling axis in hepatic glucose release and liver mitochondria homeostasis. We acknowledge that our results do not define a linear pathway from LPA through LPP1 to altered HGP. Exactly how loss of LPP1 in hepatocytes inhibits basal HGP and the component of serum responsible for lower gluconeogenic gene expression are not known. The role of LPA in attenuating HGP in WT hepatocytes and in mice lacking LPP1 is still not clear. In addition, STAT3 controls the transcription of many genes in the liver, and the repression of gluconeogenic genes could be secondary to other transcriptional modifications induced by STAT3. We also do not know the relative contribution of altered mitochondria homeostasis to HGP in the absence of LPP1. Increased ETC/OXPHOS subunit levels can indicate enhanced functional capacity or compensation

to correct inadequate functional capacity[169]. Nonetheless, these findings are significant for both uncovering metabolic relevance of LPP1 *in vivo* and for highlighting important regulatory nodes of gluconeogenesis that may be targeted to treat the excessive HGP in diabetic patients. This study lays the foundation for future work to elucidate the pathways connecting LPP1 expression to metabolic changes in HGP and mitochondria in the fasted liver.

CONCLUDING REMARKS AND FUTURE DIRECTIONS

The main goal of type 2 diabetes therapy is to reduce blood glucose levels toward the normal physiological range (70-100 mg/dL fasting and ≤180mg/dL postprandial)[28]. Reduction of blood glucose in diabetics can be achieved through promotion of insulin-stimulated glucose uptake and/or inhibition of HGP[308]. However, while mostly effective, current therapies including the insulin-sensitizing thiazolidinediones, the insulin secretagogue sulfonylureas, dipeptidyl peptidase 4 inhibitors, and even the biguanide metformin can have serious side effects and may lose their efficacy over time[28,309]. Thus, there is a need to develop safer, more efficacious treatments for type 2 diabetes, which requires a better understanding of the molecular events underlying glucose uptake and HGP.

This study identified novel mitochondria-associated pathways by which insulin-stimulated glucose uptake and fasting-induced HGP are regulated in the context of overnutrition. We have characterized a new mode of skeletal muscle insulin resistance and control of HGP mediated by the mPTP and introduced a previously unknown link between the bioactive lipid hydrolyzing enzyme LPP1, HGP and liver mitochondria homeostasis. The results described herein are a significant advance to the field of diabetes research, as both novel pathways will provide a wealth of potential targets for treatment of hyperglycemia in diabetics. With respect to the mPTP, CsA is not a feasible option for treating diabetes since CsA is well known to cause insulin resistance[310]. Our data suggest that specific inhibition of CypD may help attenuate hyperglycemia by increasing skeletal muscle glucose uptake. However, the complex tissue-specific metabolic effects of CypD deletion should serve as a note of caution if CypD is pursued as a drug target for

metabolic disease. A greater number of potential druggable targets will become apparent as future work will elucidate the molecular mechanisms underpinning mPTP-mediated changes in insulin sensitivity in various tissues and LPP1-dependent alterations in HGP.

The mechanisms by which the mPTP and LPP1 augment insulin sensitivity and HGP remain unknown. Given the physiological role of the mPTP as a mitochondrion-cytoplasm conduit, it is conceivable that blockade of the mPTP via CypD inhibition prevents the passage of a metabolite or ion which normally impedes insulin-stimulated GLUT4 trafficking and subsequent glucose uptake. In addition, closure of the mPTP may protect mitochondrial membrane potential and prevent the consumption of cytosolic ATP by ATP synthase, thereby leaving more ATP available for full insulin stimulation of GLUT4 translocation to the PM. It is interesting to note that ablation of hepatic CypD disrupted glucose and lipid metabolism in the liver. The enhanced HGP in mice lacking liver CypD may be due to increased G6pase protein[281]. The observed hepatic lipid accumulation in CypD LKO livers may be the outcome of upregulation of lipogenic genes, as CsA is known to increase expression of fatty acid synthase and acetyl-coA carboxylases 1 and 2 in the liver of rats[282]. Yet whether these effects are due to mPTP inhibition by targeting CypD or through mPTP-independent mechanisms is not known. Future work will: 1) identify the metabolite or molecule that traverses the mPTP to cause insulin resistance in skeletal muscle, 2) determine which tissue(s) is(are) responsible for the increased skeletal muscle glucose uptake in whole-body CypD KO animals, and 3) assess mitochondrial function *in situ* in the absence of CypD.

Very little is known about the role of LPP1 in liver glucose metabolism. While loss of LPP1 expression attenuates basal glucose production in hepatocytes, the LPP1

substrate LPA blunts glucagon-induced glucose production in WT hepatocytes. The latter effect may be due to direct antagonism of glucagon receptor signaling[311] by reduction of cAMP levels[75]. In mice, ablation of LPP1 increases activation of the gluconeogenic gene transcriptional repressor STAT3 and reduces PEPCK and G6Pase expression. Interestingly, mitochondrial localization of STAT3 increases activities of ETC Complexes I, II and V (ATP synthase) and decreases ROS production via induction of SOD2[295]. Given the dual role of STAT3 as an inhibitor of HGP and a regulator of mitochondrial respiration, it is possible that STAT3 is responsible for the observed changes in both HGP and liver mitochondria in fasted LPP1 KO mice. Likewise, while LPA signaling promotes Nrf2-dependent induction of antioxidant genes in hepatocytes[146], Nrf2 also represses gluconeogenesis[145], an effect that may be attributed to IL-6 mediated activation of STAT3[312]. Loss of LPP1 also reduces hepatocyte and liver PE, possibly through a phospholipase D-dependent mechanism. Reduction in liver PE could also be associated with lower mitochondrial PE. Lower mitochondrial membrane PE along with higher STAT3 activation and Nrf2 expression could alter mitochondrial protein expression, modify TCA cycle/OXPHOS, and regulate ATP and GTP stores available to fuel HGP. Future work will: 1) determine how LPA counteracts glucagon action in hepatocytes, 2) uncover how LPP1 expression regulates basal glucose production in hepatocytes, 3) identify the factor in serum responsible for suppressing gluconeogenic genes in LPP1 KO hepatocytes, 4) verify whether loss of LPP1 leads to changes in redox status and/or mitochondrial dysfunction, 5) determine if STAT3 or Nrf2 is responsible for lower gluconeogenic gene expression, altered mitochondrial homeostasis and decreased PE content in livers of LPP1 KO mice, 6) assess whether LPP1 expression affects

mitochondrial lipid composition, and 7) delineate the sequence of molecular events subsequent to LPP1 inhibition.

Overall, our findings contribute new mitochondria-related pathways regulating insulin-stimulated skeletal muscle glucose uptake and liver-derived glucose production, two vital processes controlling glycemia. Discovering the mPTP and LPP1 as crucial metabolic sensors will not only facilitate a better understanding of their respective functions but may also provide more impetus to target the mitochondrion for treatment of diabetes.

PUBLICATIONS RESULTING FROM THIS WORK

Evan P. Taddeo, Jason A. Liao, Marin E. Healy, Stefan Hargett, Sujoy Lahiri, Jill K. Slack-Davis, Chien Li, Jose L. Tomsig, Kevin R. Lynch, Thurl E. Harris, and Kyle L. Hoehn. *Lipid phosphate phosphatase 1 regulates hepatic glucose production and liver mitochondria homeostasis during fasting.* In preparation.

Rhianna C. Laker, **Evan P. Taddeo,** Yasir N. Akhtar, Mei Zhang, Kyle L. Hoehn, and Zhen Yan. *The mitochondrial permeability transition pore regulator cyclophilin D exhibits tissue-specific control of metabolic homeostasis.* In preparation.

Evan P. Taddeo, Rhianna C. Laker, David S. Breen, Yasir N. Akhtar, Brandon M. Kenwood, Jason A. Liao, Mei Zhang, Daniel J. Fazakerley, Jose L. Tomsig, Thurl E. Harris, Susanna R. Keller, Jenny D. Chow, Kevin R. Lynch, Manabu Chokki, Jeffery D. Molkentin, Nigel Turner, David E. James, Zhen Yan, and Kyle L. Hoehn. *Opening of the mitochondrial permeability transition pore links mitochondrial dysfunction to insulin resistance in skeletal muscle.* ***Molecular Metabolism,*** 3(2):124-34, 2013.

REFERENCES

1. Peppa, M., Koliaki, C., Nikolopoulos, P. & Raptis, S. a. Skeletal muscle insulin resistance in endocrine disease. *J. Biomed. Biotechnol.* **2010,** 527850 (2010).

2. Abdul-Ghani, M. a & DeFronzo, R. a. Pathogenesis of insulin resistance in skeletal muscle. *J. Biomed. Biotechnol.* **2010,** 476279 (2010).

3. Saltiel, A. R. & Pessin, J. E. Insulin signaling pathways in time and space. *Trends Cell Biol.* **12,** 65–71 (2002).

4. Martins, A. R. *et al.* Mechanisms underlying skeletal muscle insulin resistance induced by fatty acids: importance of the mitochondrial function. *Lipids Health Dis.* **11,** 30 (2012).

5. R A DeFronzo, R Gunnarsson, O Björkman, M Olsson, and J. W. Effects of insulin on peripheral and splanchnic glucose metabolism in noninsulin-dependent (type II) diabetes mellitus. *Society* **74,** 702–707 (2008).

6. Eason, R. C., Archer, H. E., Akhtar, S. & Bailey, C. J. Lipoic acid increases glucose uptake by skeletal muscles of obese-diabetic ob/ob mice. *Diabetes. Obes. Metab.* **4,** 29–35 (2002).

7. Hansen, P. a *et al.* A high fat diet impairs stimulation of glucose transport in muscle. Functional evaluation of potential mechanisms. *J. Biol. Chem.* **273,** 26157–26163 (1998).

8. Abdul-Ghani, M. a. & Defronzo, R. a. Pathogenesis of insulin resistance in skeletal muscle. *J. Biomed. Biotechnol.* **2010,** (2010).

9. Yang, C. *et al.* Syntaxin 4 heterozygous knockout mice develop muscle insulin resistance. *J. Clin. Invest.* **107,** 1211–1213 (2001).

10. Freymond, D., Bogardus, C., Okubo, M., Stone, K. & Mott, D. Impaired insulin-stimulated muscle glycogen synthase activation in vivo in man is related to low fasting glycogen synthase phosphatase activity. *J. Clin. Invest.* **82,** 1503–1509 (1988).

11. Petersen, K. F. *et al.* The role of skeletal muscle insulin resistance in the pathogenesis of the metabolic syndrome. *Proc. Natl. Acad. Sci. U. S. A.* **104,** 12587–12594 (2007).

12. Krook, A., Roth, R. a., Jiang, X. J., Zierath, J. R. & Wallberg-Henriksson, H. Insulin-stimulated Akt kinase activity is reduced in skeletal muscle from NIDDM subjects. *Diabetes* **47,** 1281–1286 (1998).

13. Hoehn, K. L. *et al.* IRS1-independent defects define major nodes of insulin resistance. *Cell Metab.* **7,** 421–433 (2008).

14. Kim, Y. B., Nikoulina, S. E., Ciaraldi, T. P., Henry, R. R. & Kahn, B. B. Normal insulin-dependent activation of Akt/protein kinase B, with diminished activation of phosphoinositide 3-kinase, in muscle in type 2 diabetes. *J. Clin. Invest.* **104,** 733–741 (1999).

15. Rowland, A. F., Fazakerley, D. J. & James, D. E. Mapping Insulin/GLUT4 Circuitry. *Traffic* **12,** 672–681 (2011).

16. Leto, D. & Saltiel, A. R. Regulation of glucose transport by insulin: traffic control of GLUT4. *Nat. Rev. Mol. Cell Biol.* **13,** 383–396 (2012).

17. Fecchi, K., Volonte, D., Hezel, M. P., Schmeck, K. & Galbiati, F. Spatial and temporal regulation of GLUT4 translocation by flotillin-1 and caveolin-3 in skeletal muscle cells. *FASEB J.* **20,** 705–707 (2006).

18. Lee, J. O. *et al.* Metformin regulates glucose transporter 4 (GLUT4) translocation through AMP-activated protein kinase (AMPK)-mediated Cbl/CAP signaling in 3T3-L1 preadipocyte cells. *J. Biol. Chem.* **287,** 44121–44129 (2012).

19. Chiang, S. H. *et al.* Insulin-stimulated GLUT4 translocation requires the CAP-dependent activation of TC10. *Nature* **410,** 944–948 (2001).

20. Mitra, P., Zheng, X. & Czech, M. P. RNAi-based analysis of CAP, Cbl, and CrkII function in the regulation of GLUT4 by insulin. *J. Biol. Chem.* **279,** 37431–37435 (2004).

21. Molero, J. C. *et al.* c-Cbl-deficient mice have reduced adiposity, higher energy expenditure, and improved peripheral insulin action. *J. Clin. Invest.* **114,** 1326–1333 (2004).

22. Kioumourtzoglou, D., Gould, G. W. & Bryant, N. J. Insulin stimulates syntaxin4 SNARE complex assembly via a novel regulatory mechanism. *Mol. Cell. Biol.* **34,** 1271–9 (2014).

23. Jewell, J. L. *et al.* Munc18c phosphorylation by the insulin receptor links cell signaling directly to SNARE exocytosis. *J. Cell Biol.* **193,** 185–199 (2011).

24. Cross, D. a, Alessi, D. R., Cohen, P., Andjelkovich, M. & Hemmings, B. a. Inhibition of glycogen synthase kinase-3 by insulin mediated by protein kinase B. *Nature* **378,** 785–9 (1995).

25. Suzuki, Y. *et al.* Insulin Control of Glycogen Metabolism in Knockout Mice Lacking the Muscle-Specific Protein Phosphatase PP1G / R GL. *Society* **21,** 2683–2694 (2001).

26. Kitamura, T. *et al.* Insulin-induced phosphorylation and activation of cyclic nucleotide phosphodiesterase 3B by the serine-threonine kinase Akt. *Mol. Cell. Biol.* **19,** 6286–6296 (1999).

27. Syed, N. a & Khandelwal, R. L. Reciprocal regulation of glycogen phosphorylase and glycogen synthase by insulin involving phosphatidylinositol-3 kinase and protein phosphatase-1 in HepG2 cells. *Mol. Cell. Biochem.* **211,** 123–136 (2000).

28. Nathan, D. M. *et al.* Medical management of hyperglycemia in type 2 diabetes: A consensus algorithm for the initiation and adjustment of therapy. *Diabetes Care* **32,** 193–203 (2009).

29. Petersen, K. F., Price, T., Cline, G. W., Rothman, D. L. & Shulman, G. I. Contribution of net hepatic glycogenolysis to glucose production during the early postprandial period. *Am. J. Physiol.* **270,** E186–E191 (1996).

30. Treadway, J., Mendys, P. & Hoover, D. Glycogen phosphorylase inhibitors for treatment of type 2 diabetes mellitus. *Expert Opin. Investig. Drugs* **10,** 439–454 (2001).

31. Roden, M., Petersen, K. F. & Schulman, G. Nuclear magnetic resonance studies of hepatic glucose metabolism in humans. *Recent Prog. Horm. Res.* **56,** 219–237 (2001).

32. Titchenell, P. M., Chu, Q., Monks, B. R. & Birnbaum, M. J. Hepatic insulin signalling is dispensable for suppression of glucose output by insulin in vivo. *Nat. Commun.* **6,** 7078 (2015).

33. Beck-Nielsen, H., Hother-Nielsen, O. & Staehr, P. Is hepatic glucose production increased in type 2 diabetes mellitus? *Curr Diab Rep* **2,** 231–236 (2002).

34. D'alessio, D. The role of dysregulated glucagon secretion in type 2 diabetes. *Diabetes, Obes. Metab.* **13,** 126–132 (2011).

35. Godoy-Matos, A. F. The role of glucagon on type 2 diabetes at a glance. *Diabetol. Metab. Syndr.* **6,** 91 (2014).

36. Cherrington, a. D. The role of hepatic insulin receptors in the regulation of glucose production. *J. Clin. Invest.* (2005). doi:10.1172/JCI200524233.3.

37. Szendroedi, J. *et al.* Abnormal hepatic energy homeostasis in type 2 diabetes. *Hepatology* **50,** 1079–1086 (2009).

38. Consoli, A. Role of liver in pathophysiology of NIDDM. *Diabetes Care* **15,** 430–441 (1992).

39. Magnusson, I., Rothman, D. L., Katz, L. D., Shulman, R. G. & Shulman, G. I. Increased rate of gluconeogenesis in type II diabetes mellitus. A 13C nuclear magnetic resonance study. *J. Clin. Invest.* **90,** 1323–1327 (1992).

40. Caton, P. W. *et al.* Metformin suppresses hepatic gluconeogenesis through induction of SIRT1 and GCN5. *J. Endocrinol.* **205,** 97–106 (2010).

41. Kim, Y. D. *et al.* Metformin inhibits hepatic gluconeogenesis through AMP-activated protein kinase-dependent regulation of the orphan nuclear receptor SHP. *Diabetes* **57,** 306–314 (2008).

42. Miller, R. a *et al.* Biguanides suppress hepatic glucagon signalling by decreasing production of cyclic AMP. *Nature* **494,** 256–60 (2013).

43. Ramnanan, C. J., Edgerton, D. S., Kraft, G. & Cherrington, a. D. Physiologic action of glucagon on liver glucose metabolism. *Diabetes, Obes. Metab.* **13,** 118–125 (2011).

44. Lam, T. K. *et al.* Mechanisms of the free fatty acid-induced increase in hepatic glucose production. *Am J Physiol Endocrinol Metab* **284,** E863–73 (2003).

45. Rebrin, K., Steil, G. M., Mittelman, S. D. & Bergman, R. N. Causal linkage between insulin suppression of lipolysis and suppression of liver glucose output in dogs. *J. Clin. Invest.* **98,** 741–749 (1996).

46. Katz, J. & Tayek, J. a. Gluconeogenesis and the Cori cycle in 12-, 20-, and 40-h-fasted humans. *Am. J. Physiol.* **275,** E537–E542 (1998).

47. Kuo, T., Harris, C. a. & Wang, J. C. Metabolic functions of glucocorticoid receptor in skeletal muscle. *Mol. Cell. Endocrinol.* **380,** 79–88 (2013).

48. Torres, T. P. *et al.* Impact of a glycogen phosphorylase inhibitor and metformin on basal and glucagon-stimulated hepatic glucose flux in conscious dogs. *J. Pharmacol. Exp. Ther.* **337,** 610–620 (2011).

49. Pernicova, I. & Korbonits, M. Metformin--mode of action and clinical implications for diabetes and cancer. *Nat. Rev. Endocrinol.* **10,** 143–156 (2014).

50. Pilkis, S., El-Maghrabi, M., McGrane, M., Pilkis, J. & Claus, T. Regulation by glucagon of hepatic pyruvate kinase, 6-phosphofructo 1-kinase, and fructose-1,6-bisphosphatase. *Fed. Proc.* **41,** 2623–2628 (1982).

51. Lin, H. V. & Accili, D. Hormonal regulation of hepatic glucose production in health and disease. *Cell Metab.* **14,** 9–19 (2011).

52. Newgard, C. B., Brady, M. J., Doherty, R. M. O. & Saltiel, A. R. Organizing Glucose Disposal. **3,** 1967–1977 (1967).

53. Rondinone, C. M. *et al.* Phosphorylation of PDE3B by phosphatidylinositol 3-kinase associated with the insulin receptor. *J. Biol. Chem.* **275,** 10093–10098 (2000).

54. Bechmann, L. P. *et al.* The interaction of hepatic lipid and glucose metabolism in liver diseases. *J. Hepatol.* **56,** 952–964 (2012).

55. Mor, I., Cheung, E. C. & Vousden, K. H. Control of glycolysis through regulation of PFK1: Old friends and recent additions. *Cold Spring Harb. Symp. Quant. Biol.* **76,** 211–216 (2011).

56. Schaftingen, E. V. Inhibition of Fructose-1, 6-bisphosphatase by Fructose 2,6-bisphosphate. *Proc. Natl. Acad. Sci.* **78,** 2861–2863 (1981).

57. Assimacopoulos-Jeannet, F. & Jeanrenaud, B. Insulin activates 6-phosphofructo-2-kinase and pyruvate kinase in the liver. Indirect evidence for an action via a phosphatase. *J. Biol. Chem.* **265,** 7202–7206 (1990).

58. Jitrapakdee, S. Transcription factors and coactivators controlling nutrient and hormonal regulation of hepatic gluconeogenesis. *Int. J. Biochem. Cell Biol.* **44,** 33–45 (2012).

59. Wang, Y., Vera, L., Fischer, W. H. & Montminy, M. The CREB coactivator CRTC2 links hepatic ER stress and fasting gluconeogenesis. *Nature* **460,** 534–537 (2009).

60. Li, X. & Kazgan, N. Mammalian Sirtuins and Energy Metabolism. *Int. J. Biol. Sci.* **7,** 575–587 (2011).

61. Puigserver, P. *et al.* Insulin-regulated hepatic gluconeogenesis through FOXO1 – PGC-1 a interaction. *Nature* **423,** 550–555 (2003).

62. Dentin, R. *et al.* Insulin modulates gluconeogenesis by inhibition of the coactivator TORC2. *Nature* **449,** 366–369 (2007).

63. Yamagata, K. *et al.* Bile acids regulate gluconeogenic gene expression via small heterodimer partner-mediated repression of hepatocyte nuclear factor 4 and Foxo1. *J. Biol. Chem.* **279,** 23158–23165 (2004).

64. Kraemer, F. B. & Shen, W.-J. Hormone-sensitive lipase: control of intracellular tri-(di-)acylglycerol and cholesteryl ester hydrolysis. *J. Lipid Res.* **43,** 1585–1594 (2002).

65. MacDougald, O. a & Burant, C. F. Obesity and metabolic perturbations after loss of aquaporin 7, the adipose glycerol transporter. *Proc. Natl. Acad. Sci. U. S. A.* **102,** 10759–10760 (2005).

66. Liu, Z., Long, W., Fryburg, D. A. & Barrett, E. J. The regulation of body and skeletal muscle protein metabolism by hormones and amino acids. *J. Nutr.* 212–217 (2006).

67. Grizard, J. *et al.* Insulin action on skeletal muscle protein metabolism during catabolic states. *Reprod. Nutr. Dev.* **39,** 61–74 (1999).

68. Houtkooper, R. H., Pirinen, E. & Auwerx, J. Sirtuins as regulators of metabolism and healthspan. *Nat. Rev. Mol. Cell Biol.* **13,** 225–238 (2012).

69. Stanya, K. J. *et al.* Direct control of hepatic glucose production by interleukin-13 in mice. *J. Clin. Invest.* **123,** 261–271 (2013).

70. Reilly, S. M. *et al.* A subcutaneous adipose tissue–liver signalling axis controls hepatic gluconeogenesis. *Nat. Commun.* **6,** 6047 (2015).

71. Inoue, H. *et al.* Role of STAT-3 in regulation of hepatic gluconeogenic genes and carbohydrate metabolism in vivo. *Nat. Med.* **10,** 168–174 (2004).

72. Bravard, A. *et al.* FTO contributes to hepatic metabolism regulation through regulation of leptin action and STAT3 signalling in liver. *Cell Commun. Signal.* **12,** 4 (2014).

73. Nie, Y. *et al.* STAT3 inhibition of gluconeogenesis is downregulated by SirT1. *Nat. Cell Biol.* **11,** 492–500 (2009).

74. Bartke, N. & Hannun, Y. a. Bioactive sphingolipids: metabolism and function. *J. Lipid Res.* **50 Suppl,** S91–S96 (2009).

75. Lin, M. E., Herr, D. R. & Chun, J. Lysophosphatidic acid (LPA) receptors: Signaling properties and disease relevance. *Prostaglandins Other Lipid Mediat.* **91,** 130–138 (2010).

76. Levine, J. S., Koh, J. S., Triaca, V. & Lieberthal, W. Lysophosphatidic acid: a novel growth and survival factor for renal proximal tubular cells. *Am. J. Physiol.* **273,** F575–F585 (1997).

77. Long, J. S., Yokoyama, K., Tigyi, G., Pyne, N. J. & Pyne, S. Lipid phosphate phosphatase-1 regulates lysophosphatidic acid- and platelet-derived-growth-factor-induced cell migration. *Biochem. J.* **394,** 495–500 (2006).

78. Hannun, Y. a & Obeid, L. M. Principles of bioactive lipid signalling: lessons from sphingolipids. *Nat. Rev. Mol. Cell Biol.* **9,** 139–150 (2008).

79. Rancoule, C. *et al.* Lysophosphatidic acid impairs glucose homeostasis and inhibits insulin secretion in high-fat diet obese mice. *Diabetologia* **56,** 1394–1402 (2013).

80. Kowalski, G. M., Carey, A. L., Selathurai, A., Kingwell, B. a. & Bruce, C. R. Plasma Sphingosine-1-Phosphate Is Elevated in Obesity. *PLoS One* **8,** 1–7 (2013).

81. Fayyaz, S., Japtok, L. & Kleuser, B. Divergent role of sphingosine 1-phosphate on insulin resistance. *Cell. Physiol. Biochem.* **34,** 134–147 (2014).

82. Gibellini, F. & Smith, T. K. The Kennedy pathway-de novo synthesis of phosphatidylethanolamine and phosphatidylcholine. *IUBMB Life* **62,** 414–428 (2010).

83. Henneberry, A., Wright, M. & McMaster, C. The major sites of cellular phospholipid synthesis and molecular determinants of Fatty Acid and lipid head group specificity. *Mol. Biol. Cell* **13,** 3148–3161 (2002).

84. Vance, D. E., Li, Z. & Jacobs, R. L. Hepatic phosphatidylethanolamine N-methyltransferase, unexpected roles in animal biochemistry and physiology. *J. Biol. Chem.* **282,** 33237–33241 (2007).

85. Stone, S. J. & Vance, J. E. Phosphatidylserine synthase-1 and -2 are localized to mitochondria-associated membranes. *J. Biol. Chem.* **275,** 34534–34540 (2000).

86. Schuiki, I. & Daum, G. Phosphatidylserine decarboxylases, key enzymes of lipid metabolism. *IUBMB Life* **61,** 151–162 (2009).

87. Nagle, C. a, Klett, E. L. & Coleman, R. a. Hepatic triacylglycerol accumulation and insulin resistance. *J. Lipid Res.* **50 Suppl,** S74–S79 (2009).

88. Bektas, M. *et al.* A novel acylglycerol kinase that produces lysophosphatidic acid modulates cross talk with EGFR in prostate cancer cells. *J. Cell Biol.* **169,** 801–811 (2005).

89. Liu, S., Murph, M., Panupinthu, N. & Mills, G. B. ATX-LPA receptor axis in inflammation and cancer. *Cell Cycle* **8,** 3695–3701 (2009).

90. Cencetti, F. *et al.* Lysophosphatidic acid stimulates cell migration of satellite cells: a role for sphingosine kinase/sphingosine 1-phosphate axis. *FEBS J.* **281,** 4467–4478 (2014).

91. Olivera, A., Rosenthal, J. & Spiegel, S. Effect of acidic phospholipids on sphingosine kinase. *J. Cell. Biochem.* **60,** 529–537 (1996).

92. Yea, K. *et al.* Lysophosphatidic acid regulates blood glucose by stimulating myotube and adipocyte glucose uptake. *J. Mol. Med.* **86,** 211–220 (2008).

93. Dusaulcy, R. *et al.* Adipose-specific disruption of autotaxin enhances nutritional fattening and reduces plasma lysophosphatidic acid. *J. Lipid Res.* **52,** 1247–1255 (2011).

94. Rapizzi, E. *et al.* Sphingosine 1-phosphate increases glucose uptake through trans-activation of insulin receptor. *Cell. Mol. Life Sci.* **66,** 3207–3218 (2009).

95. Ross, J. S. *et al.* Sphingosine Kinase 1 Is Regulated by Peroxisome Proliferator-activated Receptor α in Response to Free Fatty Acids and Is Essential for Skeletal Muscle Interleukin-6 Production and Signaling in Diet-induced Obesity. *J. Biol. Chem.* **288,** 22193–206 (2013).

96. Huang, P., Altshuller, Y., Hou, J., Pessin, J. & Frohman, M. Insulin-stimulated Plasma Membrane Fusion of Glut4 Glucose Transporter-containing Vesicles Is Regulated by Phospholipase D1. *Mol. Biol. Cell* **16,** 2614–2623 (2005).

97. Gangoiti, P. *et al.* Ceramide 1-phosphate stimulates proliferation of C2C12 myoblasts. *Biochimie* **94,** 597–607 (2012).

98. Salous, A. K., Panchatcharam, M., Sunkara, M. & Mueller, P. Mechanism of rapid elimination of lysophosphatidic acid and related lipids from the circulation of mice. 1–26

99. Im, D. S. *et al.* Characterization of sphingosine 1-phosphate-induced actions and its signaling pathways in rat hepatocytes. *Am. J. Physiol.* **272,** G1091–G1099 (1997).

100. Fang, X. *et al.* Convergence of Multiple Signaling Cascades at Glycogen Synthase Kinase 3 : Edg Receptor-Mediated Phosphorylation and Inactivation by Lysophosphatidic Acid through a Protein Kinase C-Dependent Intracellular Pathway Convergence of Multiple Signaling Cascade. (2002). doi:10.1128/MCB.22.7.2099

101. Sankella, S., Garg, A., Horton, J. D. & Agarwal, A. K. Hepatic gluconeogenesis is enhanced by phosphatidic acid which remains uninhibited by insulin in lipodystrophic Agpat2-/- mice. *J. Biol. Chem.* **289,** 4762–4777 (2014).

102. Burrows, E. L. & Bird, R. P. Obesity-associated steatotic liver exhibits aberrant or altered sphingolipid composition and preferentially accumulates ceramide species containing long chain fatty acids. **4,** 1578–1587 (2012).

103. Fayyaz, S. *et al.* Involvement of sphingosine 1-phosphate in palmitate-induced insulin resistance of hepatocytes via the S1P2 receptor subtype. *Diabetologia* **57,** 373–382 (2014).

104. Tao, C., Sifuentes, A. & Holland, W. L. Regulation of glucose and lipid homeostasis by adiponectin: Effects on hepatocytes, pancreatic β cells and adipocytes. *Best Pract. Res. Clin. Endocrinol. Metab.* **28,** 43–58 (2014).

105. Osawa, Y. *et al.* Acid sphingomyelinase regulates glucose and lipid metabolism in hepatocytes through AKT activation and AMP-activated protein kinase suppression. *FASEB J.* **25,** 1133–1144 (2011).

106. Kok, B. P. C., Venkatraman, G., Capatos, D. & Brindley, D. N. Unlike two peas in a pod: Lipid phosphate phosphatases and phosphatidate phosphatases. *Chem. Rev.* **112,** 5121–5146 (2012).

107. Tomsig, J. L. *et al.* Lipid phosphate phosphohydrolase type 1 (LPP1) degrades extracellular lysophosphatidic acid in vivo. **419,** 611–618 (2010).

108. Xu, K. *et al.* Regulation of Androgen Receptor Transcriptional Activity and Specificity by RNF6-Induced Ubiquitination. *Cancer Cell* **15,** 270–282 (2009).

109. Ariazi, E. a. *et al.* Inaugural Article: Estrogen induces apoptosis in estrogen deprivation-resistant breast cancer through stress responses as identified by global gene expression across time. *Proc. Natl. Acad. Sci.* **108,** 18879–18886 (2011).

110. Huang, Y., Zhao, B., Liu, Y. & Wang, N. Title: Peroxisome proliferator-activated receptor gamma regulates the expression of lipid phosphate phosphohydrolase 1 in human vascular endothelial cells. **86,** (2014).

111. Simon, M. F. *et al.* Expression of ectolipid phosphate phosphohydrolases in 3T3F442A preadipocytes and adipocytes. Involvement in the control of lysophosphatidic acid production. *J. Biol. Chem.* **277,** 23131–23136 (2002).

112. Sigal, Y. J., McDermott, M. I. & Morris, A. J. Integral membrane lipid phosphatases/phosphotransferases: common structure and diverse functions. *Biochem. J.* **387,** 281–293 (2005).

113. Brindley, D. N., Pilquil, C., Sariahmetoglu, M. & Reue, K. Phosphatidate degradation: Phosphatidate phosphatases (lipins) and lipid phosphate phosphatases. *Biochim. Biophys. Acta - Mol. Cell Biol. Lipids* **1791,** 956–961 (2009).

114. Brindley, D. N. & Pilquil, C. Lipid phosphate phosphatases and signaling. *J. Lipid Res.* **50 Suppl,** S225–S230 (2009).

115. Xu, J. *et al.* Lipid phosphate phosphatase-1 in the regulation of lysophosphatidate signaling. *Ann. N. Y. Acad. Sci.* **905,** 81–90 (2000).

116. Yue, J. *et al.* Mice with transgenic overexpression of lipid phosphate phosphatase-1 display multiple organotypic deficits without alteration in circulating lysophosphatidate level. *Cell. Signal.* **16,** 385–399 (2004).

117. Kai, M. *et al.* Lipid phosphate phosphatases 1 and 3 are localized in distinct lipid rafts. *J. Biochem.* **140,** 677–686 (2006).

118. Pilquil, C. *et al.* Lipid phosphate phosphatase-1 regulates lysophosphatidate-induced fibroblast migration by controlling phospholipase D2-dependent phosphatidate generation. *J. Biol. Chem.* **281,** 38418–38429 (2006).

119. Zhao, Y. *et al.* Lipid phosphate phosphatase-1 regulates lysophosphatidic acid-induced calcium release, NF-kappaB activation and interleukin-8 secretion in human bronchial epithelial cells. *Biochem. J.* **385,** 493–502 (2005).

120. Smyth, S. S. *et al.* Lipid Phosphate Phosphatases Regulate Lysophosphatidic Acid Production and Signaling in Platelets: Studies using chemical inhibitors of lipid phosphate phosphatase activity. *J. Biol. Chem.* **278,** 43214–43223 (2003).

121. Alderton, F. *et al.* G-protein-coupled Receptor Stimulation of the p42/p44 Mitogen-activated Protein Kinase Pathway Is Attenuated by Lipid Phosphate Phosphatases 1, 1a, and 2 in Human Embryonic Kidney 293 Cells. *J. Biol. Chem.* **276,** 13452–13460 (2001).

122. Haldar, D. & Lipfert, L. Export of mitochondrially synthesized lysophosphatidic acid. *J. Biol. Chem.* **265,** 11014–11016 (1990).

123. Ohba, Y. *et al.* Mitochondria-type GPAT is required for mitochondrial fusion. *EMBO J.* **32,** 1265–79 (2013).

124. Montgomery, M. K. & Turner, N. Mitochondrial dysfunction and insulin resistance: an update. *Endocr. Connect.* **4,** R1–R15 (2014).

125. Kowluru, a. Adenine and guanine nucleotide-specific succinyl-CoA synthetases in the clonal beta-cell mitochondria: Implications in the beta-cell high-energy phosphate metabolism in relation to physiological insulin secretion. *Diabetologia* **44,** 89–94 (2001).

126. Glancy, B., Wt, W., Dj, C. & Rs, B. Effect of calcium on the oxidative phosphorylation cascade in skeletal muscle mitochondria . PubMed Commons. 1–2 (2013). doi:10.1021/bi3015983.

127. Brookes, P. S., Yoon, Y., Robotham, J. L., Anders, M. W. & Sheu, S.-S. Calcium, ATP, and ROS: a mitochondrial love-hate triangle. *Am. J. Physiol. Cell Physiol.* **287,** C817–33 (2004).

128. Drose, S. & Brandt, U. Molecular mechanisms of superoxide production by the mitochondrial respiratory chain. *Adv. Exp. Med. Biol.* **748,** 145–169 (2012).

129. Raha, S., McEachern, G. E., Myint, a T. & Robinson, B. H. Superoxides from mitochondrial complex III: the role of manganese superoxide dismutase. *Free Radic. Biol. Med.* **29,** 170–180 (2000).

130. Garcia-Ruiz, C., Colell, A., Morales, A., Kaplowitz, N. & Fernandez-Checa, J. Role of oxidative stress generated from the mitochondrial electron transport chain and mitochondrial glutathione status in loss of mitochondrial function and activation of transcription factor nuclear factor-kappa B: studies with isolated mitochondria and. *Mol. Pharmacol.* **48,** 825–834 (1995).

131. Sabharwal, S. & Schumacker, P. Mitochondrial ROS in cancer: initiators, amplifiers or an Achilles' heel? *Nat. Rev. Cancer* **14,** 709–721 (2014).

132. Hayes, J. D. & Dinkova-Kostova, A. T. The Nrf2 regulatory network provides an interface between redox and intermediary metabolism. *Trends Biochem. Sci.* **39,** 199–218 (2014).

133. Dinkova-Kostova, A. T. & Abramov, A. Y. The emerging role of Nrf2 in mitochondrial function. *Free Radic. Biol. Med.* (2015). doi:10.1016/j.freeradbiomed.2015.04.036

134. Klip, a., Schertzer, J. D., Bilan, P. J., Thong, F. & Antonescu, C. Regulation of glucose transporter 4 traffic by energy deprivation from mitochondrial compromise. *Acta Physiol.* **196,** 27–35 (2009).

135. Randhawa, V. *et al.* Insulin and Hypertonicity Recruit GLUT4 to the Plasma Membrane of Muscle Cells by Using N-Ethylmaleimide-sensitive Factor-dependent SNARE Mechanisms but Different v-SNAREs: Role of TI-VAMP. *Mol. Biol. Cell* **15,** 5565–5573 (2004).

136. Del Campo, A. *et al.* Mitochondrial fragmentation impairs insulin-dependent glucose uptake by modulating Akt activity through mitochondrial Ca2+ uptake. *Am. J. Physiol. Endocrinol. Metab.* **306,** E1–E13 (2014).

137. Zhang, S.-J. *et al.* 2-Methoxyoestradiol inhibits glucose transport in rodent skeletal muscle. *Exp. Physiol.* **95,** 892–898 (2010).

138. Hoehn, K. L. *et al.* Insulin resistance is a cellular antioxidant defense mechanism. *Proc. Natl. Acad. Sci. U. S. A.* **106,** 17787–17792 (2009).

139. Menahan, L. a & Williams, R. H. Interrelationship between fatty acid oxidation and gluconeogenesis from pyruvate. *Eur. J. Biochem.* **20,** 488–493 (1971).

140. Conti, R. *et al.* Selective reversible inhibition of liver carnitine palmitoyl-transferase 1 by teglicar reduces gluconeogenesis and improves glucose homeostasis. *Diabetes* **60,** 644–651 (2011).

141. Taylor, W. M., Prpić, V., Exton, J. H. & Bygrave, F. L. Stable changes to calcium fluxes in mitochondria isolated from rat livers perfused with alpha-adrenergic agonists and with glucagon. *Biochem. J.* **188,** 443–450 (1980).

142. Arruda, A. P. *et al.* Chronic enrichment of hepatic endoplasmic reticulum–mitochondria contact leads to mitochondrial dysfunction in obesity. *Nat. Med.* (2014). doi:10.1038/nm.3735

143. Nocito, L. *et al.* The Extracellular Redox State Modulates Mitochondrial Function, Gluconeogenesis, and Glycogen Synthesis in Murine Hepatocytes. *PLoS One* **10,** e0122818 (2015).

144. Ludtmann, M. H. R., Angelova, P. R., Zhang, Y., Abramov, A. Y. & Dinkova-Kostova, A. T. Nrf2 affects the efficiency of mitochondrial fatty acid oxidation. *Biochem. J.* **457,** 415–24 (2014).

145. Uruno, A. *et al.* The Keap1-Nrf2 system prevents onset of diabetes mellitus. *Mol. Cell. Biol.* **33,** 2996–3010 (2013).

146. Venkatraman, G. *et al.* Lysophosphatidate signaling stabilizes Nrf2 and increases the expression of genes involved in drug resistance and oxidative stress responses: implications for cancer treatment. *FASEB J.* **29,** 772–785 (2014).

147. Brand, M. D. & Nicholls, D. G. Assessing mitochondrial dysfunction in cells. *Biochem. J.* **435,** 297–312 (2011).

148. Wang, R. H. *et al.* Hepatic Sirt1 deficiency in mice impairs mTorc2/Akt signaling and results in hyperglycemia, oxidative damage, and insulin resistance. *J. Clin. Invest.* **121,** 4477–4490 (2011).

149. Heilbronn, L. K., Seng, K. G., Turner, N., Campbell, L. V. & Chisholm, D. J. Markers of mitochondrial biogenesis and metabolism are lower in overweight and obese insulin-resistant subjects. *J. Clin. Endocrinol. Metab.* **92,** 1467–1473 (2007).

150. Kelley, D. E., He, J., Menshikova, E. V. & Ritov, V. B. Dysfunction of Mitochondria in Human Skeletal Muscle in Type 2 Diabetes . *Diabetes* **51,** 2944–2950 (2002).

151. Ritov, V. B. *et al.* Deficiency of subsarcolemmal mitochondria in obesity and type 2 diabetes. *Diabetes* **54,** 8–14 (2005).

152. Razak, F. & Anand, S. S. Impaired mitochondrial activity in the insulin-resistant offspring of patients with type 2 diabetes. Petersen KF, Dufour S, Befroy D, Garcia R, Shulman GI. N Engl J Med 2004; 350: 664-71. *Vasc. Med.* **9,** 223–224 (2004).

153. Brehm, A. *et al.* Increased lipid availability impairs insulin-stimulated ATP synthesis in human skeletal muscle. *Diabetes* **55,** 136–140 (2006).

154. Sparks, L. M. *et al.* Required for Mitochondrial Oxidative Phosphorylation in Skeletal Muscle. **54,** (2005).

155. Mason, S. & Wadley, G. D. Skeletal muscle reactive oxygen species: a target of good cop/bad cop for exercise and disease. *Redox Rep.* **19,** 97–106 (2014).

156. Gutiérrez, T. *et al.* Alteration in mitochondrial Ca2+ uptake disrupts insulin signaling in hypertrophic cardiomyocytes. *Cell Commun. Signal.* **12,** 1–14 (2014).

157. Galloway, C. a. & Yoon, Y. Perspectives on: SGP Symposium on Mitochondrial Physiology and Medicine: What comes first, misshape or dysfunction? The view from metabolic excess. *J. Gen. Physiol.* **139,** 455–463 (2012).

158. Bonnard, C. *et al.* Mitochondrial dysfunction results from oxidative stress in the skeletal muscle of diet-induced insulin resistant mice. *J Clin Invest* **118,** 789–800 (2008).

159. Jheng, H.-F. *et al.* Mitochondrial Fission Contributes to Mitochondrial Dysfunction and Insulin Resistance in Skeletal Muscle. *Mol. Cell. Biol.* **32,** 309–319 (2012).

160. Szendroedi, J., Phielix, E. & Roden, M. The role of mitochondria in insulin resistance and type 2 diabetes mellitus. *Nat. Rev. Endocrinol.* **8,** 92–103 (2011).

161. Cortez-Pinto, H. *et al.* Alterations in liver ATP homeostasis in human nonalcoholic steatohepatitis: a pilot study. *JAMA* **282,** 1659–1664 (1999).

162. Schmid, A. I. *et al.* Liver ATP synthesis is lower and relates to insulin sensitivity in patients with type 2 diabetes. *Diabetes Care* **34,** 448–453 (2011).

163. Anderson, N. Molecular Mechanisms and Therapeutic Targets in Steatosis and Steatohepatitis. *Pharmacol. Rev.* **60,** 311–357 (2008).

164. Sanyal, a J. *et al.* Nonalcoholic steatohepatitis: association of insulin resistance and mitochondrial abnormalities. *Gastroenterology* **120,** 1183–1192 (2001).

165. Rector, R. S. *et al.* Selective hepatic insulin resistance in a murine model heterozygous for a mitochondrial trifunctional protein defect. *Hepatology* **57,** 2213–2223 (2013).

166. Monsénégo, J. *et al.* Enhancing liver mitochondrial fatty acid oxidation capacity in obese mice improves insulin sensitivity independently of hepatic steatosis. *J. Hepatol.* **56,** 632–639 (2012).

167. Nakamura, S. *et al.* Palmitate induces insulin resistance in H4IIEC3 hepatocytes through reactive oxygen species produced by mitochondria. *J. Biol. Chem.* **284,** 14809–14818 (2009).

168. Zhai, L., Ballinger, S. W. & Messina, J. L. Role of reactive oxygen species in injury-induced insulin resistance. *Mol. Endocrinol.* **25,** 492–502 (2011).

169. Turner, N. & Heilbronn, L. K. Is mitochondrial dysfunction a cause of insulin resistance? *Trends Endocrinol. Metab.* **19,** 324–330 (2008).

170. Boushel, R. *et al.* Patients with type 2 diabetes have normal mitochondrial function in skeletal muscle. *Diabetologia* **50,** 790–796 (2007).

171. Sreekumar, R. *et al.* Impact of high-fat diet and antioxidant supplement on mitochondrial functions and gene transcripts in rat muscle. *Am. J. Physiol. Endocrinol. Metab.* **282,** E1055–E1061 (2002).

172. Turner, N. *et al.* Excess lipid availability increases mitochondrial fatty acid oxidative capacity in muscle: Evidence against a role for reduced fatty acid oxidation in lipid-induced insulin resistance in rodents. *Diabetes* **56,** 2085–2092 (2007).

173. Franko, A. *et al.* Complete failure of insulin-transmitted signaling, but not obesity-induced insulin resistance, impairs respiratory chain function in muscle. *J. Mol. Med. Berlin* **90,** 1145–1160 (2012).

174. Asmann, Y. W. *et al.* Skeletal muscle mitochondrial functions, mitochondrial DNA copy numbers, and gene transcript profiles in type 2 diabetic and nondiabetic subjects at equal levels of low or high insulin and euglycemia. *Diabetes* **55,** 3309–3319 (2006).

175. Yerby, B. *et al.* Insulin-stimulated mitochondrial adenosine triphosphate synthesis is blunted in skeletal muscles of high-fat-fed rats. *Metabolism.* **57,** 1584–1590 (2008).

176. Iossa, S. *et al.* Effect of long-term high-fat feeding on energy balance and liver oxidative activity in rats. *Br. J. Nutr.* **84,** 377–385 (2000).

177. Franko, A. *et al.* Liver adapts mitochondrial function to insulin resistant and diabetic states in mice. *J. Hepatol.* **60,** 816–823 (2014).

178. Garcia-Ruiz, C., Baulies, A., Mari, M., Garcia-Roves, P. & Fernandez-Checa, J. Mitochondrial dysfunction in non-alcoholic fatty liver disease and insulin resistance: cause or consequence? *Free Radic. Res.* **47,** 854–868 (2013).

179. Halestrap, A. P. What is the mitochondrial permeability transition pore? *J. Mol. Cell. Cardiol.* **46,** 821–831 (2009).

180. Crompton, M. & Costi, a. A heart mitochondrial Ca2(+)-dependent pore of possible relevance to re-perfusion-induced injury. Evidence that ADP facilitates pore interconversion between the closed and open states. *Biochem. J.* **266,** 33–39 (1990).

181. Haworth, R. & Hunter, D. The Ca2+-induced membrane transition in mitochondria. II. Nature of the Ca2+ trigger site. *Arch. Biochem. Biophys.* **195,** 460–467 (1979).

182. Bernardi, P. Modulation of the Mitochondrial CyclosporinA-sensitive Permeability Transition Pore by the Proton Electrochemical Gradient. *Biochemistry* **267,** 8834–8839 (1992).

183. Petronilli, V., Cola, C., Massari, S., Colonna, R. & Bernardi, P. Physiological effectors modify voltage sensing by the cyclosporin A- sensitive permeability transition pore of mitochondria. *J. Biol. Chem.* **268,** 21939–21945 (1993).

184. Wong, R., Steenbergen, C. & Murphy, E. Mitochondrial permeability transition pore and calcium handling. *Methods Mol. Biol.* **810,** 235–242 (2012).

185. Sloan, R. C. *et al.* Mitochondrial permeability transition in the diabetic heart: Contributions of thiol redox state and mitochondrial calcium to augmented reperfusion injury. *J. Mol. Cell. Cardiol.* **52,** 1009–1018 (2012).

186. Lenartowicz, E., Bernardi, P. & Azzone, G. Phenylarsine oxide induces the cyclosporin A-sensitive membrane permeability transition in rat liver mitochondria. *J. Bioenerg. Biomembr.* **23,** 679–688 (1991).

187. Crompton, M. & Cost, A. by Ca2 , inorganic phosphate and oxidative stress. **1,** (1988).

188. McStay, G., Clarke, S. J. & Halestrap, A. P. Role of critical thiol groups on the matrix surface of the adenine nucleotide translocase in the mechanism of the mitochondrial permeability transition pore. *Biochem J* **548,** 541–548 (2002).

189. Halestrap, A. P., Woodfield, K. Y. & Connern, C. P. Oxidative stress, thiol reagents, and membrane potential modulate the mitochondrial permeability transition by affecting nucleotide binding to the adenine nucleotide translocase. *J. Biol. Chem.* **272,** 3346–3354 (1997).

190. Bernardi, P. *et al.* Modulation of the mitochondrial permeability transition pore: Effect of protons and divalent cations. *J. Biol. Chem.* **267,** 2934–2939 (1992).

191. Assaly, R. *et al.* Oxidative stress, mitochondrial permeability transition pore opening and cell death during hypoxia–reoxygenation in adult cardiomyocytes. *Eur. J. Pharmacol.* **675,** 6–14 (2012).

192. Javadov, S., Karmazyn, M. & Escobales, N. Mitochondrial permeability transition pore opening as a promising therapeutic target in cardiac diseases. *J. Pharmacol. Exp. Ther.* **330,** 670–678 (2009).

193. Teodoro, J. S. *et al.* Berberine reverts hepatic mitochondrial dysfunction in high-fat fed rats: A possible role for SirT3 activation. *Mitochondrion* **13,** 637–646 (2013).

194. Kottke, M. *et al.* Mitochondrial boundary membrane contact sites in brain: points of hexokinase and creatine kinase location, and control of Ca2+ transport. *Brain* **935,** 87–102 (1988).

195. Beutner, G., Rück, A., Riede, B., Welte, W. & Brdiczka, D. Complexes between kinases, mitochondrial porin and adenylate translocator in rat brain resemble the permeability transition pore. *FEBS Lett.* **396,** 189–195 (1996).

196. Leung, A. W. C., Varanyuwatana, P. & Halestrap, A. P. The mitochondrial phosphate carrier interacts with cyclophilin D and may play a key role in the permeability transition. *J. Biol. Chem.* **283,** 26312–23 (2008).

197. Forte, M. & Bernardi, P. The permeability transition and BCL-2 family proteins in apoptosis: co-conspirators or independent agents? *Cell Death Differ.* **13,** 1287–1290 (2006).

198. Sileikyte, J. *et al.* Regulation of the inner membrane mitochondrial permeability transition by the outer membrane translocator protein (peripheral benzodiazepine receptor). *J. Biol. Chem.* **286,** 1046–1053 (2011).

199. Hafner, A. V *et al.* Regulation of the mPTP by SIRT3-mediated deacetylation of CypD at lysine 166 suppresses age-related cardiac hypertrophy. *Aging Albany NY Online* **2,** 914–923 (2010).

200. Shulga, N., Wilson-Smith, R. & Pastorino, J. G. Sirtuin-3 deacetylation of cyclophilin D induces dissociation of hexokinase II from the mitochondria. *J. Cell Sci.* **123,** 894–902 (2010).

201. Boengler, K., Hilfiker-Kleiner, D., Heusch, G. & Schulz, R. Inhibition of permeability transition pore opening by mitochondrial STAT3 and its role in myocardial ischemia/reperfusion. *Basic Res. Cardiol.* **105,** 771–785 (2010).

202. Rasola, A. *et al.* Activation of mitochondrial ERK protects cancer cells from death through inhibition of the permeability transition. *Proc. Natl. Acad. Sci. U. S. A.* **107,** 726–731 (2010).

203. Chiara, F. *et al.* Hexokinase II detachment from mitochondria triggers apoptosis through the permeability transition pore independent of voltage-dependent anion channels. *PLoS One* **3,** (2008).

204. Azarashvili, T. *et al.* Calcium-induced permeability transition in rat brain mitochondria is promoted by carbenoxolone through targeting connexin43. *Am. J. Physiol. Cell Physiol.* **300,** C707–C720 (2011).

205. Baines, C. P., Kaiser, R. a, Sheiko, T., Craigen, W. J. & Molkentin, D. Voltage-Dependent Anion Channels are Dispensable for Mitochondrial-Dependent Cell Death. *Nat. Cell Biol.* **9,** 550–555 (2009).

206. Kokoszka, J. E. *et al.* Permeability Transition Pore. **427,** 461–465 (2011).

207. Elrod, J. W. & Molkentin, J. D. Physiologic Functions of Cyclophilin D and the Mitochondrial Permeability Transition Pore. *Circ. J.* **77,** 1111–1122 (2013).

208. Kajitani, K. *et al.* Crystal structure of human cyclophilin D in complex with its inhibitor, cyclosporin A at 0.96-Å resolution. *Proteins Struct. Funct. Genet.* **70,** 1635–1639 (2008).

209. Marchler-Bauer, A. *et al.* CDD: Conserved domains and protein three-dimensional structure. *Nucleic Acids Res.* **41,** 348–352 (2013).

210. Baines, C. *et al.* Loss of cyclophilin D reveals a critical role for mitochondrial permeability transition in cell death. *Nature* **434,** (2005).

211. Matas, J. *et al.* Increased expression and intramitochondrial translocation of cyclophilin-D associates with increased vulnerability of the permeability transition

pore to stress-induced opening during compensated ventricular hypertrophy. *J. Mol. Cell. Cardiol.* **46,** 420–30 (2009).

212. Bernardi, P. The mitochondrial permeability transition pore: A mystery solved? *Front. Physiol.* **4 MAY,** 1–12 (2013).

213. Xi, J., Wang, H., Mueller, R. a., Norfleet, E. a. & Xu, Z. Mechanism for resveratrol-induced cardioprotection against reperfusion injury involves glycogen synthase kinase 3β and mitochondrial permeability transition pore. *Eur. J. Pharmacol.* **604,** 111–116 (2009).

214. Nguyen, T. T. *et al.* Cysteine 203 of cyclophilin D is critical for cyclophilin D activation of the mitochondrial permeability transition pore. *J. Biol. Chem.* **286,** 40184–92 (2011).

215. Giorgio, V. *et al.* Cyclophilin D Modulates Mitochondrial F0F1-ATP Synthase by Interacting with the Lateral Stalk of the Complex. *J. Biol. Chem.* **284,** 33982–33988 (2009).

216. Giorgio, V. *et al.* Dimers of mitochondrial ATP synthase form the permeability transition pore. *Proc. Natl. Acad. Sci. U. S. A.* **110,** 5887–92 (2013).

217. Strauss, M., Hofhaus, G., Schröder, R. R. & Kühlbrandt, W. Dimer ribbons of ATP synthase shape the inner mitochondrial membrane. *EMBO J.* **27,** 1154–1160 (2008).

218. Davies, K. M. *et al.* Macromolecular organization of ATP synthase and complex I in whole mitochondria. *Proc. Natl. Acad. Sci. U. S. A.* **108,** 14121–14126 (2011).

219. Altschuld, R. *et al.* Cyclosporin inhibits mitochondrial calcium efflux in isolated adult rat ventricular cardiomyocytes. *Am. J. Physiol.* **262,** H1699–H1704 (1992).

220. Ichas, F. & Mazat, J. P. From calcium signaling to cell death: Two conformations for the mitochondrial permeability transition pore. Switching from low- to high-conductance state. *Biochim. Biophys. Acta - Bioenerg.* **1366,** 33–50 (1998).

221. Selivanov, V. a. *et al.* A model of mitochondrial Ca2+-induced Ca2+ release simulating the Ca2+ oscillations and spikes generated by mitochondria. *Biophys. Chem.* **72,** 111–121 (1998).

222. Elrod, J. W. *et al.* Cyclophilin D controls mitochondrial pore–dependent Ca2+ exchange, metabolic flexibility, and propensity for heart failure in mice. *J. Clin. Invest.* **120,** 3680–3687 (2010).

223. Luvisetto, S., Basso, E., Petronilli, V., Bernardi, P. & Forte, M. Enhancement of anxiety, facilitation of avoidance behavior, and occurrence of adult-onset obesity in mice lacking mitochondrial cyclophilin D. *Neuroscience* **155,** 585–596 (2008).

224. Du, H. *et al.* Disease. *October* **14,** 1097–1105 (2009).

225. Cleren, C. *et al.* Promethazine protects against 1-methyl-4-phenyl-1,2,3,6-tetrahydropyridine neurotoxicity. *Neurobiol. Dis.* **20,** 701–708 (2005).

226. Miura, T. & Tanno, M. The mPTP and its regulatory proteins: Final common targets of signalling pathways for protection against necrosis. *Cardiovasc. Res.* **94,** 181–189 (2012).

227. Miura, T., Tanno, M. & Sato, T. Mitochondrial kinase signalling pathways in myocardial protection from ischaemia/reperfusion-induced necrosis. *Cardiovasc. Res.* **88,** 7–15 (2010).

228. Ong, S., Samangouei, P., Kalkhoran, S. & Hausenloy, D. The mitochondrial permeability transition pore and its role in myocardial ischemia reperfusion injury. *J. Mol. Cell. Cardiol.* **78,** 23–34 (2015).

229. Majewski, N. *et al.* Hexokinase-mitochondria interaction mediated by Akt is required to inhibit apoptosis in the presence or absence of Bax and Bak. *Mol. Cell* **16,** 819–830 (2004).

230. Juhaszova, M. *et al.* Role of glycogen synthase kinase-3β in cardioprotection. *Circ. Res.* **104,** 1240–1252 (2009).

231. Najafi, M. *et al.* Inhibition of mitochondrial permeability transition pore restores the cardioprotection by postconditioning in diabetic hearts. *J. Diabetes Metab. Disord.* **13,** 1–10 (2014).

232. Fujimoto, K., Chen, Y., Polonsky, K. S. & Dorn, G. W. Targeting cyclophilin D and the mitochondrial permeability transition enhances beta-cell survival and prevents diabetes in Pdx1 deficiency. *Proc. Natl. Acad. Sci. U. S. A.* **107,** 10214–9 (2010).

233. Chow, J. D. Y. *et al.* Genetic inhibition of hepatic acetyl-CoA carboxylase activity increases liver fat and alters global protein acetylation. *Mol. Metab.* **3,** 419–431 (2014).

234. Ozcan, L. *et al.* Calcium signaling through CaMKII regulates hepatic glucose production in fasting and obesity. *Cell Metab.* **15,** 739–751 (2012).

235. Hoehn, K. L. *et al.* Acute or Chronic Upregulation of Mitochondrial Fatty Acid Oxidation Has No Net Effect on Whole-Body Energy Expenditure or Adiposity. *Cell Metab.* **11,** 70–76 (2010).

236. Patel, S. a. *et al.* Overexpression of the adiponectin receptor AdipoR1 in rat skeletal muscle amplifies local insulin sensitivity. *Endocrinology* **153,** 5231–5246 (2012).

237. Murphy, R. C. *et al.* Detection of the abundance of diacylglycerol and triacylglycerol molecular species in cells using neutral loss mass spectrometry. *Anal. Biochem.* **366,** 59–70 (2007).

238. Kim, H., Ahn, E. & Moon, M. Profiling of human urinary phospholipids by nanoflow liquid chromatography/tandem mass spectrometry. *Analyst* **133,** 1656–1663 (2008).

239. Pulfer, M. & Murphy, R. Electrospray mass spectrometry of phospholipids. *Mass Spectrom. Rev.* **22,** 332–364 (2003).

240. Macarthur, D. G. *et al.* An Actn3 knockout mouse provides mechanistic insights into the association between ??-actinin-3 deficiency and human athletic performance. *Hum. Mol. Genet.* **17,** 1076–1086 (2008).

241. Bruce, C. R. *et al.* Overexpression of carnitine palmitoyltransferase-1 in skeletal muscle is sufficient to enhance fatty acid oxidation and improve high-fat diet-induced insulin resistance. *Diabetes* **58,** 550–558 (2009).

242. Rogers, G. W. *et al.* High throughput microplate respiratory measurements using minimal quantities of isolated mitochondria. *PLoS One* **6,** e21746 (2011).

243. Rosca, M. G. *et al.* Cardiac mitochondria in heart failure: Decrease in respirasomes and oxidative phosphorylation. *Cardiovasc. Res.* **80,** 30–39 (2008).

244. Wittig, I., Braun, H.-P. & Schägger, H. Blue native PAGE. *Nat. Protoc.* **1,** 418–428 (2006).

245. Holland, W. *et al.* Lipid mediators of insulin resistance. *Nutr. Rev.* **65,** S39–46 (2007).

246. Murrow, B. a & Hoehn, K. L. Mitochondrial regulation of insulin action. *Int. J. Biochem. Cell Biol.* **42,** 1936–1939 (2010).

247. Savage, D. B., Petersen, K. F. & Shulman, G. I. Disordered Lipid Metabolism and the Pathogenesis of Insulin Resistance. *Physiol Rev* **87,** 507–520 (2007).

248. Houstis, N., Rosen, E. & Lander, E. Reactive oxygen species have a causal role in multiple forms of insulin resistance. *Nature* **440,** 944–948 (2006).

249. Anderson, E. J. *et al.* Mitochondrial H2O2 emission and cellular redox state link excess fat intake to insulin resistance in both rodents and humans. *J. Clin. Invest.* **119,** 573–581 (2009).

250. Holland, W. L. *et al.* Inhibition of Ceramide Synthesis Ameliorates Glucocorticoid-, Saturated-Fat-, and Obesity-Induced Insulin Resistance. *Cell Metab.* **5,** 167–179 (2007).

251. Itani, S. I., Ruderman, N. B., Schmieder, F. & Boden, G. Lipid-induced insulin resistance in human muscle is associated with changes in diacylglycerol, protein kinase C, and IkappaB-alpha. *Diabetes* **51,** 2005–2011 (2002).

252. Storlien, L. H., James, D. E., Burleigh, K. M., Chisholm, D. J. & Kraegen, E. W. Fat feeding causes widespread in vivo insulin resistance, decreased energy expenditure, and obesity in rats. *Am. J. Physiol.* **251,** E576–E583 (1986).

253. Muoio, D. M. & Neufer, P. D. Lipid-induced mitochondrial stress and insulin action in muscle. *Cell Metab.* **15,** 595–605 (2012).

254. Kim, J.-A., Wei, Y. & Sowers, J. R. Role of mitochondrial dysfunction in insulin resistance. *Circ. Res.* **102,** 401–14 (2008).

255. Giorgi, C. *et al.* Mitochondrial calcium homeostasis as potential target for mitochondrial medicine. *Mitochondrion* **12,** 77–85 (2012).

256. Zorov, D. B. *et al.* Regulation and pharmacology of the mitochondrial permeability transition pore. *Cardiovasc. Res.* **83,** 213–225 (2009).

257. Zhivotovsky, B., Galluzzi, L., Kepp, O. & Kroemer, G. Adenine nucleotide translocase: a component of the phylogenetically conserved cell death machinery. *Cell Death Differ.* **16,** 1419–1425 (2009).

258. Stuart, C. a. *et al.* Slow-twitch fiber proportion in skeletal muscle correlates with insulin responsiveness. *J. Clin. Endocrinol. Metab.* **98,** 2027–2036 (2013).

259. Halestrap, a P. & Davidson, a M. Inhibition of Ca2(+)-induced large-amplitude swelling of liver and heart mitochondria by cyclosporin is probably caused by the inhibitor binding to mitochondrial-matrix peptidyl-prolyl cis-trans isomerase and preventing it interacting with the adenine nuc. *Biochem. J.* **268,** 153–160 (1990).

260. Macho, A. *et al.* Calcium Ionophoretic and apoptotic effects of ferutinin in the human jurkat T-cell line. *Biochem. Pharmacol.* **68,** 875–883 (2004).

261. Abramov, A. Y. & Duchen, M. R. Actions of ionomycin, 4-BrA23187 and a novel electrogenic Ca2+ ionophore on mitochondria in intact cells. *Cell Calcium* **33,** 101–12 (2003).

262. Colell, A., Morales, A. & Ferna, C. Direct Effect of Ceramide on the Mitochondrial Electron Transport Chain Leads to Generation of Reactive Oxygen Species. **272,** 11369–11377 (1997).

263. Chiu, T. T., Sun, Y., Koshkina, A. & Klip, A. Rac-1 superactivation triggers insulin-independent glucose transporter 4 (GLUT4) translocation that bypasses signaling defects exerted by c-Jun N-terminal kinase (JNK)- and ceramide-induced insulin resistance. *J. Biol. Chem.* **288,** 17520–17531 (2013).

264. Vyssokikh, M. Y. *et al.* Adenine nucleotide translocator isoforms 1 and 2 are differently distributed in the mitochondrial inner membrane and have distinct affinities to cyclophilin D. *Biochem. J.* **358,** 349–358 (2001).

265. Arora, K. K., Filburns, C. R. & Pederseng, P. L. Structure / Function Relationships in Hexokinase FOR THE N- AND C-TERMINAL. *J. Biol. Chem.* 18259–18266 (1993).

266. Wu, R. *et al.* Hexokinase II knockdown results in exaggerated cardiac hypertrophy via increased ROS production. *EMBO Mol. Med.* **4,** 633–646 (2012).

267. Endlicher, R. *et al.* Tissue specific sensitivity of mitochondrial permeability transition pore to Ca2+ ions. *Acta Medica (Hradec Kralove)* **52,** 69–72 (2009).

268. Tavecchio, M. *et al.* Cyclophilin D Extramitochondrial Signaling Controls Cell Cycle Progression and Chemokine-directed Cell Motility. *J. Biol. Chem.* **288,** 5553–61 (2013).

269. Tsuchiya, Y. *et al.* Palmitate-induced down-regulation of sortilin and impaired GLUT4 trafficking in C2C12 Myotubes. *J. Biol. Chem.* **285,** 34371–34381 (2010).

270. Fröjdö, S., Vidal, H. & Pirola, L. Alterations of insulin signaling in type 2 diabetes: a review of the current evidence from humans. *Biochim. Biophys. Acta* **1792,** 83–92 (2009).

271. Patergnani, S. *et al.* Calcium signaling around Mitochondria Associated Membranes (MAMs). *Cell Commun. Signal.* **9,** 19 (2011).

272. Zemel, M. B. Nutritional and endocrine modulation of intracellular calcium: implications in obesity, insulin resistance and hypertension. *Mol. Cell. Biochem.* **188,** 129–36 (1998).

273. Han, D.-H. *et al.* Deficiency of the mitochondrial electron transport chain in muscle does not cause insulin resistance. *PLoS One* **6,** e19739 (2011).

274. Fernandez-Real, J., Lopez-Bermejo, A. & Ricart, W. Cross-talk between iron metabolism and diabetes. *Diabetes* **51,** 2348–2354 (2002).

275. Frizzell, N., Lima, M. & Baynes, J. Succination of proteins in diabetes. *Free Radic. Res.* **45,** 101–109 (2011).

276. Koves, T. R. *et al.* Mitochondrial Overload and Incomplete Fatty Acid Oxidation Contribute to Skeletal Muscle Insulin Resistance. *Cell Metab.* **7,** 45–56 (2008).

277. Schooneman, M. G., Vaz, F. M., Houten, S. M. & Soeters, M. R. Acylcarnitines: Reflecting or inflicting insulin resistance? *Diabetes* **62,** 1–8 (2013).

278. Davis, E. S., Becker, a, Heitman, J., Hall, M. N. & Brennan, M. B. A yeast cyclophilin gene essential for lactate metabolism at high temperature. *Proc. Natl. Acad. Sci. U. S. A.* **89,** 11169–11173 (1992).

279. Zhang, X. *et al.* Mitofusion-2-mediated alleviation of insulin resistance in rats through reduction in lipid intermediate accumulation in skeletal muscle. *J. Biomed. Sci.* **20,** 45 (2013).

280. Hansson, M. J. *et al.* Cyclophilin D-sensitive mitochondrial permeability transition in adult human brain and liver mitochondria. *J. Neurotrauma* **28,** 143–153 (2011).

281. Lopes, P. C. *et al.* Cyclosporine A enhances gluconeogenesis while sirolimus impairs insulin signaling in peripheral tissues after 3 weeks of treatment. *Biochem. Pharmacol.* **91,** 61–73 (2014).

282. Delgado, T. *et al.* Effect of cyclosporine A on hepatic carbohydrate metabolism and hepatic gene expression in rat. *Expert Opin. Drug Metab. Toxicol.* **8,** 1223–1230 (2012).

283. Unger, R. H. Lipid overload and overflow: Metabolic trauma and the metabolic syndrome. *Trends Endocrinol. Metab.* **14,** 398–403 (2003).

284. Nunn, A. V., Bell, J. D. & Guy, G. W. Lifestyle-induced metabolic inflexibility and accelerated ageing syndrome: insulin resistance, friend or foe? *Nutr. Metab. (Lond).* **6,** 16 (2009).

285. Harmancey, R. *et al.* Insulin resistance improves metabolic and contractile efficiency in stressed rat heart. *FASEB J.* **26,** 3118–3126 (2012).

286. Barzilai, N. & Ferrucci, L. Insulin resistance and aging: A cause or a protective response? *Journals Gerontol. - Ser. A Biol. Sci. Med. Sci.* **67,** 1329–1331 (2012).

287. Guigas, B. *et al.* Metformin inhibits mitochondrial permeability transition and cell death: a pharmacological in vitro study. *Biochem. J.* **382,** 877–884 (2004).

288. Suwa, M., Egashira, T., Nakano, H., Sasaki, H. & Kumagai, S. Metformin increases the PGC-1alpha protein and oxidative enzyme activities possibly via AMPK phosphorylation in skeletal muscle in vivo. *J. Appl. Physiol.* **101,** 1685–1692 (2006).

289. Rossetti, L. *et al.* Effect of Metformin Treatment on Insulin Action in Diabetic Rats: In Vivo and In Vitro Correlations. *Metabolism* **39,** 425–435 (1990).

290. Rancoule, C. *et al.* Involvement of autotaxin/lysophosphatidic acid signaling in obesity and impaired glucose homeostasis. *Biochimie* **96,** 140–143 (2014).

291. Smyth, S. S., Cheng, H.-Y., Miriyala, S., Panchatcharam, M. & Morris, A. J. Roles of lysophosphatidic acid in cardiovascular physiology and disease. *Biochim. Biophys. Acta* **1781,** 563–570 (2008).

292. Liu, L. *et al.* Nutrient sensing by the mitochondrial transcription machinery dictates oxidative phosphorylation. *J. Clin. Invest.* **124,** 768–784 (2014).

293. Horvath, S. E. & Daum, G. Lipids of mitochondria. *Prog. Lipid Res.* **52,** 590–614 (2013).

294. Osman, C. *et al.* The genetic interactome of prohibitins: Coordinated control of cardiolipin and phosphatidylethanolamine by conserved regulators in mitochondria. *J. Cell Biol.* **184,** 583–596 (2009).

295. Meier, J. a. & Larner, A. C. Toward a new STATe: The role of STATs in mitochondrial function. *Semin. Immunol.* **26,** 20–28 (2014).

296. Vial, G. *et al.* Effects of a high-fat diet on energy metabolism and ROS production in rat liver. *J. Hepatol.* **54,** 348–356 (2011).

297. Van Der Veen, J. N., Lingrell, S., Da Silva, R. P., Jacobs, R. L. & Vance, D. E. The concentration of phosphatidylethanolamine in mitochondria can modulate ATP production and Glucose Metabolism in Mice. *Diabetes* **63,** 2620–2630 (2014).

298. Simo, K. a. *et al.* Altered lysophosphatidic acid (LPA) receptor expression during hepatic regeneration in a mouse model of partial hepatectomy. *Hpb* **16,** 534–542 (2014).

299. Jiang, W. *et al.* Acetylation Regulates Gluconeogenesis by Promoting PEPCK1 Degradation via Recruiting the UBR5 Ubiquitin Ligase. *Mol. Cell* **43,** 33–44 (2011).

300. Ariotti, N. *et al.* Caveolae regulate the nanoscale organization of the plasma membrane to remotely control Ras signaling. *J. Cell Biol.* **204,** 777–792 (2014).

301. Kiss, Z., Crilly, K. S. & Anderson, W. H. From Phosphatidylethanolamine : Modulation of Sphingosine 1-Phosphate- Induced Mitogenesis By Ethanolamine. **391,** 383–391 (1997).

302. Tasseva, G. *et al.* Phosphatidylethanolamine deficiency in mammalian mitochondria impairs oxidative phosphorylation and alters mitochondrial morphology. *J. Biol. Chem.* **288,** 4158–4173 (2013).

303. Burgess, S. C. *et al.* Impaired tricarboxylic acid cycle activity in mouse livers lacking cytosolic phosphoenolpyruvate carboxykinase. *J. Biol. Chem.* **279,** 48941–48949 (2004).

304. Holmström, K. M. *et al.* Nrf2 impacts cellular bioenergetics by controlling substrate availability for mitochondrial respiration. *Biol. Open* **2,** 761–70 (2013).

305. Rexroth, S. *et al.* Reactive oxygen species target specific tryptophan site in the mitochondrial ATP synthase. *Biochim. Biophys. Acta - Bioenerg.* **1817,** 381–387 (2012).

306. Zhang, Y., Marcillat, O., Giulivi, C., Ernster, L. & Davies, K. J. The Oxidative Inactivtion of Mitochondrial Electron Transport Chain Components and ATPase. *J Biol Chem* **265,** 16330–16336 (1990).

307. Cízková, A. *et al.* Development of a human mitochondrial oligonucleotide microarray (h-MitoArray) and gene expression analysis of fibroblast cell lines from 13 patients with isolated F1Fo ATP synthase deficiency. *BMC Genomics* **9,** 38 (2008).

308. Inzucchi, S. CLINICIAN ' S CORNER Oral Antihyperglycemic Therapy for Type 2 Diabetes Scientific Review. **06520,** 360–372 (2008).

309. Kahn, S. E. *et al.* Glycemic durability of rosiglitazone, metformin, or glyburide monotherapy. *N. Engl. J. Med.* **355,** 2427–2443 (2006).

310. Wahlstrom, H. *et al.* Inhibition of insulin release by cyclosporine and production of peripheral insulin resistance in the dog. *Transplantation* **49,** 600–604 (1990).

311. Nguyen, G. H., French, R. & Radhakrishna, H. Protein kinase A inhibits lysophosphatidic acid induction of serum response factor via alterations in the actin cytoskeleton. *Cell. Signal.* **16,** 1141–1151 (2004).

312. Wruck, C. J. *et al.* Nrf2 induces interleukin-6 (IL-6) expression via an antioxidant response element within the IL-6 promoter. *J. Biol. Chem.* **286,** 4493–4499 (2011).